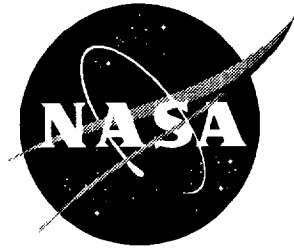# Development of a Rotor-Body Coupled Analysis for an Active Mount Aeroelastic Rotor Testbed

Matthew L. Wilbur
U.S. Army Research Laboratory
Vehicle Technology Center
Langley Research Center, Hampton, Virginia

June 1998

Available from the following:

Contents

Tables

Figures

Symbols

$[A]$	mobility matrix
A_X	roll displacement, deg
A_Y	pitch displacement, deg
A_Z	yaw displacement, deg
a	speed of sound, ft/s
$[B]$	motion matrix
b	rotor blade index
C	damping
$[C]$	impedance matrix
C_D	drag coefficient
C_L	lift coefficient
C_Q	torque coefficient
c	damping for sample model, lb-s/ft
D	rotor drag, lb
$[D]$	load transfer matrix
$\mathbf{d}_a$	displacement vector of Stewart platform joint for actuator a
$\mathbf{d}_g$	displacement vector of simulated center of gravity
$[E]$	system loads due to motion matrix
EI	bending stiffness
F	force, lb
$\{F\}$	force vector
F_I	force at interface joint of sample model, lb
$\{F_I\}$	interface force vector
$\{F_0\}$	uncoupled rotor force vector
F_X	axial force, lb
F_Y	side force, lb
F_Z	normal force, lb
f_j	jth time step in time history
GJ	torsional stiffness
H	harmonic input amplitudes for ARES-II hub motion in CAMRAD-II model
$[I]$	identity matrix
$\mathbf{i, j, k}$	unit vectors
J	number of time steps in time history
K	spring stiffness
k	spring stiffness of sample model, lb/ft
L	rotor lift, lb
L_X	axial displacement, in.

L_Y	side displacement, in.
L_Z	normal displacement, in.
$\mathbf{l}_a$	vector from longeron joint of actuator a to Stewart platform joint of actuator a
l_A	length of actuator a, in.
M	moment, in-lb
M_{tip}	hover tip Mach number
M_X	rolling moment, in-lb
M_Y	pitching moment, in-lb
M_Z	yawing moment, in-lb
m	mass of sample model, slugs
N	number of rotor blades
n	harmonic number
nP	frequency, n times rotor rotational speed Ω
Q	rotor torque, ft-lb
R	rotor radius, ft
$[\mathbf{R}_g]$	rotation matrix about simulated center of gravity
$\mathbf{r}_a$	vector from fixed-system balance center to Stewart platform joint for actuator a
$\mathbf{r}_g$	vector from fixed-system balance center to simulated center of gravity
$\mathbf{r}_{ga}$	vector from simulated center of gravity to Stewart platform joint for actuator a
$T(\psi)$	azimuthally varying signal for generation of hub motion in CAMRAD-II model of ARES-II
$\{\mathbf{U}\}$	control vector for Stewart platform motion
V_{tip}	rotor hover tip speed, ft/s
V_∞	forward flight velocity, ft/s
w_j	weighting factor for harmonic analysis
$\{\mathbf{X}\}$	displacement vector
$\{\mathbf{x}_I\}$	interface displacement vector
$\{\mathbf{x}\}$	displacement vector of sample model
x_I	displacement at interface joint of sample model, ft
α_{TPP}	rotor tip-path-plane angle of attack, deg or rad
θ	rotation angle, rad
μ	rotor advance ratio
ρ	density, slugs/ft^3
ψ	azimuth angle, deg or rad, 0° over helicopter tail and increases with counterclockwise rotation
ψ_b	azimuth angle of bth blade, deg
Ω	rotor rotational speed, rad/s

Subscripts:

a, A	actuator number

B	referenced to body-fixed coordinate system attached to ARES-II fixed-system balance
b	rotor blade index
c	cosine component
corr	corrected
FB	fixed balance
g	simulated center of gravity
H	hub interface joint
I	interface joint
L	referenced to body-fixed coordinate system attached to ARES-II longeron
m	mth degree of freedom
n	harmonic
RB	rotating balance
S	swashplate interface joint
s	sine component
x	axial
y	side
z	normal
θ_x	roll
θ_y	pitch
θ_z	yaw
0	uncoupled rotor condition

Superscript:

T	transposed

Abbreviations:

ARES	Aeroelastic Rotor Experimental System
ARES-II	second generation version of Aeroelastic Rotor Experimental System
BRR	Basic Research Rotor
CAMRAD-II	second generation version of Comprehensive Analytical Model of Rotorcraft Aerodynamics and Dynamics
c.g.	center of gravity
DADS	Dynamic Analysis and Design System
dof	degree of freedom
FFT	Fast Fourier Transform
mag	magnitude
NASA	National Aeronautics and Space Administration
TDT	Langley Transonic Dynamics Tunnel

Dots over a symbol indicate derivative with respect to time.

Summary

Helicopters have historically had significant vibration problems that require stringent design specifications for helicopter subsystems. The primary source of the vibratory loads may be traced to the main-rotor system where the rotor blades are excited by the periodic aerodynamic environment. The resulting vibratory loads are transmitted down the main-rotor shaft into the helicopter fuselage. Generally the effects of the rotor coupling with the fuselage response are ignored in rotor system analysis. However, these effects are often important and may significantly alter the helicopter system response. At the Langley Research Center, an active mount rotorcraft testbed is being developed for use in the Langley Transonic Dynamics Tunnel. This testbed, the second generation version of the Aeroelastic Rotor Experimental System (ARES-II), can impose rotor hub motions and measure the response so that rotor-body coupling phenomena may be investigated. An analytical method for coupling an aeroelastically scaled model rotor system to the ARES-II is developed in the current study. Models of the testbed and the rotor system are developed in independent analyses, and an impedance-matching approach is used to couple the rotor system to the testbed. The development of the analytical models and the coupling method is examined, and individual and coupled results are presented for the testbed and rotor system. Coupled results are presented with and without applied hub motion, and system loads and displacements are examined. The results show that a closed-loop control system is necessary to achieve desired hub motions, that proper modeling requires including the loads at the rotor hub and rotor control system, and that the strain-gauge balance placed in the rotating system of the ARES-II provides the best loads results.

1. Introduction

1.1. Motivation

Aeroelastic testing of model-scale helicopter rotors has been performed in the Langley Transonic Dynamics Tunnel (TDT) since the 1960s. Since 1976, the bulk of this testing has been accomplished by using the Aeroelastic Rotor Experimental System (ARES), a generic rotorcraft testbed designed for the performance, stability, and dynamic loads evaluation of new rotor concepts. Currently, a second generation version of the testbed is under development at the TDT. This testbed is called ARES-II (fig. 1.1) and has been designed for the evaluation of dynamic loads due to rotor-body coupling and for extended rotor stability testing. To comprehend fully the expected capability of the ARES-II, new analysis techniques must be established. These techniques will be used to develop pretest predictions, to formulate efficient test plans, and to develop safety-of-flight criteria for safe, practical wind tunnel testing. The goal of the current research is to develop analytical techniques for the prediction of rotor-body coupling effects. Because the ARES-II may be used for testing of many model rotor system designs, developing a coupling method that permits rotor-off treatment of the testbed for evaluation and verification is
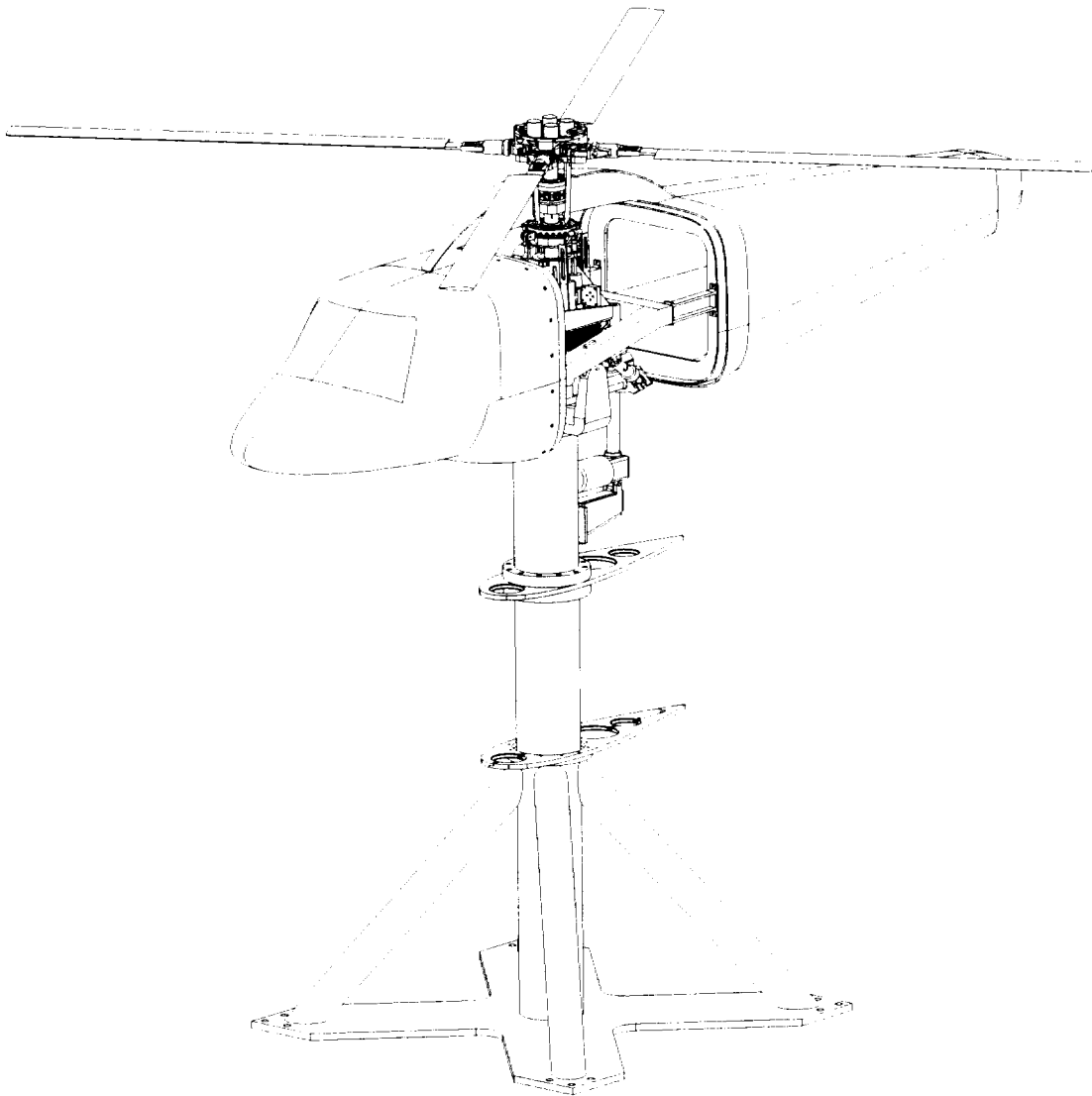

Figure 1.1. ARES-II rotor research testbed.

necessary. Therefore, a method is employed which permits the development of independent math models of the testbed and the rotor system before the rotor-to-body coupling is accomplished.

1.2. Background

Helicopters have historically had significant vibration problems. These vibrations can, at times, be severe and are responsible for a great number of stringent design requirements for helicopter subsystems. Vibratory loads cause crew and passenger fatigue and discomfort, reduce overall system reliability, and increase maintenance costs. For military helicopters, vibratory response can make targeting operations difficult. Further, vibration levels must be attenuated for the helicopter to be accepted by the public as a viable means of civil transportation. Achievements in vibration reduction, however, are quickly being offset by the requirement for higher flight speeds. Reductions in flight vibrations, therefore, are becoming more and more difficult to attain. For these reasons, helicopter vibration reduction has been, and continues to be, a primary area of rotorcraft research in industry, academia, and government organizations throughout the world.

In 1976, a NASA advisory council challenged the helicopter research community with the goal of "the jet smooth helicopter," a maximum vibratory loading of $0.02g$ throughout the straight-and-level flight envelope. To date, no production helicopter has achieved this goal. Advances in vibration control, however, have been significant. Vibration levels had dropped from $0.3g$–$0.6g$ in the mid-1950s to about $0.1g$ in the early 1980s (ref. 1). The methods used to attain these reduced levels of vibration have been documented by Reichert in a 1981 paper surveying the developed techniques (ref. 1). Although somewhat dated, the paper presents the bulk of vibration reduction techniques in use on production aircraft today. Furthermore, little additional progress has been made toward achieving the jet smooth goal since Reichert's paper was published.

It is widely accepted that the primary source of helicopter vibratory loads may be traced to the main-rotor system. Other loads exist (e.g., fuselage airloads, rotor-fuselage aerodynamic interference, drive train loads, tail rotor loads); however, the effects of these loads are typically small when compared with those produced by the main rotor that are passed down the main-rotor shaft into the fuselage. Therefore, the traditional methods of helicopter vibration reduction have usually consisted of means to reduce the vibratory loads generated by the main rotor.

Traditionally, the method used to determine vibration levels throughout the fuselage has been to analyze the rotor as an isolated system when calculating the loads imposed on a fixed rotor shaft. These loads were then applied independently to an analytical model of the fuselage to determine vibration levels at locations throughout the helicopter. However, rotor-body couplings have been known for some time to exist between rotor systems and the fuselage that can alter the loads. Several analytical techniques have been implemented to couple the rotor system to the fuselage. One such technique is known as "impedance matching," where the load and displacement fields at the interface between the rotor system and the fuselage are matched. References 2 through 6 are representative of rotor-body coupling research using impedance-matching methods. An advantage of the impedance-matching method is that the rotor and body may be treated by using different independent analyses. Therefore, one is free to choose the analyses that can best model the individual systems.

1.3. Scope

The scope of the current research includes the development of an impedance-matching method suitable for coupling a generic research rotor to the ARES-II rotorcraft testbed. The ARES-II testbed is capable of six-degree-of-freedom actuation of the rotor hub through a motion-based system called a Stewart platform. Therefore, this system and its control must be modeled as well. A three-step approach is used for the analysis. First, independent analytical models of the ARES-II and the Basic Research Rotor (BRR), the rotor system chosen for this study, are developed (sections 4.1 and 4.2). Second, the developed models of the ARES-II and the BRR are used to generate a set of impedance matrices representing the load-displacement relationships at the interface joints on each model (sections 5.3.1 and 5.3.2). These interface joints are the points at which the two systems are joined during the coupling phase of the analysis. Finally, the two systems are coupled together by enforcing displacement and load compatibility conditions through simple linear algebraic manipulations of the impedance matrices (section 5.3.3). A survey of the available analyses was undertaken to decide which would provide the best independent models of

the ARES-II and the BRR, the rotor system chosen for this study. The most recently available, state-of-the-art analysis for rotor systems is CAMRAD-II, the second generation version of the Comprehensive Analytical Model of Rotorcraft Aerodynamics and Dynamics (refs. 7 and 8). This program was chosen for the Basic Research Rotor modeling. To model the ARES-II, the Dynamic Analysis and Design System (DADS), a multibody dynamics analysis, was chosen (refs. 9 and 10). Alternatively, a finite-element code could have been used. The ARES-II, however, is a relatively stiff system with discrete areas of flexibility—a system a multibody dynamics code is well suited to model. Additionally, DADS offers a superior interface for visualizing the testbed motion and for implementing the control of the motion-based platform.

The impedance-matching methods proposed in references 2 through 6 have been used for guidance in this study. However, two enhancements have been included in the current effort that are not evident in the literature. First, the controlled motion-based platform of the ARES-II is unique among rotor testbeds. For this work, the impedance-matching method has been extended to include the motions introduced by the platform. Second, two load paths have been modeled between the testbed and the rotor system in the current work—the hub and the rotor control system. Only the hub load path is evident throughout the literature. The rotor control system load path is shown to be necessary to provide an accurate assessment of the system loads.

1.4. Organization of Study

The rest of the study is organized in the following manner:

Section 2. Basic Rotorcraft Analysis: This section provides a brief introduction to rotorcraft analysis for readers unfamiliar with such techniques. Basic rotor system definitions, control, performance, aerodynamics, and dynamics are discussed.

Section 3. Rotorcraft Wind Tunnel Test Apparatus: This section provides a complete description of the ARES-II testbed and the BRR.

Section 4. Analytical Models of ARES-II and BRR: This section describes the DADS model of the ARES-II and the CAMRAD-II model of the BRR. Also described is the development of the equations necessary to prescribe motion of the ARES-II Stewart platform.

Section 5. Dynamic Analysis Using Impedance Matching: This section describes the application and limitations of the impedance-matching approach as applied to the ARES-II and the BRR. A simple spring-mass-damper system is used to convey the proper impedance-matching techniques. A complete description of the steps necessary to develop the impedance models and coupling equations for the ARES-II and the BRR are included.

Section 6. Presentation of Results: The results obtained with the individual models of the ARES-II and the BRR are discussed in this section. Also included are coupled rotor-testbed results for actuated and unactuated motion of the ARES-II Stewart platform.

2. Basic Rotorcraft Analysis

This section provides a brief introduction to rotorcraft analysis for readers who are unfamiliar with such techniques. Several good texts (refs. 11 through 14) are available which discuss rotor system aerodynamics, dynamics, and stability in detail. This discussion emphasizes the major analytical techniques used in analyzing the Basic Research Rotor (BRR) system.

2.1. Definitions

2.1.1. Azimuth

For most helicopters, the main-rotor system rotates in a counterclockwise direction (when viewed from above) at an angular rate of Ω in radians per second. Azimuthal blade position is denoted by ψ and is indexed so that $\psi = 0°$ occurs when the blade chosen to be the reference blade is over the aircraft tail and increases in the direction

3

of rotor rotation. Typically, rotor blades are equally spaced azimuthally so that a general relationship exists between each blade and the reference blade; that is

$$\psi_b = \psi + \frac{2b\pi}{N} \tag{2.1}$$

where b is the blade number, N is the number of rotor blades, ψ is the azimuth of the reference blade in radians, and ψ_b is the azimuth of the bth blade in radians. Therefore, by using equation (2.1), the reference blade is the bth blade.

2.1.2. Rotor Speed Parameters

Several important parameters are associated with the rotational speed of the rotor system. The rotor tip speed in hover is defined by

$$V_{tip} = \Omega R \tag{2.2}$$

where R is the rotor radius in feet. An associated parameter is the rotor hover tip Mach number given by the following equation:

$$M_{tip} = \frac{V_{tip}}{a} \tag{2.3}$$

where a is the test medium speed of sound in feet per second. The hover tip Mach number is typically used to ensure proper aerodynamic scaling when testing rotor systems for performance characteristics in the Langley Transonic Dynamics Tunnel.

Rotor advance ratio is typically used to refer to the forward flight speed of a helicopter and is defined by

$$\mu = \frac{V_\infty \cos \alpha_{TPP}}{V_{tip}} \tag{2.4}$$

where V_∞ is the forward flight speed and α_{TPP} is the rotor tip-path-plane angle of attack with respect to V_∞. A well-designed rotor system with good performance characteristics may be able to reach $\mu = 0.45$. A poor performing rotor system may have difficulty in attaining $\mu = 0.35$.

2.1.3. Articulated Rotor Hubs

An articulated rotor hub has three hinges for each blade: the flap hinge, the lead-lag hinge, and the pitch bearing, each of which is shown in figure 2.1 for the rotor hub used with the BRR. The lead-lag and flap hinges permit blade motions in the plane and out of the plane of rotation, respectively. The pitch bearing allows each blade to change angle of attack under the influence of the rotor control system.

2.1.4. Coordinate Systems

Referring to the "fixed system" and the "rotating system" is typical in rotorcraft analysis. Generally, the fixed system consists of the helicopter fuselage and its components. The rotating system consists of the rotor and all components operating at the same rotational speed as the rotor system such as the main-rotor shaft and rotating control system components. For the purposes of this study, however, the rotating system is considered to include only those rotor system components that are part of the rotor hub or the blades. All other rotating-system components, including the rotor control system and rotor shaft, are considered to be part of the fixed system. The reasons for this consideration become evident in section 4.2.2.

The coordinate system referred to throughout this report is a typical rotorcraft fixed-system coordinate frame oriented as shown in figure 2.2. Unless otherwise specified, all motions and loads are identified with respect to this

4
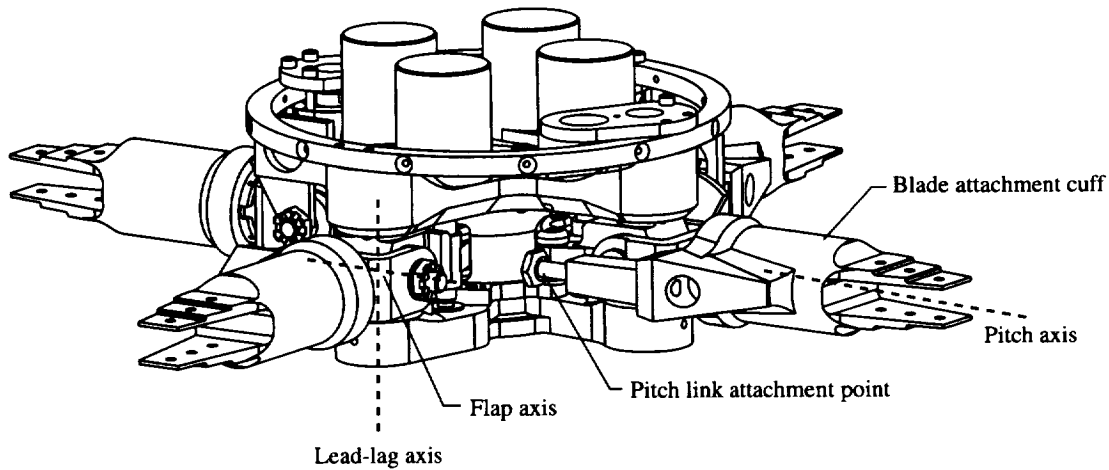
Figure 2.1. Basic Research Rotor articulated hub.
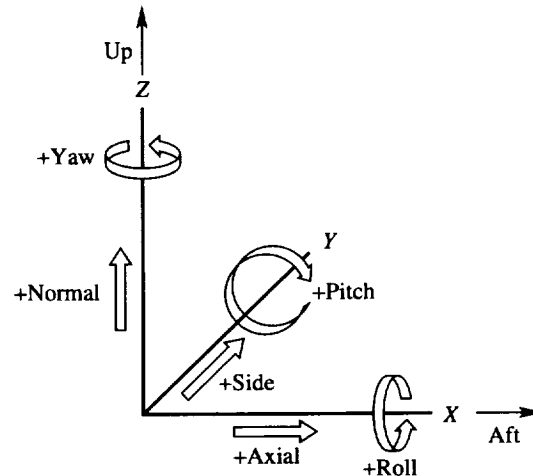
Figure 2.2. Fixed-system coordinate frame.

coordinate frame. For example, a "positive axial force" is a load oriented along the +X-axis, and a "negative pitching moment" is a moment defined by using the right-hand rule along the -Y-axis.

2.2. Rotor Control System

The rotor control system consists of the swashplate, swashplate actuators, and the pitch links. A close-up view of the control system of the ARES-II with the BRR articulated hub is shown in figure 2.3. The swashplate has both rotating and stationary sections. The rotating section turns with the hub and serves as the lower attachment point for the pitch links. The upper end of each pitch link is attached to the pitch horn which is part of the blade cuff. Both ends of the pitch links have spherical rod-end bearings to permit rotational motions at the joints. The stationary section of the swashplate is mounted to the shaft with a large spherical bearing that is free to travel up and down the rotor shaft. This arrangement eliminates two degrees of freedom from the swashplate (fore and aft and side to side), and the nonrotating scissors (fig. 2.3) eliminate a third degree of freedom (rotation about the shaft). The remaining three degrees of freedom are constrained by three swashplate actuators. The actuators control the swashplate position up and down the rotor shaft and the swashplate tilt from side to side and fore and aft.

5
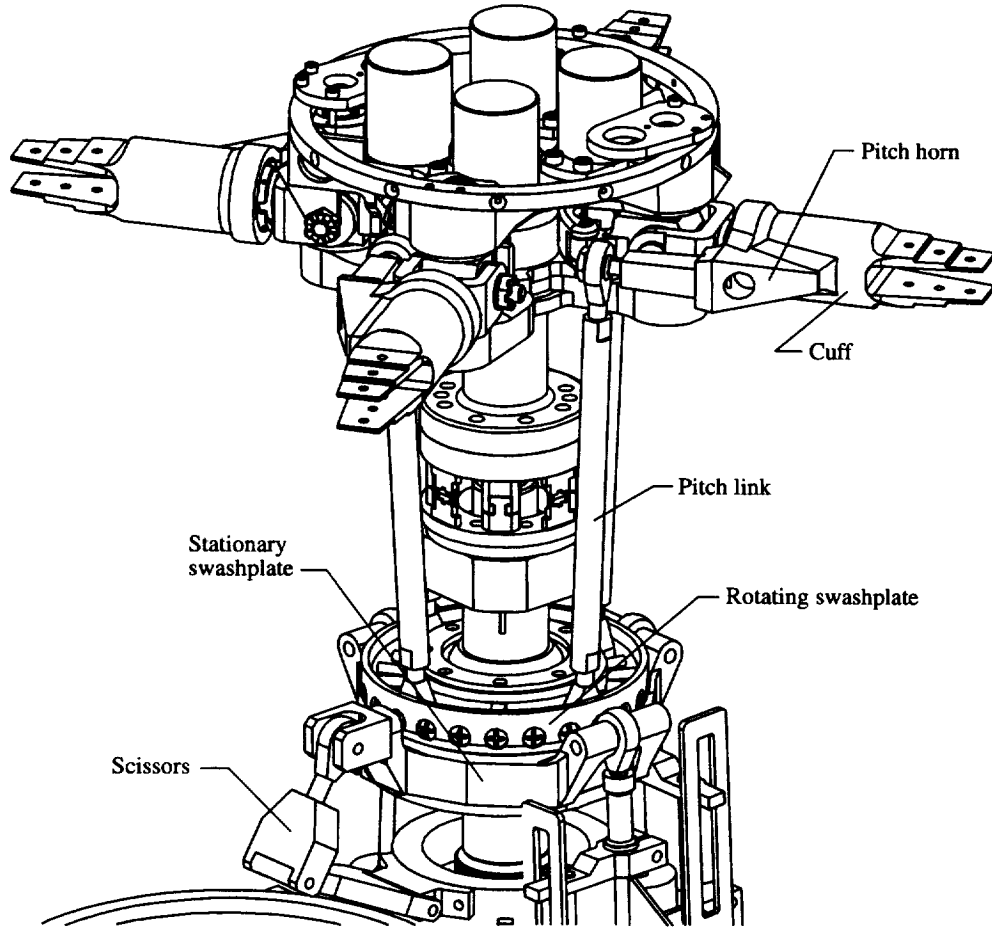
Figure 2.3. ARES-II control system with BRR hub.

For control systems with the pitch links trailing the blades, a lowering of the swashplate increases the pitch on all the blades collectively. Thus, raising and lowering the swashplate controls the "collective" pitch of the blades. By tilting the swashplate, a "cyclic" blade pitch schedule may be induced; this means that a sinusoidal oscillation of blade pitch is induced as a function of azimuth. Because the swashplate has two axes of tilt (i.e., fore and aft and side to side), two cyclic controls are necessary. The cyclic control that induces forward or aft motion of the helicopter is called longitudinal cyclic, and the control that induces right or left sideward motion of the helicopter is called lateral cyclic.

2.3. Rotor Performance

Because this study focuses on rotor dynamics, little needs to be said regarding rotor performance; however, some explanation is necessary because rotor performance parameters are used to define trim targets in section 5. Generally, three parameters are of primary concern for rotor performance: rotor-generated lift, propulsive force, and torque required. Each of these parameters is normally nondimensionalized so that comparisons may be made between rotor systems regardless of size. However, the typical nondimensionalization factors for fixed-wing aircraft fail when applied to rotary-wing aircraft in hover flight ($V_\infty = 0$). The accepted equations for nondimensionalization of rotor systems allow for treatment of both the hover and forward flight conditions as follows:

$$C_L = \frac{L}{\pi R^2 \rho (\Omega R)^2} \tag{2.5}$$

6

$$C_D = \frac{D}{\pi R^2 \rho (\Omega R)^2} \qquad (2.6)$$

$$C_Q = \frac{Q}{\pi R^3 \rho (\Omega R)^2} \qquad (2.7)$$

where L is lift, D is drag (or propulsive force), Q is torque, ρ is density, R is rotor radius, and Ω is rotor rotational speed. Notice that drag D is used for propulsive force. For a wind axis system, lift is normally considered positive up and drag positive aft. Therefore, referring to the propulsive force (which is oriented forward) as "negative drag" is typical.

2.4. Rotor Aerodynamics

The rotor system develops its thrust by inducing a mass flow, or induced velocity, downward through the rotor. The total flow through the rotor, or inflow, is a combination of the flight and induced velocities. This inflow is a highly nonuniform and volatile flow field that is difficult to model and to analyze. The inflow is, however, a critical characteristic in the determination of rotor aerodynamic loads because the local inflow directly affects the local blade section angle of attack. Further, the rotor system aerodynamics represents the primary forcing function responsible for the dynamic response. Therefore, a good model of the rotor system aerodynamics, and hence, a good model of the inflow, is necessary.

The rotor inflow is influenced by the flight velocity and the rotor wake. Therefore, a representation of the rotor wake structure (blade tip vortices and inboard blade vortex sheets) is necessary to calculate the rotor inflow. In CAMRAD-II, wake models are available based on the research results of Landgrebe (ref. 15), Kocurek and Tangler (ref. 16), Scully (ref. 17), and Johnson (ref. 18).

References 15 through 18 describe two approaches to model the rotor wake: the prescribed wake and the free wake. The simpler of the two is the prescribed wake methodology. In the prescribed wake method, a series of trajectories is calculated for the tip vortices and the inboard wake sheet based on rotor operating conditions. The inflow environment is calculated based on the position and the circulation strength of the wake elements at each azimuthal step in the analysis. An example of the wake geometry obtained with this method is shown for hover and forward flight in figure 2.4. The second approach is the free wake methodology in which the tip vortex trajectory is allowed to distort based on the conditions of the surrounding airflow; this results in the most realistic aerodynamic environment. An example of the wake geometry obtained with this method is shown in figure 2.5. For this study, a wake model based on the second approach, the Johnson free wake methodology (ref. 18), has been used for all calculations to obtain the greatest possible model fidelity.

2.5. Rotor Dynamics

Main-rotor system dynamic response is the primary contributor to helicopter vibratory loads. The aerodynamic environment of the rotor system in forward flight produces periodic blade loads at frequencies that are harmonics of the rotor rotational speed. Therefore, these frequencies are the primary concern of the helicopter dynamicist. Then, referring to the frequencies as referenced to the rotor speed becomes convenient. Thus, the terminology n per revolution, n per rev, and nP is introduced. Each refers to n times the rotor rotational speed Ω or $n\Omega$ as is sometimes observed in the literature. As a simple example, consider the BRR at its nominal operating speed of 660 rpm or 11 Hz. A frequency of 22 Hz would be considered 2 per rev; a frequency of 33 Hz, 3 per rev; and so forth. Throughout this report, the nomenclature n per rev and nP will be used interchangeably to refer to frequencies. As in any structural dynamics problem, the natural frequencies of the rotor blades are of considerable concern. However, their calculation is considerably complicated because of the rotational environment of the rotor system. Figure 2.6 shows the Southwell or "fan" diagram of the BRR as calculated by CAMRAD-II. This figure shows rotor blade frequencies in both Hertz and per rev as a function of rotor speed in revolutions per minute. The lowest two frequencies are rigid-body lead-lag and flap modes representing rotation about the lead-lag and flap hinges. The higher frequencies are elastic blade modes that have the general appearance of pinned-free elastic

7

(a) Hover.   (b) Forward flight.
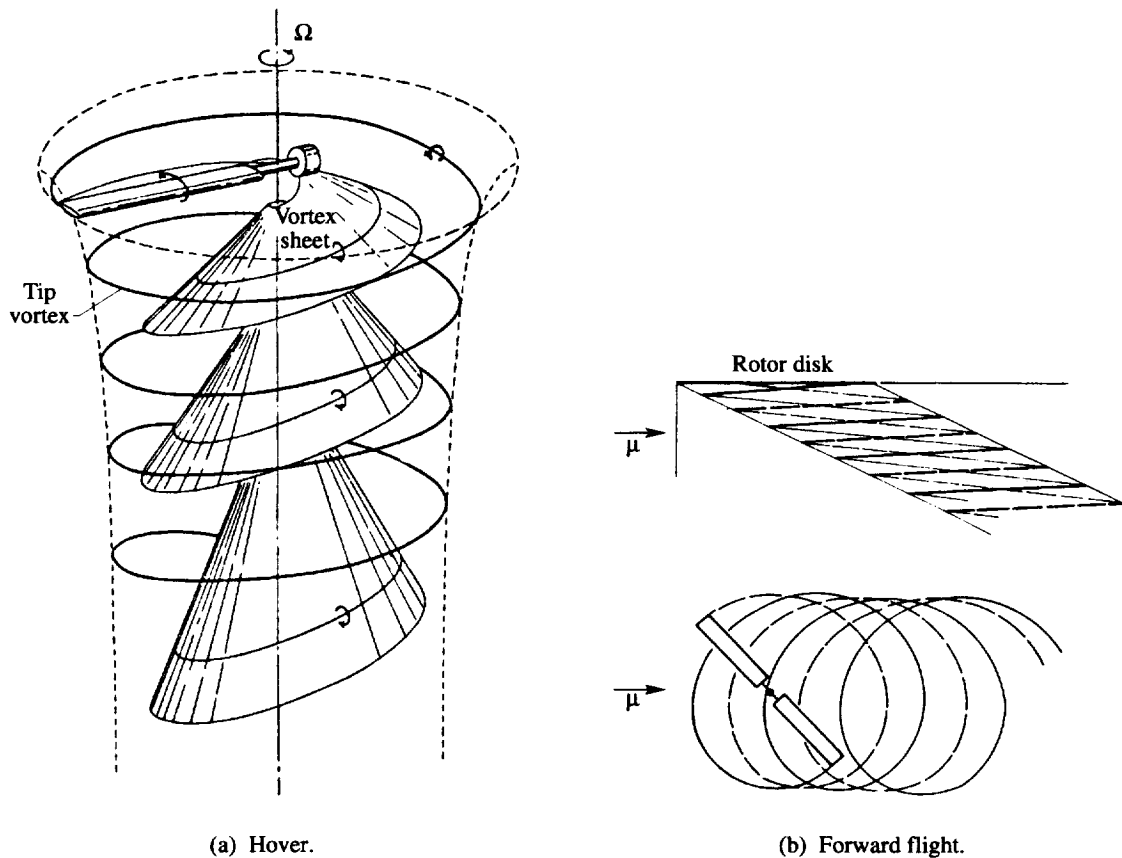
Figure 2.4. Prescribed wake geometry for hover and forward flight. Forward flight geometry shows only tip vortex trajectory.

Figure 2.5. Free wake geometry in forward flight. Only tip vortex trajectories are shown.

beam modes. The per-rev lines in figure 2.6 represent the frequencies at which the aerodynamic forcing functions excite the blade modes.

The rotor system dynamics problem is one of forced response in which the aerodynamic loads supply the forcing functions at discrete frequencies (i.e., per rev). The next concern is the determination of which frequencies have the greatest effect on the helicopter vibratory loads. Appendix A contains a detailed development of the manner in which rotating-blade loads are transferred down the shaft into the fuselage or fixed-system components of

8
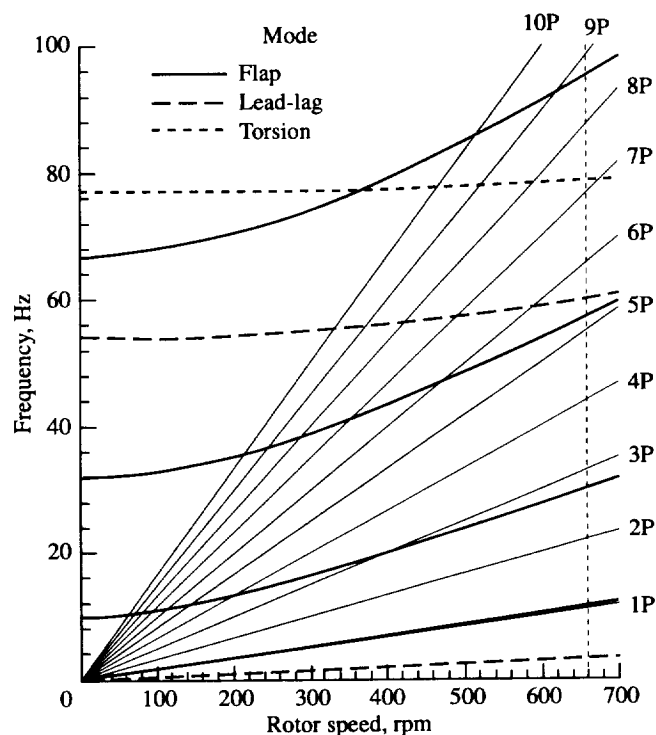
Figure 2.6. Basic Research Rotor rotating frequencies. Vertical dashed line at 660 rpm represents nominal operating speed of BRR.

the aircraft. Here it is sufficient to point out that the rotor system normally acts as a loads filter for the fixed system, passing down only loads whose frequencies are integer multiples of the blade passage frequency (i.e., frequencies of kN per rev, where k is an integer and N is the number of blades). For a four-bladed rotor system such as the BRR, the blade passage frequency is 4 per rev so that only loads having frequencies of 4P, 8P, 12P, and so forth are passed to the fixed system. As shown in appendix A, these fixed-system loads result from loads in the rotor system at frequencies of kN per rev and $(k \pm 1)N$ per rev. Therefore, for the BRR, 4-per-rev fixed-system loads are generated by 3P, 4P, and 5P loads in the rotor system, and 8-per-rev fixed-system loads are generated by 7P, 8P, and 9P loads in the rotor system. Furthermore, the harmonic loads generally become smaller with increasing frequency. Therefore, considering only frequencies at 9 per rev and below is typical in rotor dynamics analysis of four-bladed rotor systems. This is a key point in the analysis of rotor-body coupled systems since only two fixed-system frequencies (4P and 8P) are considered critical for the analysis of a four-bladed rotor.

3. Rotorcraft Wind Tunnel Test Apparatus

The scope of the current research does not include any wind tunnel testing. However, since the objective is to develop analytical models of rotorcraft wind tunnel test hardware, descriptions are provided in this section to acquaint the reader with the apparatus necessary to perform such testing. This description gives the reader a more thorough appreciation of the basis for model-scale aeroelastic rotor testing in the Langley Transonic Dynamics Tunnel.

3.1. Langley Transonic Dynamics Tunnel

The Langley Transonic Dynamics Tunnel (TDT) is a continuous-flow pressure tunnel capable of speeds up to Mach 1.2 at stagnation pressures up to 1 atm. The TDT has a slotted test section that is 16 ft square with cropped corners and a cross-sectional area of 248 ft^2. Either air or Refrigerant-12 (R-12), a heavy gas, may be used as the test medium. For rotorcraft research, a test medium density of 0.006 slug/ft^3 is typically used. The TDT is particularly suited for rotorcraft testing because of three advantages associated with the heavy gas. First, the high density

9

of the test medium permits model rotor components to be heavier; thereby, structural design requirements are eased while dynamic similarity is maintained. Second, the low speed of sound of R-12 permits much lower rotor rotational speeds and forward flight velocities to match full-scale Mach numbers; thus, the centrifugal blade forces are eased and the drive system power requirements are reduced. Furthermore, the lower rotational speeds translate into a smaller control bandwidth when using active control techniques that depend upon harmonic actuation. Third, the high-density environment increases the Reynolds number throughout the test envelope and permits a more accurate simulation of the full-scale aerodynamic environment. A more detailed discussion of the advantages of the heavy gas test medium and further discussions on rotorcraft testing in the TDT are presented in reference 19.

3.2. Aeroelastic Rotor Experimental System

The second generation version of the Aeroelastic Rotor Experimental System (ARES-II) model-scale helicopter rotor testbed is currently under development at the TDT. The stand-mounted testbed is intended for use in defining rotor-body coupling phenomena by using aeroelastically scaled model rotor systems. Sections 3.2.1 through 3.2.3 describe the testbed and its major subsystems. These subsystems include a stand and longeron component (section 3.2.1), an actively controlled hydraulic Stewart platform (section 3.2.2), and a rotor pylon section (section 3.2.3). Figures 3.1 through 3.6 provide various views of the testbed. Figure 3.1 shows the ARES-II with the BRR installed. The fuselage shell left-side panel has been removed to show the placement of the rotor pylon within the shell. The aerodynamic fairing normally installed around the stand has also been removed to show stand details. Figure 3.2 shows the testbed with the rotor blades and the fuselage shell removed. A close-up view of the upper portion of the ARES-II is shown in figure 3.3. Figures 3.4 through 3.6 show detailed views of the rotor pylon and the Stewart platform. For all views, the ARES-II drive belts and miscellaneous hardware have been removed for clarity.

3.2.1. Stand and Longeron

The ARES-II stand (fig. 3.2) is constructed of a steel baseplate, a steel central column, four steel support columns, a steel yoke to support the longeron, and two airfoil-shaped aluminum ribs to support an aerodynamic fairing during wind tunnel testing. The longeron (figs. 3.2 through 3.5) is constructed of three steel box beams each 2 in. square and a 1-in-diameter steel bar. Aluminum fittings placed on the longeron (fig. 3.5) provide support for the hydraulically controlled Stewart platform. Figures 3.3 and 3.4 clearly identify the longeron and its placement on the stand. The connection between the stand and longeron is a revolute joint oriented to allow pitching motions of the longeron relative to the stand. An electric motor-driven screw-jack actuator placed behind the stand is used to control the pitch motion of the longeron. This arrangement permits the adjustment of rotor pylon pitch (or shaft angle of attack), a feature necessary for proper trim of rotor systems in forward flight.

The ARES-II stand is designed to be soft mounted to the TDT floor with elastomeric pads placed at the four corners of the stand baseplate. This arrangement permits limited flexibility and allows tuning of the ARES-II rigid-body frequencies. Alternatively, the stand may be hard mounted to the floor.

3.2.2. Stewart Platform

A hydraulically actuated Stewart platform is placed between the stand-longeron assembly and the rotor pylon. It consists of a six-degree-of-freedom baseplate that is driven by six hydraulic actuators attached to the longeron. The platform is similar in function to those commonly in use on aircraft motion-based simulators and allows six-degree-of-freedom actuation of the rotor pylon which is rigidly attached to the Stewart platform baseplate. Figure 3.4 shows the rotor pylon exploded from the longeron and Stewart platform assembly. This view shows the orientation of the Stewart platform actuators with respect to the longeron. Figure 3.5 shows a close-up view of the Stewart platform. The actuators are connected to the longeron brackets by spherical rod-end bearings. The piston rod of each actuator is connected to the Stewart platform baseplate with a spherical rod-end bearing. The actuator rod connections provide a three-point restraint for the baseplate; thereby, six-degree-of-freedom control of the platform is allowed. Two of the rod-baseplate joints are labeled in figure 3.5; the third is hidden from view.
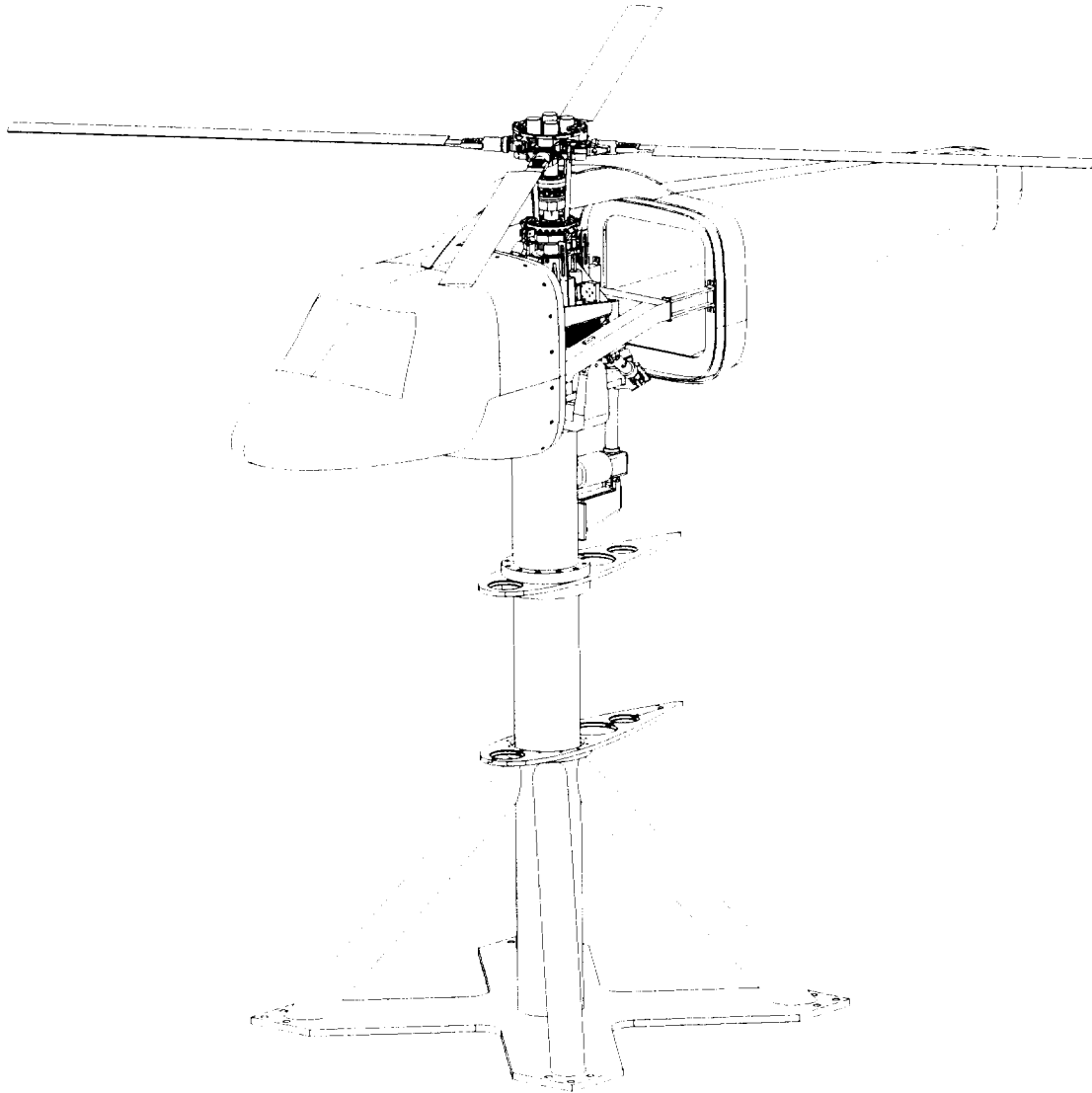
Figure 3.1. ARES-II with Basic Research Rotor installed.

The ARES-II Stewart platform provides a limited range of motion about the nominal centered position of the platform. Translational motions are limited in range to ±0.4 in. and rotational motions to ±2.0°. For this study, the nominal translational and rotational rotor pylon motions applied are ± 0.01 in. and ±0.05°, respectively, well within the range of motion of the Stewart platform.

3.2.3. Rotor Pylon

Figure 3.6 provides a detailed view of the rotor pylon. The rotor pylon consists of the rotor control system, the rotor drive system, and the force measurement system. As mentioned earlier, the rotor hub and pitch links are not considered part of the rotor pylon. They are shown only to provide a complete view of the assembled system. The rotor control system consists of three fly-by-wire hydraulic swashplate actuators and a standard rise-and-fall swashplate. The rotor drive system is powered by a variable-frequency synchronous motor rated at 47-hp output at 12000 rpm. The motor is connected to the rotor shaft through a belt-driven, two-stage speed reduction system.

Instrumentation on the rotor pylon provides continuous display of swashplate control settings, rotor speed, and rotor forces and moments. A 30-channel slip-ring assembly placed in the rotor shaft permits the transfer of

11
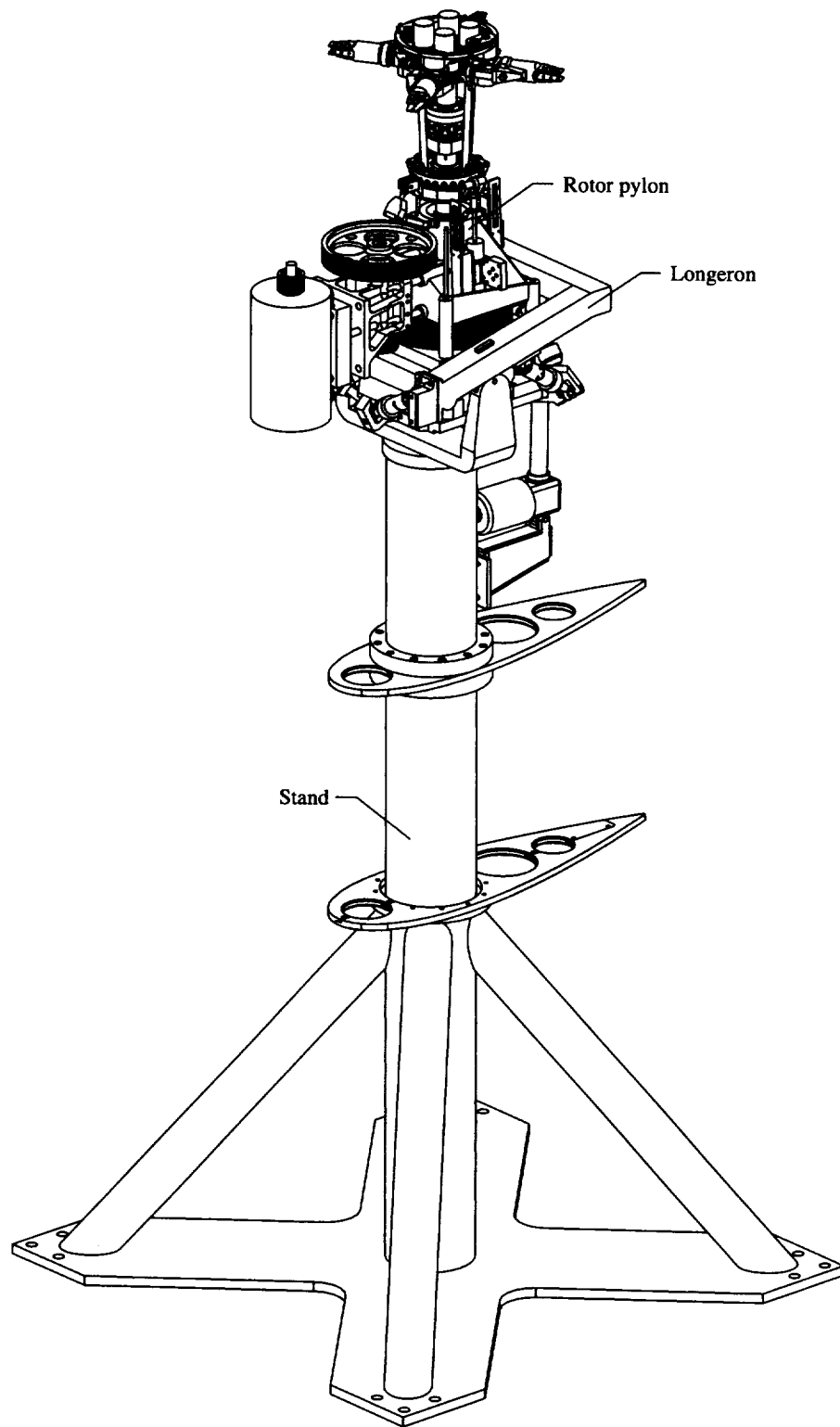
Figure 3.2. ARES-II with aerodynamic shell removed. Drive belts and miscellaneous hardware are not shown for clarity.

Longeron

Pitch axis

Yoke

Screw jack

Pitch actuator
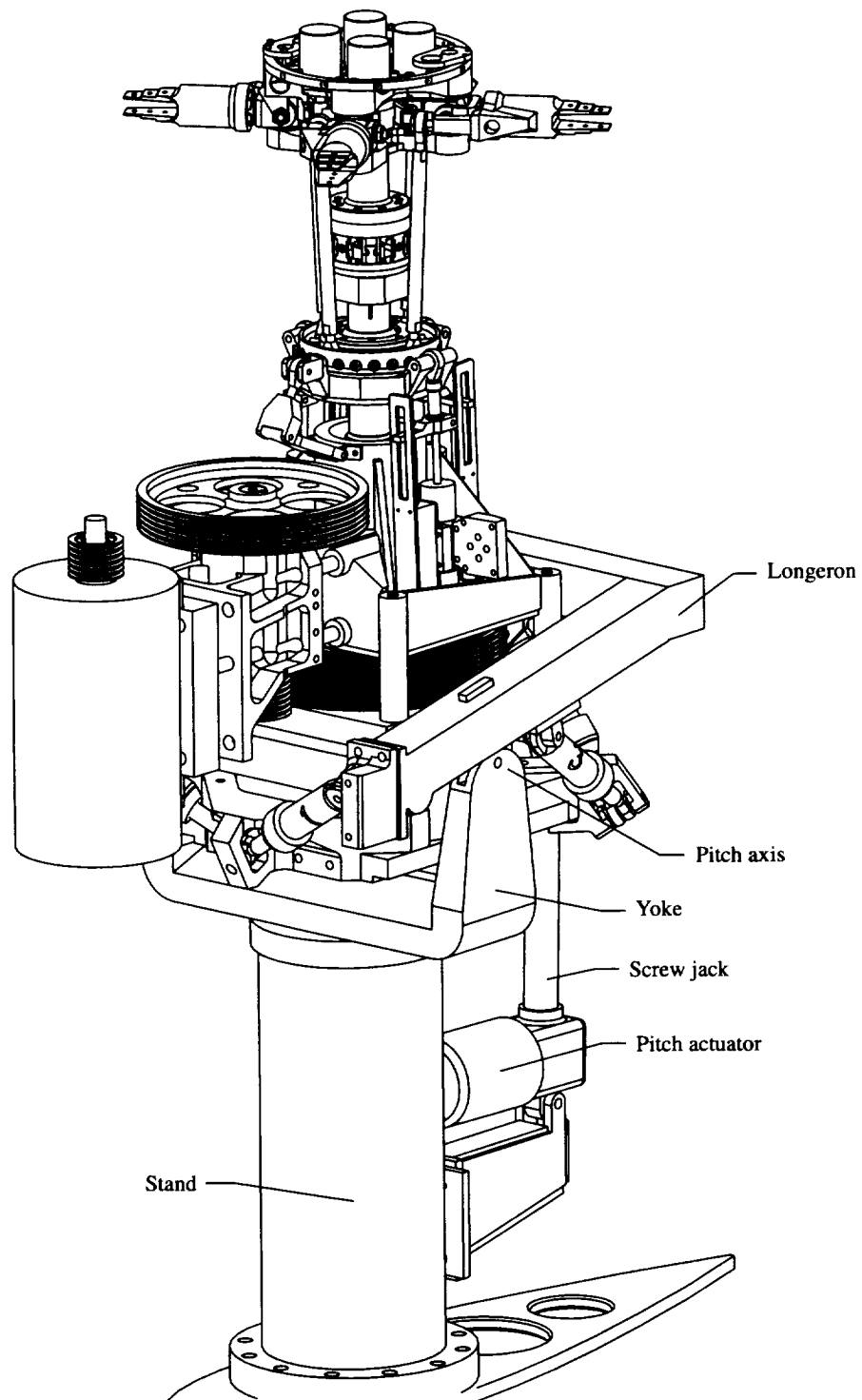
Stand

Figure 3.3. ARES-II upper stand components.
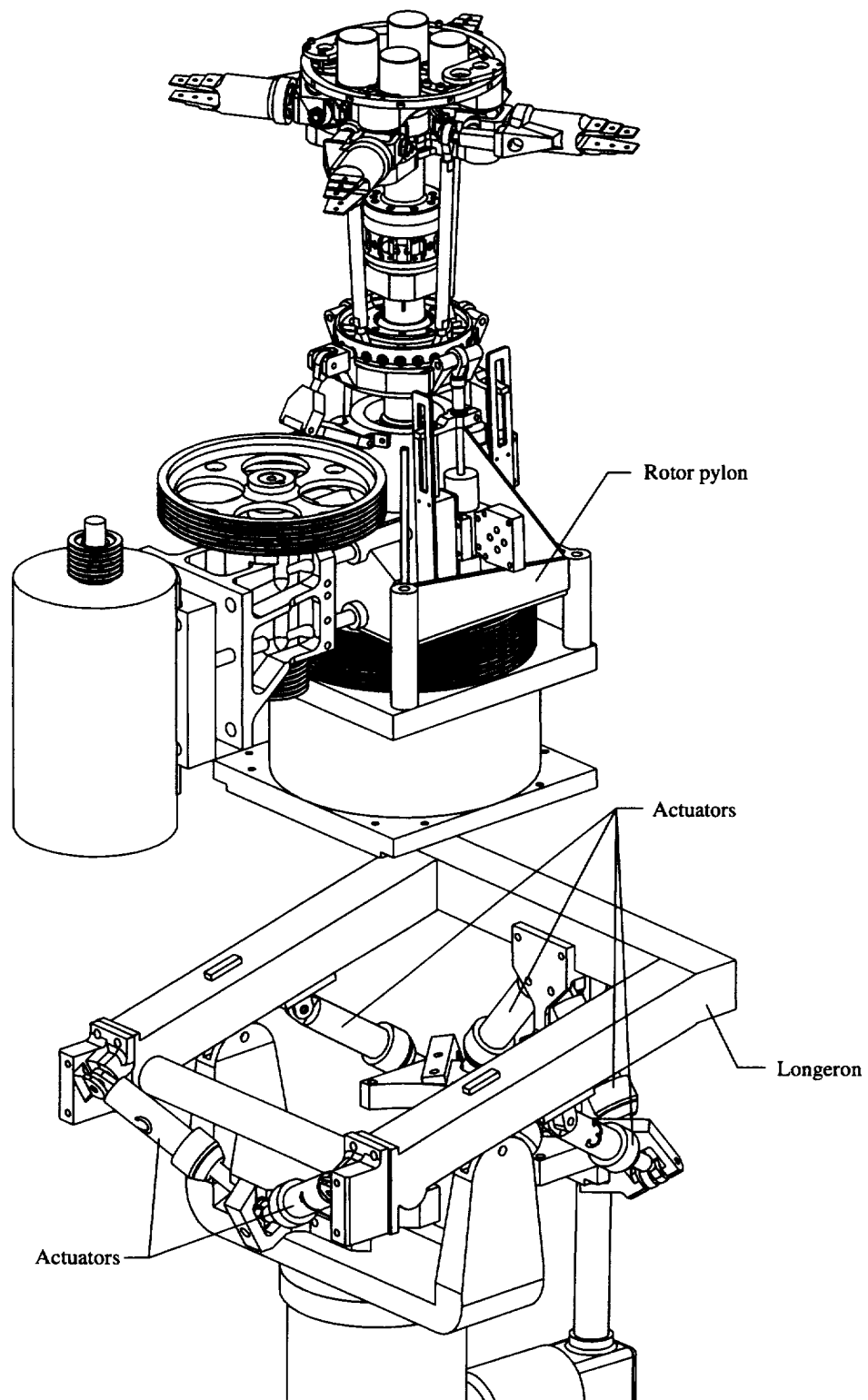
Figure 3.4. Exploded view of ARES-II rotor pylon and Stewart platform.
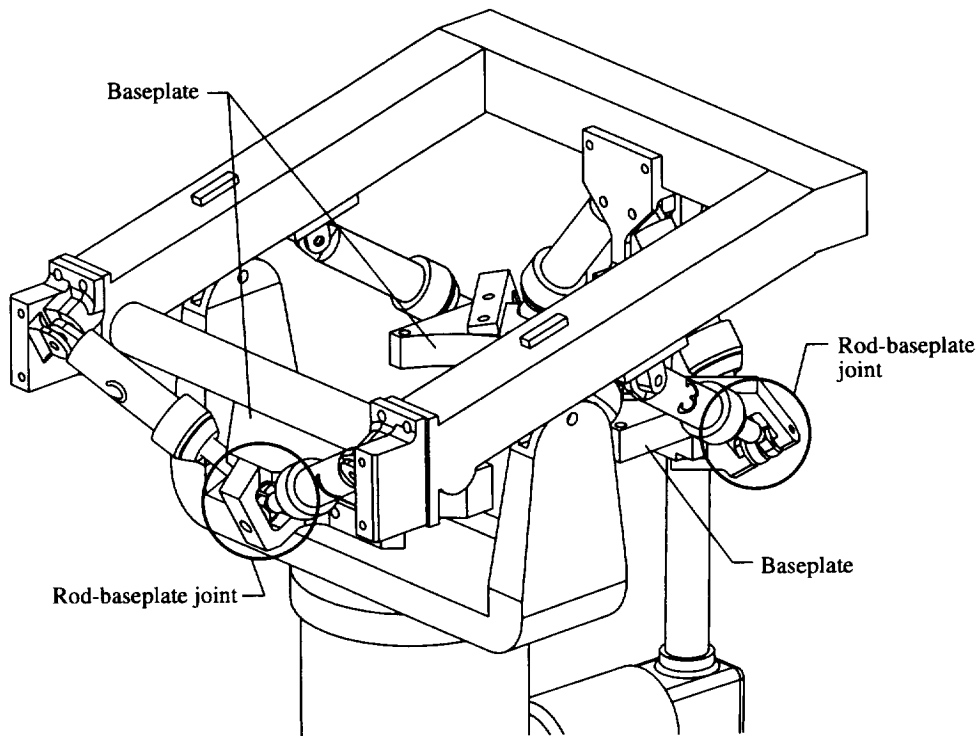
Figure 3.5. Close-up view of Stewart platform components.

rotating-system data to the fixed system. Fixed-system forces and moments are measured by a six-component strain-gauge balance placed at the bottom of the rotor pylon. This balance is called the fixed-system balance. Rotating-system forces and moments are measured by a second six-component strain-gauge balance. This balance is placed just below the rotor hub between the rotor shaft and the mast and rotates with the shaft assembly. This balance is called the rotating balance.

3.3. Basic Research Rotor

For the initial investigation on the ARES-II, the BRR is the rotor system chosen. The BRR is a four-bladed, articulated rotor system designed for generic rotorcraft wind tunnel research, but it is not intended to represent any full-scale flight vehicle hardware.

3.3.1. Rotor Hub

A four-bladed articulated rotor hub is used for the BRR. The hub lead-lag and flap hinges are coincident and placed 3.0 in. from the center of rotation, with the pitch bearing placed directly outboard of the hinges. Rotary potentiometers placed on the hub and geared to the blade cuffs permit measurement of blade lead-lag, flap, and pitch angles. Lead-lag dampers are used on the hub with an effective damping output of 980 in-lb-s/rad. Kinematic coupling due to the control system configuration induces a pitch-flap coupling ratio of 0.5, flap up–pitch down; that is, the coupling produces a 0.5° nose-down blade pitch for each degree of upward (positive) blade-flap displacement.

3.3.2. Rotor Blades

The BRR blades are untwisted, rectangular planform research blades with NACA 0012 airfoils. The blades are not representative of those used on any full-scale helicopter; however, they have been designed with model-scale dynamic properties similar to those used on full-scale helicopters. The blades have a chord of 3.625 in. and, when installed on the rotor hub, have a radius of 56.224 in.

15
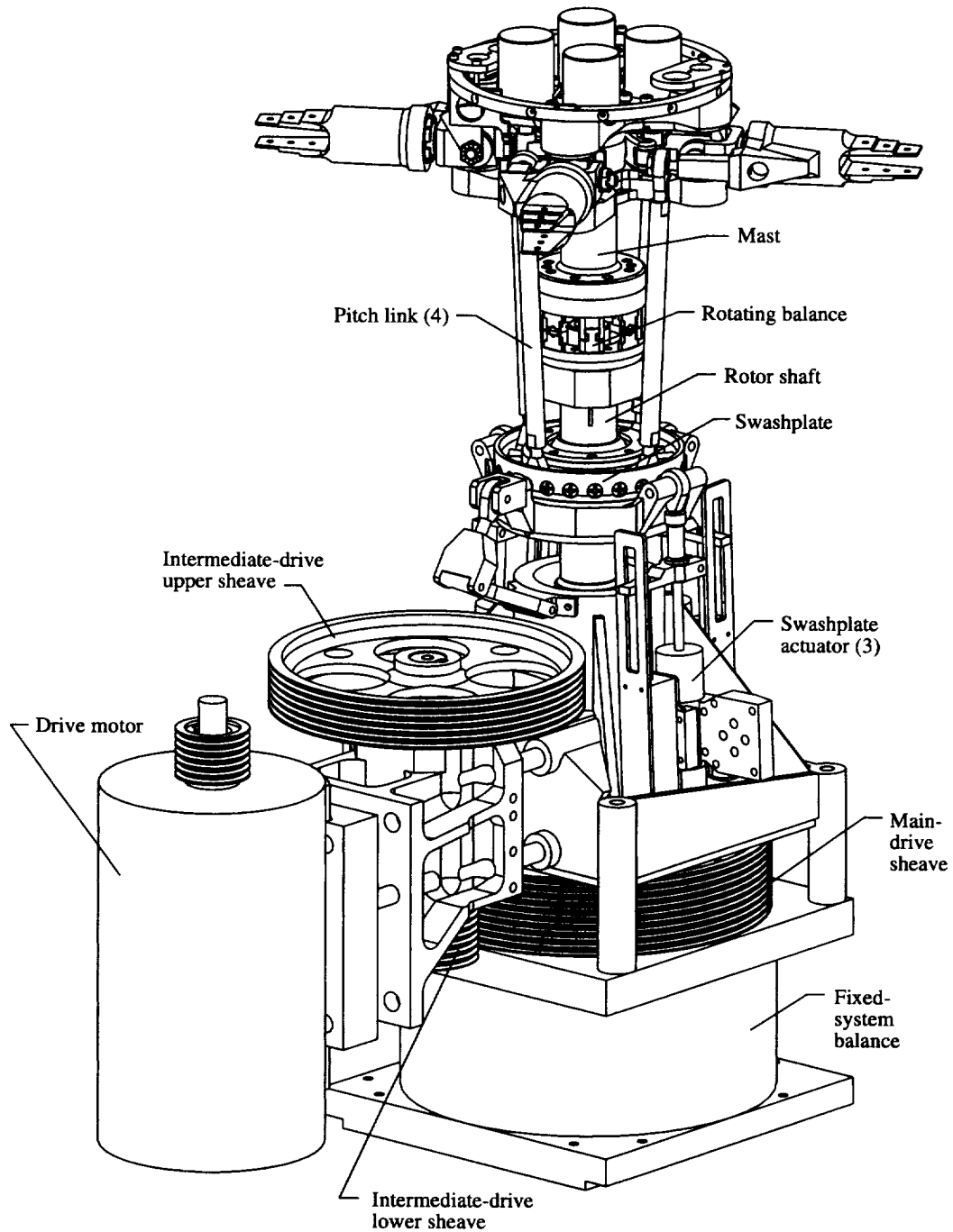
Figure 3.6. ARES-II rotor pylon consisting of rotor drive, control, and force measurement systems. Drive belts and miscellaneous hardware are not shown for clarity.

4. Analytical Models of ARES-II and BRR

Coupling dynamic systems with an impedance-matching approach requires the development of impedance matrices that describe the load-displacement relationships at the interfaces connecting the individual systems. The individual systems are then coupled by imposing load and displacement compatibility conditions on the matrices. Therefore, the first step in the development of an impedance-matching method for coupling the BRR to the ARES-II testbed is the development of individual analytical models of the two systems. This method has the

16

advantage of allowing the selection of the best analysis for each system to be analyzed. For the ARES-II, a finite-element code could have been chosen to develop the model. However, the Dynamic Analysis and Design System (DADS), a multibody dynamics code, was selected to be used because DADS has a significant advantage over a standard purpose finite-element code in the areas of motion visualization, active control interfaces, and hydraulic system modeling. For the BRR model, the second generation version of the Comprehensive Analytical Model of Rotorcraft Aerodynamics and Dynamics (CAMRAD-II) has been chosen. Each of these analyses offers strengths in their respective areas that could not have been matched were a model of the complete system developed in a single analysis. This section presents an overview of the model formulations in each analysis. The development of the impedance matrices using results from these models and the coupling analysis is detailed in section 5. Appendixes B and C provide the reader with detailed program inputs.

4.1. DADS Model of ARES-II

DADS (refs. 9 and 10) is a time-marching computer analysis that simulates physical systems by numerically integrating a set of differential algebraic equations assembled by the program according to geometry, mass, stiffness, damping, joint, and external load information provided by the user. The results of the numerical integration are supplied as time histories of body positions and system loads. Although the program is primarily a multibody dynamics analysis utilizing rigid-body components connected with joints, flexibility may be included at the joints and beam elements or component mode synthesis may be used to model elastic structures. For the ARES-II, a model consisting of rigid bodies, flexible joints, and a beam element has been developed. For this model, component mass and inertia characteristics have been defined by using the Pro/ENGINEER solid-modeling, computer-aided-design software. Component stiffness and damping characteristics have been defined with known experimentally determined values and estimates obtained from simple analytical models. The construction of the DADS model of the ARES-II is discussed from the ground up in section 4.1.1. Figures 3.2 through 3.6 are useful to the reader in visualizing the model developed. Section 4.1.2 details the analysis necessary to determine the time-varying actuator lengths for control of the ARES-II motion platform.

4.1.1. ARES-II Model Construction

The ARES-II stand is shown in figure 4.1 modeled with two rigid bodies (the base and yoke) and one elastic beam (the post). For wind tunnel testing, the stand is constrained to the floor with elastomeric pads placed at each of the four corners of the stand baseplate. These pads permit pitch, roll, and normal displacements of the stand but restrain axial, side, and yaw displacements. The pads are modeled in DADS by four spring elements with damping and constraints to eliminate the axial, side, and yaw degrees of freedom of the stand.

The ARES-II longeron is modeled as a rigid body. A revolute joint is placed between the longeron and the stand yoke to control rotor pylon pitch. The linear screw-jack actuator placed between the stand and the longeron to control shaft angles is not modeled; instead a rotational driver constraint is placed at the location of the shaft angle revolute joint to control relative pitch motion between the stand and longeron.

All brackets and fittings for the attachment of the Stewart platform actuators to the longeron are modeled as rigid bodies and are rigidly attached to the longeron. The connections between the actuators and the brackets are modeled as universal joints. These joints are oriented such that the rotational degree of freedom about the longitudinal axis of the actuator is eliminated. Thus, the actuators do not spin but still have the necessary freedom of motion to actuate the pylon components. The connection of the piston rod portion of the actuators to the actuator bodies is modeled by translational joints. Control elements are also modeled to provide means to drive each actuator according to a specified schedule. The connection between the actuator rods and the Stewart platform baseplate is modeled with spherical joints.

The ARES-II fixed-system balance is modeled as two rigid bodies (top and bottom plates) connected by a six-degree-of-freedom elastic joint with damping. The bottom plate of the balance is rigidly attached to the baseplate of the Stewart platform. A large rigid body consisting of the main-shaft housing, the intermediate-shaft housing, and the drive motor is rigidly mounted to the top of the fixed-system balance. The main-rotor shaft and sheave, intermediate shaft and upper and lower sheaves, and the drive motor sheave are all modeled as rigid bodies with

17
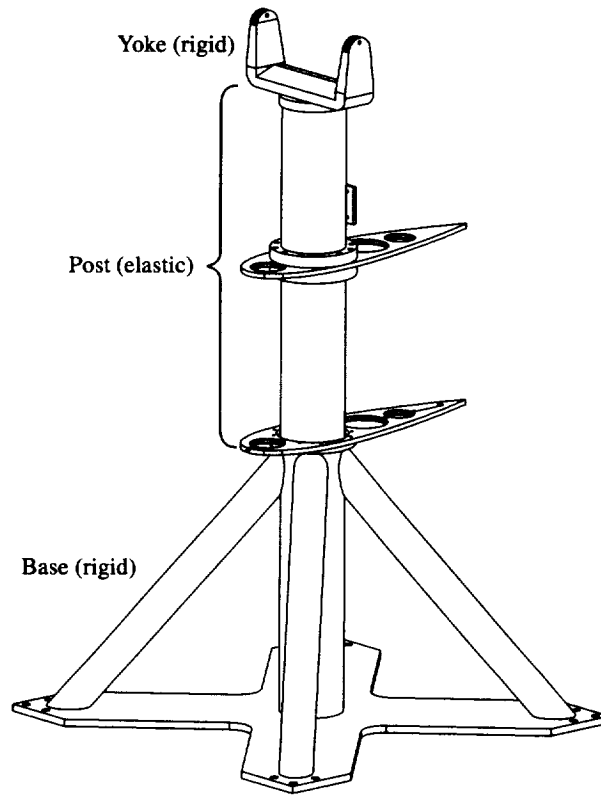
Figure 4.1. ARES-II stand.

rotational degrees of freedom. The main shaft is connected to the main-shaft housing, the intermediate shaft to the intermediate-shaft housing, and the drive-motor sheave to the drive motor through revolute joints. Constraint equations are used to model the proper drive reduction ratios between the drive motor sheave and the upper sheave on the intermediate shaft, and between the lower sheave on the intermediate shaft and the main sheave.

The mass of the swashplate, pitch links, and swashplate actuators was chosen to be included in the DADS model of the ARES-II. Therefore, these components are massless in the CAMRAD-II rotor system model. Their mass is included in that of the main-shaft housing. The interface joint for the swashplate, then, is included in the rigid-body model of the main-shaft housing.

The rotating balance, like the fixed-system balance, is modeled as two rigid bodies connected by a six-degree-of-freedom elastic joint with damping. The bottom plate of the rotating balance is rigidly attached to the top of the main shaft. The mast is modeled as a rigid body and rigidly attached to the top plate of the rotating balance. The interface joint for the rotor hub is included in the rigid-body model of the mast.

4.1.2. Actuator Motion Analysis

A means is necessary to control the ARES-II Stewart platform actuators so that prescribed rotor pylon motions may be imposed. To do so one must assume a center of motion for the rotor pylon, or "simulated center of gravity." The equations may then be generated to develop schedules of actuator lengths as a function of the desired simulated c.g. motions. To simplify the analysis, a rigid structure is assumed so that dynamic response does not interfere with the desired motions.

To begin the analysis, numbering the actuators as shown in figure 4.2 is useful. Two coordinate systems are necessary. One is called the "B-frame" (fig. 4.3), a body-fixed coordinate system on the fixed-system balance with

18
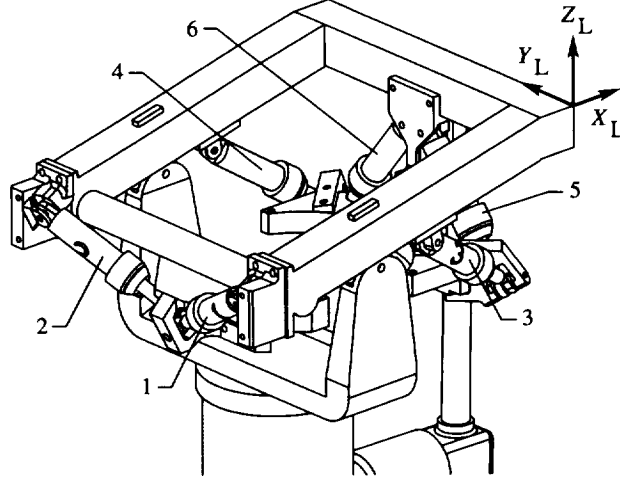
Figure 4.2. ARES-II actuator numbering.

its origin at the balance center. The second is called the "L -frame" (fig. 4.2) and is fixed to the longeron with the same orientation as the B-frame when the balance is in the nominal centered position.

A set of vectors may be defined from the balance center to the joints between the Stewart platform actuators and the baseplate. These vectors are defined as r_1 through r_6 for actuators 1 through 6 and are referenced to the balance coordinate frame (fig. 4.3). For the ARES-II configuration these vectors are

$$\left.\begin{array}{l} \mathbf{r}_1 = -7.206\mathbf{i}_B \qquad\qquad\; - 2.237\mathbf{k}_B \\[4pt] \mathbf{r}_2 = -6.821\mathbf{i}_B \qquad\qquad\; - 2.030\mathbf{k}_B \\[4pt] \mathbf{r}_3 = -7.348\mathbf{i}_B - 5.724\mathbf{j}_B - 2.629\mathbf{k}_B \\[4pt] \mathbf{r}_4 = -7.348\mathbf{i}_B + 5.724\mathbf{j}_B - 2.629\mathbf{k}_B \\[4pt] \mathbf{r}_5 = -7.113\mathbf{i}_B - 5.450\mathbf{j}_B - 2.862\mathbf{k}_B \\[4pt] \mathbf{r}_6 = -7.113\mathbf{i}_B + 5.450\mathbf{j}_B - 2.862\mathbf{k}_B \end{array}\right\} \qquad (4.1)$$

where the dimensions are in inches. Another vector is defined from the balance center to the arbitrarily selected simulated c.g. (fig. 4.3). This vector is defined as

$$\mathbf{r}_g = r_{g_x}\mathbf{i}_B + r_{g_y}\mathbf{j}_B + r_{g_z}\mathbf{k}_B \qquad (4.2)$$

Therefore, six vectors from the simulated c.g. to the Stewart platform baseplate joints may be generated with

$$\mathbf{r}_{ga} = -\mathbf{r}_g + \mathbf{r}_a \qquad (4.3)$$

where the subscript a denotes the referenced actuator (e.g., $\mathbf{r}_{g1}$ is the vector from the simulated c.g. to the baseplate joint for actuator 1).

Assume now a desired translational displacement vector for the simulated c.g. with respect to the longeron coordinate system L as follows:

$$\mathbf{d}_g = d_{g_x}\mathbf{i}_L + d_{g_y}\mathbf{j}_L + d_{g_z}\mathbf{k}_L \qquad (4.4)$$

19
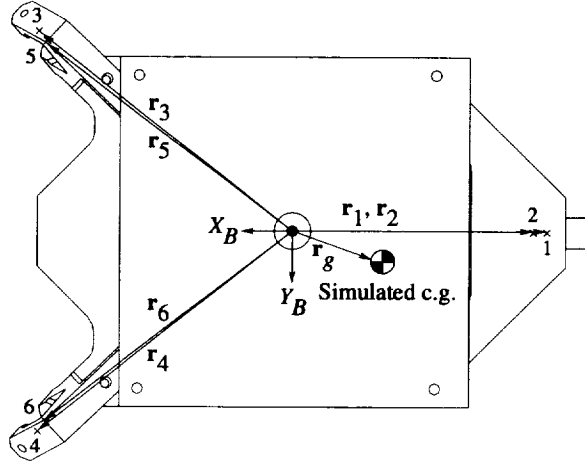
(a) Top view.
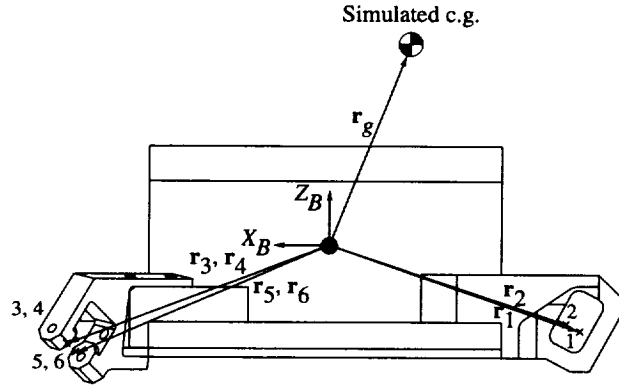
(b) Side view.

Figure 4.3. Vectors for motion analysis. Views are of fixed-system balance mounted on Stewart platform baseplate.

To obtain the desired translation of the simulated c.g., each Stewart platform baseplate joint must translate an equal distance. Therefore, the actuated displacement of each joint for simulated c.g. translation is

$$\mathbf{d}_a = \mathbf{d}_g \tag{4.5}$$

To calculate joint displacement for rotations about the simulated c.g., however, requires the application of a rotation of each vector $\mathbf{r}_{ga}$ and then a translation of $-\mathbf{r}_{ga}$. To illustrate, assume a single-axis rotation θ_{x_g} through the simulated c.g. where the rotation is with respect to the longeron coordinate system L. The matrix equation for the joint displacement is

$$
\begin{Bmatrix} d_{a_x} \\ d_{a_y} \\ d_{a_z} \end{Bmatrix} =
\begin{bmatrix}
1 & 0 & 0 \\
0 & \cos\theta_{x_g} & -\sin\theta_{x_g} \\
0 & \sin\theta_{x_g} & \cos\theta_{x_g}
\end{bmatrix}
\begin{Bmatrix} r_{ga_x} \\ r_{ga_y} \\ r_{ga_z} \end{Bmatrix} -
\begin{Bmatrix} r_{ga_x} \\ r_{ga_y} \\ r_{ga_z} \end{Bmatrix}
\tag{4.6}
$$

The general form of equation (4.6) is

$$\{\mathbf{d}_a\} = [\mathbf{R}_{x_g}]\{\mathbf{r}_{ga}\} - \{\mathbf{r}_{ga}\} \tag{4.7}$$

20

Therefore, in a mathematical sense, all rotations must be completed before the translation occurs. If a rotation sequence of y-x-z (pitch-roll-yaw) is assumed, the complete rotation matrix may be written as

$$
[\mathbf{R}_g] =
\begin{bmatrix}
\cos\theta_y \cos\theta_z & & \sin\theta_y \cos\theta_z \\
-\sin\theta_x \sin\theta_y \sin\theta_z & -\cos\theta_x \sin\theta_z & +\sin\theta_x \cos\theta_y \sin\theta_z \\
& & \\
\cos\theta_y \sin\theta_z & & \sin\theta_y \sin\theta_z \\
+\sin\theta_x \sin\theta_y \cos\theta_z & \cos\theta_x \cos\theta_z & -\sin\theta_x \cos\theta_y \cos\theta_z \\
& & \\
-\cos\theta_x \sin\theta_y & \sin\theta_x & \cos\theta_x \cos\theta_y
\end{bmatrix}
\tag{4.8}
$$

Combining the results for actuator displacement due to translation and rotation of the simulated c.g. yields

$$
\{\mathbf{d}_a\} = [\mathbf{I}]\{\mathbf{d}_g\} + \left[[\mathbf{R}_g] - [\mathbf{I}]\right]\{\mathbf{r}_{ga}\}
\tag{4.9}
$$

Position vectors may be developed for each actuator when the Stewart platform is placed in its nominal or reference position. The position vectors are denoted $\mathbf{l}_a$ and represent the relative position of the Stewart platform joint of the actuator with respect to the actuator joint at the longeron. These vectors are

$$
\left.
\begin{aligned}
\mathbf{l}_1 &= 1.869\mathbf{i}_L + 6.580\mathbf{j}_L - 3.987\mathbf{k}_L \\
\mathbf{l}_2 &= 2.254\mathbf{i}_L - 6.580\mathbf{j}_L - 3.780\mathbf{k}_L \\
\mathbf{l}_3 &= 6.346\mathbf{i}_L + 1.376\mathbf{j}_L - 4.384\mathbf{k}_L \\
\mathbf{l}_4 &= 6.346\mathbf{i}_L - 1.376\mathbf{j}_L - 4.384\mathbf{k}_L \\
\mathbf{l}_5 &= \qquad\quad - 4.825\mathbf{j}_L - 6.062\mathbf{k}_L \\
\mathbf{l}_6 &= \qquad\quad 4.825\mathbf{j}_L - 6.062\mathbf{k}_L
\end{aligned}
\right\}
\tag{4.10}
$$

Then, the actuator lengths may be determined by

$$
l_a = \left|\mathbf{l}_a + \mathbf{d}_a\right|
\tag{4.11}
$$

For control of the DADS model Stewart platform actuators, equations (4.9) through (4.11) are used to calculate schedules for each actuator length. These results are applied as time-varying distance constraints between the joints at each end of the actuators.

4.1.3. DADS Model Results

Because DADS is a time-marching analysis simulating the physical system through numerical integration, the output is a set of time histories. Thus, no eigenanalysis is available to determine system frequencies and modes. Instead, it is typical to "excite" the DADS model and measure the response in a manner similar to physical-model shake testing. Alternatively, a displace-and-release (or "pluck") excitation may be used to identify the basic free-response characteristics of the model.

The damped natural frequencies of the DADS model of the ARES-II have been identified by displacing the hub interface joint, then releasing and allowing free-vibration response. Fast Fourier Transforms of the loads measured at the fixed-system balance during the free response are shown in figure 4.4. For the axial and pitch response, the ARES-II was excited by plucking the hub interface joint axially. Side and roll responses were generated by plucking the hub joint to the side; the normal response, by plucking the hub joint vertically; and the yaw
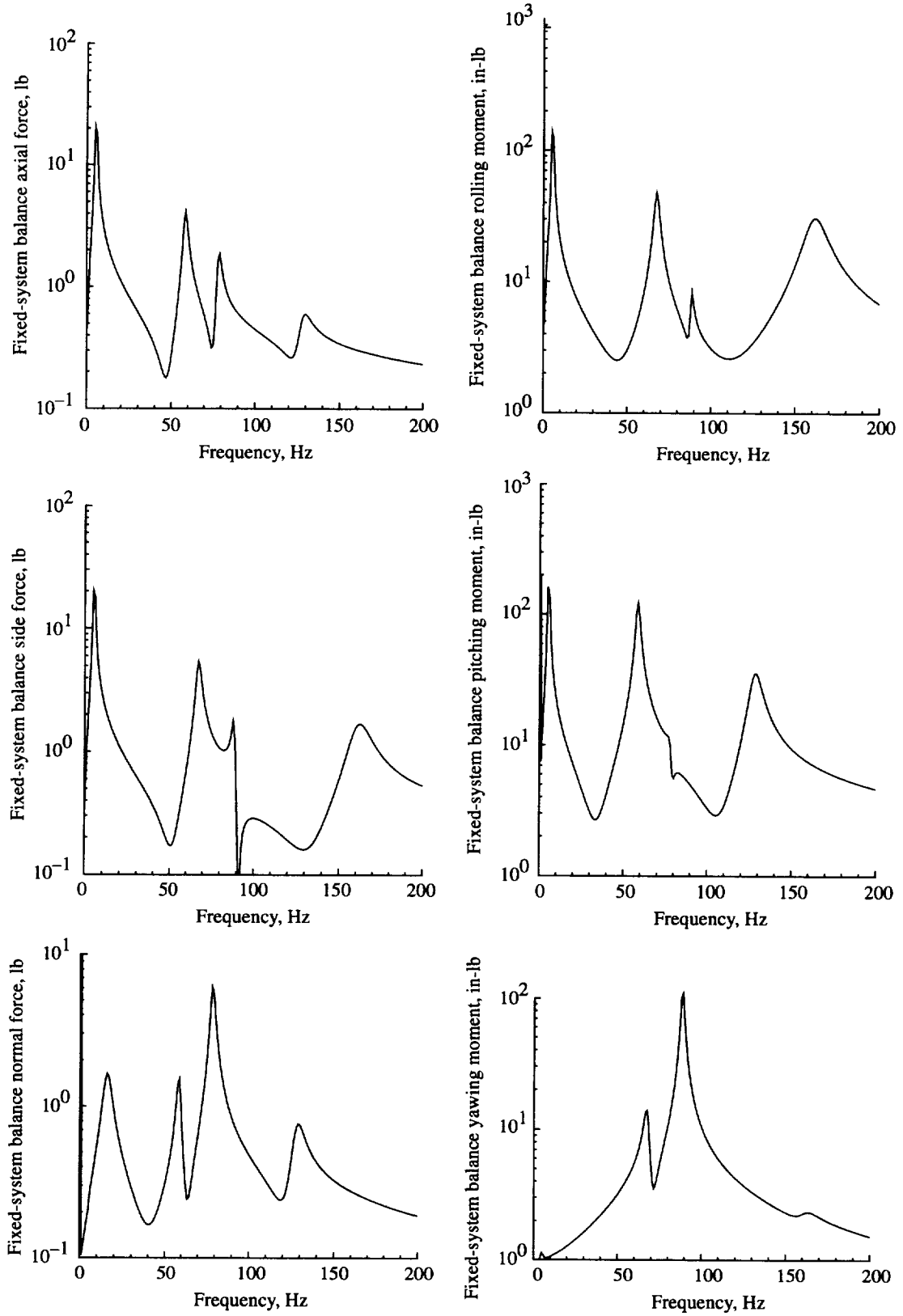
Figure 4.4. FFTs of ARES-II free-response measured at fixed-system balance.

response, by plucking with a yawing moment at the hub joint. The FFTs in figure 4.4 have been used to identify the damped natural frequencies and to estimate the modal characteristics of the ARES-II system; these are presented in table 4.1.

Significant modal coupling exists for the ARES-II elastic modes because the c.g. of the rotor pylon is above and forward of the fixed-system balance flexibility. Therefore, axial motions of the ARES-II rotor pylon generate pitch response. The associated vertical acceleration of the c.g. due to pitching then generates normal (vertical) response. Similarly, roll and yaw motions couple with side motions of the rotor pylon. The information presented in table 4.1 are estimates based on the results of figure 4.4 and a physical understanding of the ARES-II. No experimental data were available that defined the stiffness and damping of the ARES-II elastomeric stand mounting pads. Therefore, a trial-and-error approach was used to define these properties to obtain rigid-body pitch and roll frequencies of 5 Hz with 8 percent critical damping. The elastic modes are listed with the component estimated to be the most dominant first and the least dominant last. For example, the first elastic mode at 58 Hz is considered primarily an axial mode with pitch and normal coupled response. To obtain a more accurate assessment of the ARES-II frequencies and modal identification would require the development of a finite-element model and an eigenanalysis.

4.2. CAMRAD-II Model of the BRR

CAMRAD-II is a state-of-the-art rotorcraft analysis that can model a wide range of rotorcraft configurations. For this study, CAMRAD-II was used to develop a complete aerodynamic and dynamic model of the BRR. The kinematic effects of the swashplate control system were included in the model. However, because the weight of the swashplate and control system was included in the DADS model, these components were considered massless in the CAMRAD-II model.

The development of a detailed CAMRAD-II model consists of two stages. The first stage is the development of the "rotorcraft shell" model. The CAMRAD-II rotorcraft shell allows the user to input a general set of rotorcraft information to construct models of most common rotor system configurations. The shell effectively eliminates much of the tedious work involved in generating a model because it constructs much of the detailed system model. The second stage is the development of the "core" model. The core model allows the user to supply detailed information regarding the system to be modeled; this permits the generation of configurations that cannot be fully constructed by the shell. The development of the core model is, however, more complicated and may easily require input data an order of magnitude more than that required by the shell.

4.2.1. BRR Shell Model

The rotor system model of the BRR was initially generated by using rotorcraft shell input. Because each blade is, in theory, identical, only one blade is modeled. Phasing routines internal to CAMRAD-II allow for the calculation of system response by using all four blades. The hub is modeled as a rigid body inboard of the flap and lead-lag hinges. A second rigid body is modeled between the hinges and the pitch bearing. A third rigid body extends

Table 4.1. Damped Natural Frequencies and Modes of ARES-II

Frequency, Hz	Mode
5	Rigid pitch
5	Rigid roll
17	Rigid normal
58	Elastic axial/pitch/normal
67	Elastic side/roll/yaw
79	Elastic normal/axial/pitch
90	Elastic yaw/side/roll
131	Elastic normal/pitch/axial
163	Elastic side/roll

from the pitch bearing to the outboard end of the rotor blade cuff. The blade is modeled by using 5 finite-element beams with 19 aerodynamic panels distributed radially. The kinematic effects of the control system are included by providing detailed placement of the pitch horn and pitch link attachment points.

4.2.2. BRR Core Model

Enhancement of the model generated by the rotorcraft shell is necessary to permit the implementation of prescribed hub motions. These hub motions, as shown in section 5.3.2, are necessary to develop the rotor system impedance matrices for the coupling analysis. Additionally, the hub mass and inertia characteristics calculated by the rotorcraft shell are generally inaccurate. Therefore, the core model was used to prescribe the proper hub mass and inertia.

Figure 4.5 shows a schematic of the model developed. The boxes in the figure represent components available for use in CAMRAD-II models. The component type is listed at the bottom of each box (e.g., rigid body, Fourier series) and the component name, if any, is listed at the top of each box. The circles in figure 4.5 represent joints between structural components of the CAMRAD-II model. The value inside the circle specifies the number of motion degrees of freedom that the joint permits. Labels next to the joints identify the joint function.

The CAMRAD-II model that was generated represents the ARES-II/BRR in configuration only. The stand and pylon components shown in figure 4.5 are dimensioned to represent the ARES-II but have no stiffness or mass properties. Thus, the ARES-II portion of the CAMRAD-II model is strictly a kinematic, but not dynamic, representation of the testbed. It is modeled only to impose the BRR hub motions required for development of the rotor impedance matrix described in section 5.3.2.3. The BRR model, however, is a complete dynamic and aerodynamic

Figure 4.5. Schematic of CAMRAD-II model of BRR.

24

representation of the rotor system. As shown in figure 4.5, the model consists of a rigid body component named "stand" which is rigidly attached to the ground. To permit prescribed hub motion, a rigid body component named "pylon" is installed at the top of the stand component with a six-degree-of-freedom (6-dof) joint. All rotor system components as generated by the rotorcraft shell in section 4.2.1 are attached to the pylon component. The dashed box at the left of the figure shows the control input portion of the model. Harmonic input amplitudes may be prescribed for each of the six possible joint motions. These amplitudes are input to a Fourier series component that generates a set of six azimuthally varying signals by using the equation

$$T(\psi) = \sum_{n=0}^{8} (H_{n_c} \cos n\psi + H_{n_s} \sin n\psi)$$

where H_{n_c} and H_{n_s} are the harmonic inputs, $T(\psi)$ is the output signal, and only the mean and first eight harmonics of motion are considered. The six output signals are combined into a single vector by a "summer" component that inputs the signals to the 6-dof joint between the stand and pylon components. Actuator features internal to the 6-dof joint process the vector and generate linear and angular motions of the pylon and, thus, the hub.

Output components are included in the model to display hub motion, hub loads at the hub interface joint, and swashplate loads at the swashplate interface joint. These output components resolve loads in the fixed-system frame for the mean and 4P and 8P harmonic forces and moments. This procedure offered the advantage of having to process only 4P and 8P loads in the coupling procedure instead of processing 3P, 4P, 5P, 7P, 8P, and 9P loads as would be required if the loads were resolved in the rotating frame. Thus, an effective revolute joint is placed between the rotor hub and the mast of the ARES-II model, which although not representative of the configuration of the physical model, is effective in producing efficient results due to the reduction in excitation frequencies considered.

5. Dynamic Analysis Using Impedance Matching

Dynamic analysis of systems through impedance-matching approaches can be useful. However, as with any engineering analysis approach, one must be careful to consider the limitations and assumptions of the application. For impedance matching, two such limitations stand out. First, impedance matching is a frequency-dependent technique. Therefore, impedance characteristics must be defined for each component to be coupled at each frequency of interest. Second, impedance-matching approaches are developed with linear theory. Therefore, only systems that are linear by nature or whose characteristics are linear in a region of interest are suitable for analysis by impedance matching. For rotorcraft application, in which one may be interested in coupling a rotor system to a fuselage model, the first of these limitations is generally not of considerable concern. Because the rotor system is the primary contributor to helicopter vibratory loads and the rotor-generated forcing functions applied to the fuselage are harmonic in nature, only a few such frequencies of interest exist in a rotorcraft application. Typically, rotor dynamics applications are restricted to those frequencies below 9P for a four-bladed rotor system. Therefore, for the Basic Research Rotor, which passes to the fixed system only steady loads and loads at 4P and 8P, only two frequencies exist for which impedance characteristics must be developed (i.e., 4P and 8P). The second limitation of impedance matching, however, is of greater concern in rotorcraft analysis. Although fixed-systems structures (i.e., fuselages, testbeds, and whirl stands) are typically modeled by using linear theory, the rotor system is inherently nonlinear. This nonlinearity is of particular concern at low flight speeds ($\mu \leq 0.15$) where blade tip vortices impinge on the following blades, and high flight speeds ($\mu \geq 0.30$) where rotor blade stall produces nonlinear response. Therefore, the application of impedance matching to couple a rotor system to a fuselage or test stand requires that the rotor impedance model be developed about a steady-state flight condition of interest. Additionally, the results must be carefully checked to ensure that rotor system response remains within a linear range.

25

The term "impedance" often has different meanings which depend upon the application used. For this study, impedance is defined as the force-displacement relationship that exists for a system degree of freedom when an interface joint location is being driven by a prescribed oscillatory motion at a particular frequency of interest. Also of interest is system "mobility," which is defined as the displacement-force relationship that exists for a system degree of freedom when an interface joint location is being subjected to a prescribed oscillatory force at a particular frequency of interest. Both impedance and mobility, as shown in section 5.1, may be represented by square matrices. Further, system mobility is shown to be the inverse of system impedance. Therefore, the term "impedance matching" is appropriate for system coupling using either impedance matrices, mobility matrices, or both.

Section 4 discussed the DADS model of the ARES-II and the CAMRAD-II model of the BRR. This section discusses how these models are used to develop impedance representations of each system and details the impedance-matching approach developed to couple the two systems. For this study, two interface joints are used: one at the joint between the hub and mast of the main-rotor shaft and the other at the joint between the swashplate and the main-rotor shaft.

5.1. Sample Coupled Model

A simple model is used to demonstrate the principles of the coupling analysis. This model is shown in figure 5.1. Two systems are shown which are to be coupled at the interface joint I. System A consists of three one-degree-of-freedom (1-dof) masses. Spring k_1 and damper c_1 are placed between the ground and m_1; an actuator is placed between masses m_1 and m_2; and another spring k_2 and damper c_2 are placed between masses m_2 and m_3. The interface joint for the system is placed on m_3. System B consists of one 1-dof mass with a spring k_3 and damper c_3. The interface joint for system B is placed at one end of the spring-damper so that the spring-damper lies between the interface joint and the mass. System A is a 2-dof system due to the constraint that exists because of the actuator. This constraint equation may be expressed as

$$x_2 = x_1 + l_A \tag{5.1}$$
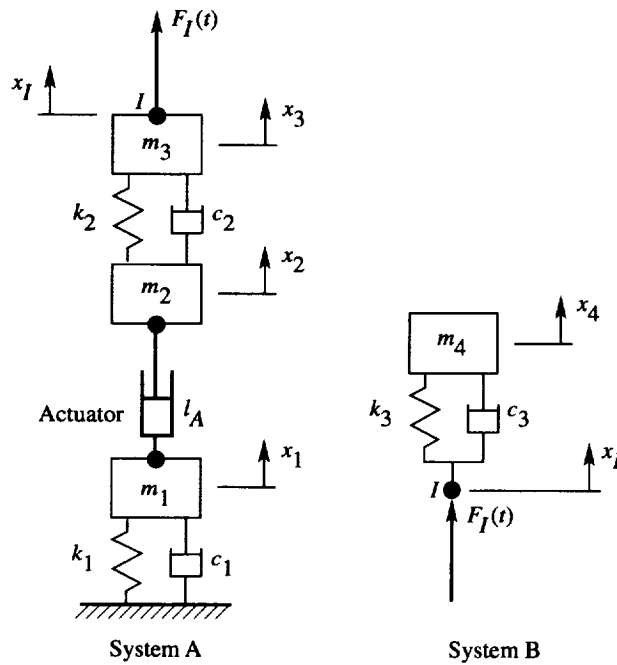
Figure 5.1. Sample model.

26

The remaining two generalized coordinates for system A include x_1 and x_3. The equations of motion for these two coordinates may be easily generated. They are

$$
\left.
\begin{aligned}
(m_1 + m_2)\ddot{x}_1 + m_2\ddot{l}_A + (c_1 + c_2)\dot{x}_1 - c_2(\dot{x}_3 - \dot{l}_A) + (k_1 + k_2)x_1 - k_2(x_3 - l_A) &= 0 \\
m_3\ddot{x}_3 + c_2(\dot{x}_3 - \dot{x}_1 - \dot{l}_A) + k_2(x_3 - x_1 - l_A) &= F_I(t)
\end{aligned}
\right\}
\tag{5.2}
$$

Because the actuator may be used to force system motion, the equations of motion are written as

$$
\left.
\begin{aligned}
(m_1 + m_2)\ddot{x}_1 + (c_1 + c_2)\dot{x}_1 - c_2\dot{x}_3 + (k_1 + k_2)x_1 - k_2x_3 &= -m_2\ddot{l}_A - c_2\dot{l}_A - k_2l_A \\
m_3\ddot{x}_3 + c_2(\dot{x}_3 - \dot{x}_1) + k_2(x_3 - x_1) &= F_I(t) + c_2\dot{l}_A + k_2l_A
\end{aligned}
\right\}
\tag{5.3}
$$

Now let

$$
\left.
\begin{aligned}
F_I(t) &= F_{I_c} \cos \Omega t + F_{I_s} \sin \Omega t \\
l_A(t) &= l_{A_c} \cos \Omega t + l_{A_s} \sin \Omega t
\end{aligned}
\right\}
\tag{5.4}
$$

where F_{I_c}, F_{I_s}, l_{A_c}, and l_{A_s} are constant and Ω is the frequency of the applied force or actuation. If steady-state responses are assumed in the form

$$
\left.
\begin{aligned}
x_1(t) &= x_{1_c} \cos \Omega t + x_{1_s} \sin \Omega t \\
x_3(t) &= x_{3_c} \cos \Omega t + x_{3_s} \sin \Omega t
\end{aligned}
\right\}
\tag{5.5}
$$

a matrix expression for the solution of the steady-state response may be written as

$$
\begin{bmatrix}
-\Omega^2(m_1 + m_2) + k_1 + k_2 & \Omega(c_1 + c_2) & -k_2 & -c_2\Omega \\
-\Omega(c_1 + c_2) & -\Omega^2(m_1 + m_2) + k_1 + k_2 & c_2\Omega & -k_2 \\
-k_2 & -\Omega c_2 & k_2 - \Omega^2 m_3 & \Omega c_2 \\
\Omega c_2 & -k_2 & -\Omega c_2 & k_2 - \Omega^2 m_3
\end{bmatrix}
\begin{Bmatrix}
x_{1_c} \\
x_{1_s} \\
x_{3_c} \\
x_{3_s}
\end{Bmatrix}
$$

$$
=
\begin{Bmatrix}
\Omega^2 m_2 l_{A_c} - c_2\Omega l_{A_s} - k_2 l_{A_c} \\
\Omega^2 m_2 l_{A_s} + c_2\Omega l_{A_c} - k_2 l_{A_s} \\
F_{I_c} + k_2 l_{A_c} + c_2\Omega l_{A_s} \\
F_{I_s} - c_2\Omega l_{A_c} + k_2 l_{A_s}
\end{Bmatrix}
\tag{5.6}
$$

5.1.1. Mobility Matrix Development

A numerical example is used to illustrate the development of the sample model mobility matrices. Let $m_1 = m_2 = m_3 = 1.0$ slug, $k_1 = k_2 = 10.0$ lb/ft, and $c_1 = c_2 = 2.0$ lb-s/ft. To develop the mobility matrices for m_1 and m_3, the force input at the interface is set to a unit cosine force ($F_{I_c} = 1.0$, $F_{I_s} = 0.0$) and the actuator is held fixed ($l_{A_c} = l_{A_s} = 0.0$). For an excitation frequency of $\Omega = 2\pi$ rad/s, the vector x resulting from the solution of equation (5.6) is

$$\left\{ \begin{array}{c} x_{1_c} \\ x_{1_s} \\ x_{3_c} \\ x_{3_s} \end{array} \right\} = \left\{ \begin{array}{c} -0.001343 \\ -0.006917 \\ -0.025186 \\ 0.012510 \end{array} \right\} \tag{5.7}$$

Similarly, the result when a unit sine force ($F_{I_c} = 0.0$, $F_{I_s} = 1.0$) is applied and the actuator is held fixed ($l_{A_c} = l_{A_s} = 0.0$) is

$$\left\{ \begin{array}{c} x_{1_c} \\ x_{1_s} \\ x_{3_c} \\ x_{3_s} \end{array} \right\} = \left\{ \begin{array}{c} 0.006917 \\ -0.001343 \\ -0.012510 \\ -0.025186 \end{array} \right\} \tag{5.8}$$

With the results from equations (5.7) and (5.8), a mobility matrix may be generated for either m_1 or m_3. Because the interface joint is on m_3, it is necessary that the mobility matrix for this mass be developed. The development of the mobility matrix for m_1 is optional for the coupling analysis but is useful if complete system motion is desirable.

The general method for developing a mobility matrix is to place the cosine and sine components of the degree-of-freedom displacement due to a unit cosine forcing function at the interface joint in the first column of the mobility matrix. Likewise, the second column of the matrix is filled with the cosine and sine components of the degree-of-freedom displacement due to a unit sine forcing function at the interface joint. For m_3, then, the mobility matrix is

$$[A_3] = \begin{bmatrix} -0.025186 & -0.012510 \\ 0.012510 & -0.025186 \end{bmatrix} \tag{5.9}$$

Because the system is linear, the mobility matrix may be developed by using only the results from either the cosine force or the sine force. Throughout this work, a sine excitation has been used so that the mobility matrix for the mth degree of freedom may be generated by

$$[A_m] = \begin{bmatrix} x_{m_s} & x_{m_c} \\ -x_{m_c} & x_{m_s} \end{bmatrix} \tag{5.10}$$

Therefore, by using a mobility matrix, the motion of a degree of freedom may be determined if the applied force at the interface is known; that is,

$$\left\{ \begin{array}{c} x_{m_c} \\ x_{m_s} \end{array} \right\} = [A_m] \left\{ \begin{array}{c} F_{I_c} \\ F_{I_s} \end{array} \right\}$$

(5.11)

5.1.2. Motion Matrix Development

Besides generating the mobility matrix for the sample system A, the effect of actuator motion on system performance is necessary. These effects may be included as a matrix component as well. For this study, this matrix is called the "motion matrix" and will be denoted by $[B_m]$ for each degree of freedom m of interest. The motion matrix may be generated in a manner similar to the mobility matrix. With the numerical example, equation (5.6) is solved for an absence of force input ($F_{I_c} = 0.0$, $F_{I_s} = 0.0$) while either a unit cosine motion ($l_{A_c} = 1.0$, $l_{A_s} = 0.0$) or a unit sine motion ($l_{A_c} = 0.0$, $l_{A_s} = 1.0$) is effected by the actuator. The motion matrix is assembled in the same manner as the mobility matrix. For the sample system, the resulting motion matrix for m_3 is

$$[B_3] = \begin{bmatrix} -0.047323 & -0.220797 \\ 0.220797 & -0.047323 \end{bmatrix}$$

(5.12)

Note that for this application an "ideal" actuator is assumed so that pure cosine and sine motions are provided by the actuator.

Now, by using superposition, a matrix equation can be developed which defines system motion due to the application of an external force at the interface joint and due to actuation. This equation is

$$\left\{ \begin{array}{c} x_{I_c} \\ x_{I_s} \end{array} \right\} = [A_3] \left\{ \begin{array}{c} F_{I_c} \\ F_{I_s} \end{array} \right\} + [B_3] \left\{ \begin{array}{c} l_{A_c} \\ l_{A_s} \end{array} \right\}$$

(5.13)

5.1.3. Impedance Matrix Development

Now an impedance matrix is developed for sample system B. The equation of motion for this simple system is

$$m_4 \ddot{x}_4 + c_3 \dot{x}_4 + k_3 x_4 = c_3 \dot{x}_I + k_3 x_I$$

(5.14)

If

$$\left. \begin{array}{l} x_I = x_{I_c} \cos \Omega t + x_{I_s} \sin \Omega t \\ x_4 = x_{4_c} \cos \Omega t + x_{4_s} \sin \Omega t \end{array} \right\}$$

(5.15)

a matrix equation may be written for the system as

$$\begin{bmatrix} k_3 - \Omega^2 m_4 & \Omega c_3 \\ -\Omega c_3 & k_3 - \Omega^2 m_3 \end{bmatrix} \left\{ \begin{array}{c} x_{4_c} \\ x_{4_s} \end{array} \right\} = \begin{bmatrix} k_3 & \Omega c_3 \\ -\Omega c_3 & k_3 \end{bmatrix} \left\{ \begin{array}{c} x_{I_c} \\ x_{I_s} \end{array} \right\}$$

(5.16)

For this example, let $k_4 = 10.0$ lb/ft, $c_3 = 2.0$ lb-s/ft, $m_4 = 1.0$ slug, and $\Omega = 2\pi$ rad/s. Prescribed unit cosine and unit sine motions of the interface joint are applied individually and equation (5.16) solved for $\{x_4\}$. For the prescribed unit cosine ($x_{I_c} = 1.0$, $x_{I_s} = 0.0$) motion,

$$\left\{ \begin{array}{c} x_{4_c} \\ x_{4_s} \end{array} \right\} = \left\{ \begin{array}{c} -0.133286 \\ 0.483109 \end{array} \right\} \tag{5.17}$$

For the prescribed unit sine ($x_{I_c} = 0.0$, $x_{I_s} = 1.0$) motion,

$$\left\{ \begin{array}{c} x_{4_c} \\ x_{4_s} \end{array} \right\} = \left\{ \begin{array}{c} -0.483109 \\ -0.133286 \end{array} \right\} \tag{5.18}$$

However, to complete the coupling analysis, the force at the joint F_I is necessary, not the motion of m_4. This force is described by

$$F_I(t) = k_3(x_4 - x_I) + c_3(\dot{x}_4 - \dot{x}_I) \tag{5.19}$$

or

$$\left. \begin{array}{l} F_{I_c} = k_3(x_{4_c} - x_{I_c}) + \Omega c_3(x_{4_s} - x_{I_s}) \\[2mm] F_{I_s} = k_3(x_{4_s} - x_{I_s}) + \Omega c_3(-x_{4_c} + x_{I_c}) \end{array} \right\} \tag{5.20}$$

The impedance matrix [C] may then be developed in a manner identical to the mobility and motion matrices described previously. The impedance matrix is thus determined from the results of equations (5.17), (5.18), and (5.20) as

$$[\mathbf{C}] = \begin{bmatrix} -5.2619 & -19.0724 \\ 19.0724 & -5.2619 \end{bmatrix} \tag{5.21}$$

Finally, the following force equation for the interface joint may be written by using the impedance matrix:

$$\left\{ \begin{array}{c} F_{I_c} \\ F_{I_s} \end{array} \right\} = [\mathbf{C}] \left\{ \begin{array}{c} x_{I_c} \\ x_{I_s} \end{array} \right\} \tag{5.22}$$

5.1.4. Coupled Analysis

To develop the analysis to couple systems A and B of figure 5.1, some compatibility condition must exist at the interface joint I of each system. For this analysis, the compatibility conditions include displacement and force at the interface joint $\{x_I\}$ and $\{F_I\}$, respectively. Substituting equation (5.22) into equation (5.13) to ensure that force compatibility exists at the interface joint and solving for $\{x_I\}$ to ensure that displacement compatibility exists as well give

$$\left\{ \begin{array}{c} x_{I_c} \\ x_{I_s} \end{array} \right\} = \left[[\mathbf{I}] - [\mathbf{A}_3][\mathbf{C}] \right]^{-1} [\mathbf{B}_3] \left\{ \begin{array}{c} I_{A_c} \\ I_{A_s} \end{array} \right\} \tag{5.23}$$

30

Substituting equation (5.23) into equation (5.22) yields the following equation for the interface force:

$$\left\{ \begin{array}{c} F_{I_c} \\ F_{I_s} \end{array} \right\} = [C]\Big[[I] - [A_3][C]\Big]^{-1}[B_3]\left\{ \begin{array}{c} l_{A_c} \\ l_{A_s} \end{array} \right\} \tag{5.24}$$

Equations (5.23) and (5.24) represent the interface displacement and force for the completely assembled and coupled system. The results are valid for the frequency for which the mobility matrix $[A_3]$, the motion matrix $[B_3]$, and the impedance matrix $[C]$ were developed. For the coupled sample system at an actuation frequency Ω of 2π rad/s, the results for $l_{A_c} = 1.0$, $l_{A_s} = 0.0$ are

$$\left. \begin{array}{c} \left\{ \begin{array}{c} x_{I_c} \\ x_{I_s} \end{array} \right\} = \left\{ \begin{array}{c} 0.044853 \\ 0.177474 \end{array} \right\} \\ \\ \left\{ \begin{array}{c} F_{I_c} \\ F_{I_s} \end{array} \right\} = \left\{ \begin{array}{c} -3.6209 \\ -0.0784 \end{array} \right\} \end{array} \right\} \tag{5.25}$$

Note also that $x_3 = x_I$ so that the motion of m_3 has been obtained as well. Other system motion results may be obtained by developing the following mobility matrix for m_1:

$$[A_1] = \begin{bmatrix} -0.001343 & 0.006917 \\ -0.006917 & -0.001343 \end{bmatrix} \tag{5.26}$$

and by using equations (5.1), (5.11), and (5.16). The results are

$$\left\{ \begin{array}{c} x_{I_c} \\ x_{I_s} \end{array} \right\} = [A_1]\left\{ \begin{array}{c} F_{I_c} \\ F_{I_s} \end{array} \right\} = \left\{ \begin{array}{c} 0.004321 \\ 0.025151 \end{array} \right\} \tag{5.27}$$

$$\left\{ \begin{array}{c} x_{2_c} \\ x_{2_s} \end{array} \right\} = \left\{ \begin{array}{c} x_{1_c} \\ x_{1_s} \end{array} \right\} + \left\{ \begin{array}{c} l_{A_c} \\ l_{A_s} \end{array} \right\} = \left\{ \begin{array}{c} 1.004321 \\ 0.025151 \end{array} \right\} \tag{5.28}$$

$$\left\{ \begin{array}{c} x_{4_c} \\ x_{4_s} \end{array} \right\} = \begin{bmatrix} k_3 - \Omega^2 m_4 & \Omega c_3 \\ -\Omega c_3 & k_3 - \Omega^2 m_4 \end{bmatrix}^{-1} \begin{bmatrix} k_3 & \Omega c_3 \\ -\Omega c_3 & k_3 \end{bmatrix}\left\{ \begin{array}{c} x_{I_c} \\ x_{I_s} \end{array} \right\}$$

$$= \left\{ \begin{array}{c} -0.091718 \\ -0.001986 \end{array} \right\} \tag{5.29}$$

31

5.2. Comments and Observations Regarding Impedance Matching

Several characteristics of the impedance-matching method developed in section 5.1 are noteworthy. First, the method as presented is only useful for dynamic systems undergoing steady-state forced response at discrete frequencies. Second, a 1-dof response of a single location on a system is representable by a 2×2 matrix for each frequency of interest. Therefore, for complete 6-dof response of an interface joint or other location, a 12×12 matrix is necessary. Multiple 12×12 matrices are necessary for multiple excitation frequencies. Third, all response matrices may be developed with similar techniques.

It is evident as well that a relationship exists between a mobility and an impedance matrix. To verify this relationship, one need only recall variations of equations (5.11) and (5.22) such as

$$\left. \begin{array}{l} \{x\} = [A]\{F\} \\ \{F\} = [C]\{x\} \end{array} \right\}$$

In practice, the only reason to use both a mobility matrix and an impedance matrix is to identify the manner in which the response matrices were developed. A mobility matrix is defined by applying a forcing function and examining the motion response. The impedance matrix is developed by applying a motion and examining the force response.

5.3. Application of Impedance Matching to ARES-II and Basic Research Rotor

Most techniques developed in section 5.1 are directly applicable to the analysis of the ARES-II testbed and the BRR. However, some modifications are required to model the rotor system properly. The following sections detail the procedures necessary to couple the two systems.

5.3.1. ARES-II Impedance Modeling

Two load paths exist for the transfer of loads between the ARES-II and the BRR. These paths include the rotor hub connection to the mast and the swashplate connection to the main-rotor shaft and main-shaft housing. The largest load transfers occur at the rotor hub connection. The swashplate, however, restrains the pitch links and thus carries the loads generated by blade pitching moments and control. As shown, the swashplate loads may, at times, represent a significant portion of the harmonic load transfer from the rotating system to the fixed system. Therefore, to neglect these loads would introduce an uncertainty as to the validity of the model. Furthermore, because one goal of this study is to define the loads sensed by both the rotating and the nonrotating balances, including the swashplate load path is necessary because the rotating balance is unable to measure these loads. Note that including the swashplate loads in the analysis represents a departure from the standard practice evident in the literature where, almost universally, the swashplate loads are neglected.

The DADS model of the ARES-II described in section 4.1 is used to develop the necessary impedance characteristics of the hub and swashplate interface joints. Within the DADS model, the two interface joints at the hub and swashplate are included as points of interest to ease load application and to identify system response. These two interface joints and their orientation are shown in figure 5.2. The main-rotor shaft assembly in the DADS model can rotate. However, for this study resolving all forces and moments in the nonrotating system is convenient because the number of frequencies required for analysis is reduced to two: 4 per rev and 8 per rev. Therefore, the main-rotor shaft is held fixed, and a rotational joint is assumed at the interface between the mast and the rotor hub. As a result, none of the rotational inertia of the main-rotor shaft assembly or drive system is included in the model. These effects, however, are considered minimal when compared with the rotational inertia of the rotor system. Additionally, because no drive system flexibility is modeled, including the drive system inertias would be relatively meaningless.

5.3.1.1. Harmonic analysis.
In contrast with the dynamic analysis of the ARES-II testbed presented in section 4.1.3 in which all frequencies were excited with an initial displacement, the development of an impedance-matching analysis requires examination of the system steady-state response due to harmonic excitation. Therefore,
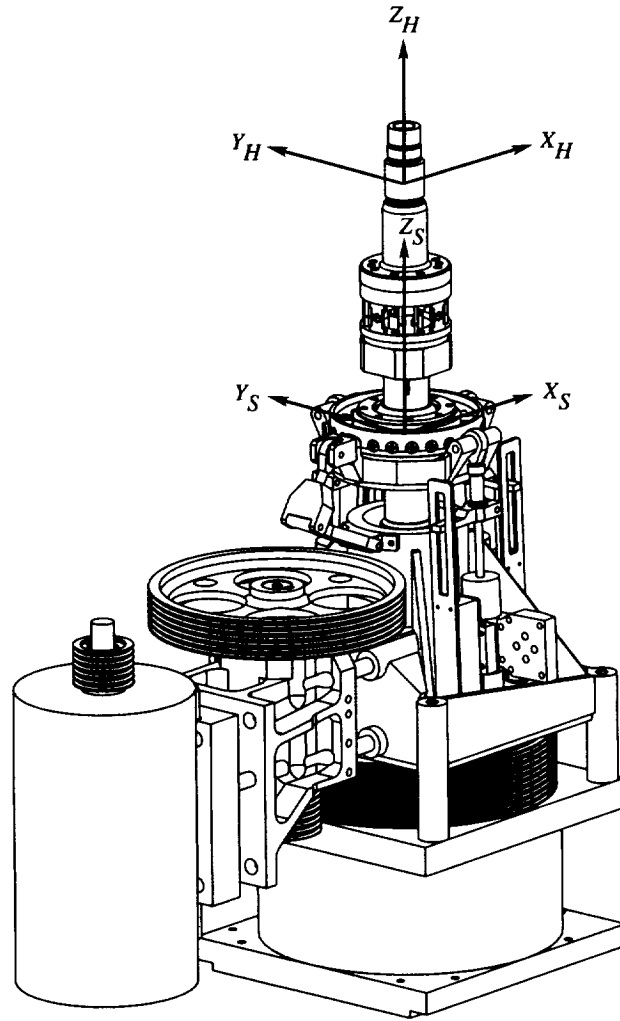
Figure 5.2. Location and orientation of interface joints on ARES-II pylon.

a significant amount of time-history data is generated with DADS throughout the analysis of the ARES-II testbed to relate the excitation and response at discrete frequencies. Additionally, a reduction of the steady-state responses to constant coefficients is necessary to develop the required impedance matrices. Because DADS is a simulation analysis that uses a time-marching integration solution, all transient response must decay before an accurate assessment of the steady-state amplitude of motion may be obtained. These steady-state amplitudes are often obtained with an FFT algorithm that generally requires a substantial length of time-history data for accurate analysis. However, since the impedance-matching analysis requires discrete frequencies of interest, an alternative approach is suggested.

A harmonic analysis of the time-history data generated by DADS is used that is similar to the conditional sampling method used in reference 7. With this method, only one complete cycle of data is necessary for analysis. The length of the cycle must be equal to the period of the rotor rotational frequency. For the BRR, a rotor system operating at 660 rpm, this period is 0.09091 s. For accurate results, this method also requires that most transient response has decayed. However, the harmonic analysis is much less affected by any remaining transients than the FFT.

For the analysis, the time-history window W is divided into J time steps ($\Delta t = W/J$) and evaluation takes place over $J + 1$ samples. Sample 1 of the window is aligned in the time history with $\psi = 0°$ and sample $J + 1$ with $\psi = 360°$ (reference blade over the tail for the first and last time steps). The index j is used to denote the time step (i.e., $j = 1$ to $J + 1$), and a weighting factor w_j is necessary for the analysis. At the window endpoints ($j = 1$ and $j = J + 1$), $w_j = 1/2J$, and elsewhere, $w_j = 1/J$. The components of each harmonic may then be obtained by

$$
\left.
\begin{aligned}
f_{c_n} &= \sum_{j=1}^{J+1} 2w_j\, f_j\, \cos n\psi_j \\[2mm]
f_{s_n} &= \sum_{j=1}^{J+1} 2w_j\, f_j\, \sin n\psi_j
\end{aligned}
\right\}
\tag{5.30}
$$

where n is the harmonic number, f_j is the amplitude of the signal at the jth time step in the time history, ψ_j is the azimuth of the jth time step, and f_{c_n} and f_{s_n} are the cosine and sine amplitude components for the nth harmonic of the time history.

For this study, it has been found that a simulation time of only 0.5 s is required for the decay of transient response before good quality harmonic analysis results are obtained. Therefore, the time-history window from which results have been obtained runs from 0.5 to 0.59091 s; this, compared with the 2.5 s of data required for FFT analysis, represents a significant savings in computation time. This harmonic analysis approach has been used for all cases in which time-history data analysis was required throughout this study.

5.3.1.2. ARES-II mobility matrix. Because applying a harmonic force and observing the associated displacements throughout the DADS model is simpler than applying a pure harmonic displacement and observing the forces, the necessary mobility matrices are generated directly with the DADS model of the ARES-II. To generate a full set of mobility matrices at the two frequencies of interest, 4P and 8P, requires 12 independent executions of the analysis. Six runs are required in which each force and moment is applied to the hub interface joint using superimposed 4-per-rev and 8-per-rev forces and moments. An identical set of force and moment runs are required for application of load to the swashplate interface joint. Because the analytical model of the ARES-II is completely linear, only sine excitations were used to develop the mobility matrices.

The general form for the mobility equation (eq. (5.11)) may be written for a 6-dof interface joint as

$$
\begin{Bmatrix} \{x\} \\ \{y\} \\ \{z\} \\ \{\theta_x\} \\ \{\theta_y\} \\ \{\theta_z\} \end{Bmatrix}
=
\begin{bmatrix}
[A_{x/x}] & [A_{x/y}] & [A_{x/z}] & [A_{x/\theta_x}] & [A_{x/\theta_y}] & [A_{x/\theta_z}] \\
[A_{y/x}] & [A_{y/y}] & [A_{y/z}] & [A_{y/\theta_x}] & [A_{y/\theta_y}] & [A_{y/\theta_z}] \\
[A_{z/x}] & [A_{z/y}] & [A_{z/z}] & [A_{z/\theta_x}] & [A_{z/\theta_y}] & [A_{z/\theta_z}] \\
[A_{\theta_x/x}] & [A_{\theta_x/y}] & [A_{\theta_x/z}] & [A_{\theta_x/\theta_x}] & [A_{\theta_x/\theta_y}] & [A_{\theta_x/\theta_z}] \\
[A_{\theta_y/x}] & [A_{\theta_y/y}] & [A_{\theta_y/z}] & [A_{\theta_y/\theta_x}] & [A_{\theta_y/\theta_y}] & [A_{\theta_y/\theta_z}] \\
[A_{\theta_z/x}] & [A_{\theta_z/y}] & [A_{\theta_z/z}] & [A_{\theta_z/\theta_x}] & [A_{\theta_z/\theta_y}] & [A_{\theta_z/\theta_z}]
\end{bmatrix}
\begin{Bmatrix} \{F_x\} \\ \{F_y\} \\ \{F_z\} \\ \{M_x\} \\ \{M_y\} \\ \{M_z\} \end{Bmatrix}
\tag{5.31}
$$

where the displacement and rotation column vectors and the force and moment column vectors are each cosine and sine pairs (i.e., $\{x\} = \{x_c \ x_s\}^T$, $\{F_x\} = \{F_{x_c} \ F_{x_s}\}^T$), and the mobility matrices are each 2×2 and represent the displacement due to the applied force as described by the subscripts (i.e., $[A_{x/y}]$ is the mobility matrix for the x-displacement due to a force applied in the y-direction). Therefore, a single DADS run in which a forcing function is applied to an interface joint allows the generation of one matrix column of the large matrix in equation (5.31).

The eight 12×12 mobility matrices generated for the ARES-II are given in the following equations:

For hub interface joint response due to 4P hub interface joint force and moment excitation,

$$[A_{H/H_4}] = 10^{-5} \times$$

```
                                  A
 4.0638 -0.5832  0.0000  0.0000 | 0.0782 -0.1072|  0.0000  0.0000  0.3939 -0.0275  0.0000  0.0000
 0.5832  4.0638  0.0000  0.0000 | 0.1072  0.0782|  0.0000  0.0000  0.0275  0.3939  0.0000  0.0000
 0.0000  0.0000  2.5037 -0.3089   0.0000  0.0000 -0.3132  0.0149  0.0000  0.0000  0.0188  0.0019
 0.0000  0.0000  0.3089  2.5037   0.0000  0.0000 -0.0149 -0.3132  0.0000  0.0000 -0.0019  0.0188
 0.0790 -0.1073  0.0005  0.0000   0.2830 -0.2024  0.0000  0.0000  0.0035 -0.0053  0.0000  0.0000
 0.1073  0.0790  0.0000  0.0005   0.2024  0.2830  0.0000  0.0000  0.0053  0.0035  0.0000  0.0000
 0.0000  0.0000 -0.3132  0.0149   0.0000  0.0000  0.0446 -0.0014  0.0000  0.0000  0.0004 -0.0001
 0.0000  0.0000 -0.0149 -0.3132   0.0000  0.0000  0.0014  0.0446  0.0000  0.0000  0.0001  0.0004
 0.3939 -0.0275  0.0000  0.0000   0.0035 -0.0053  0.0000  0.0000  0.0486 -0.0020  0.0000  0.0000
 0.0275  0.3939  0.0000  0.0000   0.0053  0.0035  0.0000  0.0000  0.0020  0.0486  0.0000  0.0000
 0.0000  0.0000  0.0188  0.0019   0.0000  0.0000  0.0004 -0.0001  0.0000  0.0000  0.0462 -0.0012
 0.0000  0.0000 -0.0019  0.0188   0.0000  0.0000  0.0001  0.0004  0.0000  0.0000  0.0012  0.0462
```

$$(5.32a)$$

For hub interface joint response due to 4P swashplate interface joint force and moment excitation,

$$[A_{H/S_4}] = 10^{-5} \times$$

```
                                  B
 1.3119 -0.3382  0.0000  0.0000 | 0.0778 -0.1071|  0.0000  0.0000  0.2391 -0.0228  0.0000  0.0000
 0.3382  1.3119  0.0000  0.0000 | 0.1071  0.0778|  0.0000  0.0000  0.0228  0.2391  0.0000  0.0000
 0.0000  0.0000  0.4134 -0.1672   0.0000  0.0000 -0.1592  0.0104  0.0000  0.0000  0.0188  0.0019
 0.0000  0.0000  0.1672  0.4134   0.0000  0.0000 -0.0104 -0.1592  0.0000  0.0000 -0.0019  0.0188
 0.0501 -0.0637  0.0000  0.0001   0.2469 -0.2013  0.0000  0.0000  0.0034 -0.0053  0.0000  0.0000
 0.0637  0.0501 -0.0001  0.0000   0.2013  0.2469  0.0000  0.0000  0.0053  0.0034  0.0000  0.0000
 0.0000  0.0000 -0.0917  0.0072   0.0000  0.0000  0.0083 -0.0004  0.0000  0.0000  0.0004 -0.0001
 0.0000  0.0000 -0.0072 -0.0917   0.0000  0.0000  0.0004  0.0083  0.0000  0.0000  0.0001  0.0004
 0.1397 -0.0151  0.0000  0.0000   0.0034 -0.0053  0.0000  0.0000  0.0122 -0.0010  0.0000  0.0000
 0.0151  0.1397  0.0000  0.0000   0.0053  0.0034  0.0000  0.0000  0.0010  0.0122  0.0000  0.0000
 0.0000  0.0000  0.0218  0.0012   0.0000  0.0000  0.0004 -0.0001  0.0000  0.0000  0.0108 -0.0002
 0.0000  0.0000 -0.0012  0.0218   0.0000  0.0000  0.0001  0.0004  0.0000  0.0000  0.0002  0.0108
```

$$(5.32b)$$

For swashplate interface joint response due to 4P hub interface joint force and moment excitation,

$$[A_{S/H_4}] = 10^{-5} \times \overset{B}{\begin{bmatrix} 1.3120 & -0.3382 & 0.0000 & 0.0000 & 0.0498 & -0.0637 & 0.0000 & 0.0000 & 0.1397 & -0.0151 & 0.0000 & 0.0000 \\ 0.3382 & 1.3120 & 0.0000 & 0.0000 & 0.0637 & 0.0498 & 0.0000 & 0.0000 & 0.0151 & 0.1397 & 0.0000 & 0.0000 \\ 0.0000 & 0.0000 & 0.4134 & -0.1672 & 0.0000 & 0.0000 & -0.0917 & 0.0072 & 0.0000 & 0.0000 & 0.0218 & 0.0012 \\ 0.0000 & 0.0000 & 0.1672 & 0.4134 & 0.0000 & 0.0000 & -0.0072 & -0.0917 & 0.0000 & 0.0000 & -0.0012 & 0.0218 \\ 0.0782 & -0.1071 & 0.0001 & 0.0002 & 0.2469 & -0.2013 & 0.0000 & 0.0000 & 0.0034 & -0.0053 & 0.0000 & 0.0000 \\ 0.1071 & 0.0782 & -0.0002 & 0.0001 & 0.2013 & 0.2469 & 0.0000 & 0.0000 & 0.0053 & 0.0034 & 0.0000 & 0.0000 \\ 0.0000 & 0.0000 & -0.1592 & 0.0104 & 0.0000 & 0.0000 & 0.0083 & -0.0004 & 0.0000 & 0.0000 & 0.0004 & -0.0001 \\ 0.0000 & 0.0000 & -0.0104 & -0.1592 & 0.0000 & 0.0000 & 0.0004 & 0.0083 & 0.0000 & 0.0000 & 0.0001 & 0.0004 \\ 0.2391 & -0.0228 & 0.0000 & 0.0000 & 0.0034 & -0.0052 & 0.0000 & 0.0000 & 0.0122 & -0.0010 & 0.0000 & 0.0000 \\ 0.0228 & 0.2391 & 0.0000 & 0.0000 & 0.0052 & 0.0034 & 0.0000 & 0.0000 & 0.0010 & 0.0122 & 0.0000 & 0.0000 \\ 0.0000 & 0.0000 & 0.0188 & 0.0019 & 0.0000 & 0.0000 & 0.0004 & -0.0001 & 0.0000 & 0.0000 & 0.0108 & -0.0002 \\ 0.0000 & 0.0000 & -0.0019 & 0.0188 & 0.0000 & 0.0000 & 0.0001 & 0.0004 & 0.0000 & 0.0000 & 0.0002 & 0.0108 \end{bmatrix}}$$

(5.32c)

For swashplate interface joint response due to 4P swashplate interface joint force and moment excitation,

$$[A_{S/S_4}] = 10^{-6} \times \begin{bmatrix} 1.6600 & -2.1453 & 0.0002 & 0.0000 & 0.4965 & -0.6367 & 0.0000 & 0.0000 & 1.3877 & -0.1484 & 0.0000 & 0.0000 \\ 2.1453 & 1.6600 & 0.0000 & 0.0002 & 0.6367 & 0.4965 & 0.0000 & 0.0000 & 0.1484 & 1.3877 & 0.0000 & 0.0000 \\ -0.0001 & 0.0000 & -3.3920 & -1.0835 & -0.0001 & 0.0000 & -0.9123 & 0.0704 & 0.0000 & 0.0000 & 0.2177 & 0.0125 \\ 0.0000 & -0.0001 & 1.0835 & -3.3920 & 0.0000 & -0.0001 & -0.0704 & -0.9123 & 0.0000 & 0.0000 & -0.0125 & 0.2177 \\ 0.4979 & -0.6374 & 0.0019 & -0.0001 & 2.4687 & -2.0124 & 0.0000 & 0.0000 & 0.0341 & -0.0525 & 0.0000 & 0.0000 \\ 0.6374 & 0.4979 & 0.0001 & 0.0019 & 2.0124 & 2.4687 & 0.0000 & 0.0000 & 0.0525 & 0.0341 & 0.0000 & 0.0000 \\ 0.0000 & 0.0000 & -0.9123 & 0.0704 & 0.0000 & 0.0000 & 0.0821 & -0.0040 & 0.0000 & 0.0000 & 0.0037 & -0.0008 \\ 0.0000 & 0.0000 & -0.0704 & -0.9123 & 0.0000 & 0.0000 & 0.0040 & 0.0821 & 0.0000 & 0.0000 & 0.0008 & 0.0037 \\ 1.3877 & -0.1484 & 0.0000 & 0.0000 & 0.0341 & -0.0524 & 0.0000 & 0.0000 & 0.1212 & -0.0096 & 0.0000 & 0.0000 \\ 0.1484 & 1.3877 & 0.0000 & 0.0000 & 0.0524 & 0.0341 & 0.0000 & 0.0000 & 0.0096 & 0.1212 & 0.0000 & 0.0000 \\ 0.0000 & 0.0000 & 0.2176 & 0.0125 & 0.0000 & 0.0000 & 0.0037 & -0.0008 & 0.0000 & 0.0000 & 0.1079 & -0.0021 \\ 0.0000 & 0.0000 & -0.0125 & 0.2176 & 0.0000 & 0.0000 & 0.0008 & 0.0037 & 0.0000 & 0.0000 & 0.0021 & 0.1079 \end{bmatrix}$$

(5.32d)

For interface joint response due to 8P hub interface joint force and moment excitation,

$$[A_{H/H_8}] = 10^{-4} \times \begin{bmatrix} -0.1067 & -0.0372 & 0.0000 & 0.0001 & 0.0333 & 0.0220 & 0.0000 & 0.0000 & 0.0117 & -0.0022 & 0.0000 & 0.0000 \\ 0.0372 & -0.1067 & -0.0001 & 0.0000 & -0.0220 & 0.0333 & 0.0000 & 0.0000 & 0.0022 & 0.0117 & 0.0000 & 0.0000 \\ 0.0000 & 0.0000 & 0.6536 & -1.7950 & 0.0000 & 0.0000 & -0.0348 & 0.0523 & 0.0000 & 0.0000 & 0.0859 & -0.2239 \\ 0.0000 & 0.0000 & 1.7950 & 0.6536 & 0.0000 & 0.0000 & -0.0523 & -0.0348 & 0.0000 & 0.0000 & 0.2239 & 0.0859 \\ 0.0334 & 0.0220 & 0.0001 & -0.0002 & -0.1544 & -0.0218 & 0.0000 & 0.0000 & -0.0007 & 0.0010 & 0.0000 & 0.0000 \\ -0.0220 & 0.0334 & 0.0002 & 0.0001 & 0.0218 & -0.1544 & 0.0000 & 0.0000 & -0.0010 & -0.0007 & 0.0000 & 0.0000 \\ 0.0000 & 0.0000 & -0.0348 & 0.0523 & 0.0000 & 0.0000 & 0.0043 & -0.0017 & 0.0000 & 0.0000 & -0.0026 & 0.0064 \\ 0.0000 & 0.0000 & -0.0523 & -0.0348 & 0.0000 & 0.0000 & 0.0017 & 0.0043 & 0.0000 & 0.0000 & -0.0064 & -0.0026 \\ 0.0117 & -0.0022 & 0.0000 & 0.0000 & -0.0007 & 0.0010 & 0.0000 & 0.0000 & 0.0036 & -0.0003 & 0.0000 & 0.0000 \\ 0.0022 & 0.0117 & 0.0000 & 0.0000 & -0.0010 & -0.0007 & 0.0000 & 0.0000 & 0.0003 & 0.0036 & 0.0000 & 0.0000 \\ 0.0000 & 0.0000 & 0.0862 & -0.2237 & 0.0000 & 0.0000 & -0.0026 & 0.0064 & 0.0000 & 0.0000 & 0.0131 & -0.0286 \\ 0.0000 & 0.0000 & 0.2237 & 0.0862 & 0.0000 & 0.0000 & -0.0064 & -0.0026 & 0.0000 & 0.0000 & 0.0286 & 0.0131 \end{bmatrix}$$

(5.32e)

For hub interface joint response due to 8P swashplate interface joint force and moment excitation,

$$[A_{H/S_8}] = 10^{-4} \times \begin{bmatrix}
-0.1530 & -0.0170 & 0.0000 & 0.0001 & 0.0333 & 0.0220 & 0.0000 & 0.0000 & -0.0033 & -0.0013 & 0.0000 & 0.0000 \\
0.0170 & -0.1530 & -0.0001 & 0.0000 & -0.0220 & 0.0333 & 0.0000 & 0.0000 & 0.0013 & -0.0033 & 0.0000 & 0.0000 \\
0.0000 & 0.0000 & 0.4239 & -1.3717 & 0.0000 & 0.0000 & -0.0184 & 0.0477 & 0.0000 & 0.0000 & 0.0859 & -0.2237 \\
0.0000 & 0.0000 & 1.3717 & 0.4239 & 0.0000 & 0.0000 & -0.0477 & -0.0184 & 0.0000 & 0.0000 & 0.2237 & 0.0859 \\
0.0395 & 0.0141 & 0.0001 & -0.0001 & -0.1578 & -0.0216 & 0.0000 & 0.0000 & -0.0008 & 0.0009 & 0.0000 & 0.0000 \\
-0.0141 & 0.0395 & 0.0001 & 0.0001 & 0.0216 & -0.1578 & 0.0000 & 0.0000 & -0.0009 & -0.0008 & 0.0000 & 0.0000 \\
0.0000 & 0.0000 & -0.0139 & 0.0394 & 0.0000 & 0.0000 & 0.0007 & -0.0014 & 0.0000 & 0.0000 & -0.0026 & 0.0064 \\
0.0000 & 0.0000 & -0.0394 & -0.0139 & 0.0000 & 0.0000 & 0.0014 & 0.0007 & 0.0000 & 0.0000 & -0.0064 & -0.0026 \\
-0.0036 & -0.0008 & 0.0000 & 0.0000 & -0.0007 & 0.0010 & 0.0000 & 0.0000 & 0.0000 & -0.0001 & 0.0000 & 0.0000 \\
0.0008 & -0.0036 & 0.0000 & 0.0000 & -0.0010 & -0.0007 & 0.0000 & 0.0000 & 0.0001 & 0.0000 & 0.0000 & 0.0000 \\
0.0000 & 0.0000 & 0.0655 & -0.1724 & 0.0000 & 0.0000 & -0.0025 & 0.0059 & 0.0000 & 0.0000 & 0.0096 & -0.0284 \\
0.0000 & 0.0000 & 0.1724 & 0.0655 & 0.0000 & 0.0000 & -0.0059 & -0.0025 & 0.0000 & 0.0000 & 0.0284 & 0.0096
\end{bmatrix}$$

(5.32f)

For swashplate interface joint response due to 8P hub interface joint force and moment excitation,

$$[A_{S/H_8}] = 10^{-4} \times \begin{bmatrix}
-0.1530 & -0.0170 & 0.0000 & 0.0001 & 0.0394 & 0.0141 & 0.0000 & 0.0000 & -0.0036 & -0.0008 & 0.0000 & 0.0000 \\
0.0170 & -0.1530 & -0.0001 & 0.0000 & -0.0141 & 0.0394 & 0.0000 & 0.0000 & 0.0008 & -0.0036 & 0.0000 & 0.0000 \\
0.0000 & 0.0000 & 0.4237 & -1.3717 & 0.0000 & 0.0000 & -0.0139 & 0.0394 & 0.0000 & 0.0000 & 0.0652 & -0.1725 \\
0.0000 & 0.0000 & 1.3717 & 0.4237 & 0.0000 & 0.0000 & -0.0394 & -0.0139 & 0.0000 & 0.0000 & 0.1725 & 0.0652 \\
0.0333 & 0.0220 & 0.0001 & -0.0002 & -0.1578 & -0.0216 & 0.0000 & 0.0000 & -0.0007 & 0.0010 & 0.0000 & 0.0000 \\
-0.0220 & 0.0333 & 0.0002 & 0.0001 & 0.0216 & -0.1578 & 0.0000 & 0.0000 & -0.0010 & -0.0007 & 0.0000 & 0.0000 \\
0.0000 & 0.0000 & -0.0184 & 0.0477 & 0.0000 & 0.0000 & 0.0007 & -0.0014 & 0.0000 & 0.0000 & -0.0025 & 0.0059 \\
0.0000 & 0.0000 & -0.0477 & -0.0184 & 0.0000 & 0.0000 & 0.0014 & 0.0007 & 0.0000 & 0.0000 & -0.0059 & -0.0025 \\
-0.0033 & -0.0013 & 0.0000 & 0.0000 & -0.0008 & 0.0009 & 0.0000 & 0.0000 & 0.0000 & -0.0001 & 0.0000 & 0.0000 \\
0.0013 & -0.0033 & 0.0000 & 0.0000 & -0.0009 & -0.0008 & 0.0000 & 0.0000 & 0.0001 & 0.0000 & 0.0000 & 0.0000 \\
0.0000 & 0.0000 & 0.0861 & -0.2235 & 0.0000 & 0.0000 & -0.0026 & 0.0064 & 0.0000 & 0.0000 & 0.0096 & -0.0284 \\
0.0000 & 0.0000 & 0.2235 & 0.0861 & 0.0000 & 0.0000 & -0.0064 & -0.0026 & 0.0000 & 0.0000 & 0.0284 & 0.0096
\end{bmatrix}$$

(5.32g)

For swashplate interface joint response due to 8P swashplate interface joint force and moment excitation,

$$[A_{S/S_8}] = 10^{-4} \times \begin{bmatrix}
-0.1242 & -0.0107 & 0.0000 & 0.0000 & 0.0394 & 0.0141 & 0.0000 & 0.0000 & -0.0033 & -0.0008 & 0.0000 & 0.0000 \\
0.0107 & -0.1242 & 0.0000 & 0.0000 & -0.0141 & 0.0394 & 0.0000 & 0.0000 & 0.0008 & -0.0033 & 0.0000 & 0.0000 \\
0.0000 & 0.0000 & 0.3138 & -1.0547 & 0.0000 & 0.0000 & -0.0131 & 0.0365 & 0.0000 & 0.0000 & 0.0652 & -0.1724 \\
0.0000 & 0.0000 & 1.0547 & 0.3138 & 0.0000 & 0.0000 & -0.0365 & -0.0131 & 0.0000 & 0.0000 & 0.1724 & 0.0652 \\
0.0395 & 0.0141 & 0.0000 & -0.0001 & -0.1577 & -0.0216 & 0.0000 & 0.0000 & -0.0008 & 0.0009 & 0.0000 & 0.0000 \\
-0.0141 & 0.0395 & 0.0001 & 0.0000 & 0.0216 & -0.1577 & 0.0000 & 0.0000 & -0.0009 & -0.0008 & 0.0000 & 0.0000 \\
0.0000 & 0.0000 & -0.0131 & 0.0366 & 0.0000 & 0.0000 & 0.0006 & -0.0013 & 0.0000 & 0.0000 & -0.0025 & 0.0059 \\
0.0000 & 0.0000 & -0.0366 & -0.0131 & 0.0000 & 0.0000 & 0.0013 & 0.0006 & 0.0000 & 0.0000 & -0.0059 & -0.0025 \\
-0.0033 & -0.0008 & 0.0000 & 0.0000 & -0.0008 & 0.0009 & 0.0000 & 0.0000 & 0.0000 & -0.0001 & 0.0000 & 0.0000 \\
0.0008 & -0.0033 & 0.0000 & 0.0000 & -0.0009 & -0.0008 & 0.0000 & 0.0000 & 0.0001 & 0.0000 & 0.0000 & 0.0000 \\
0.0000 & 0.0000 & 0.0654 & -0.1723 & 0.0000 & 0.0000 & -0.0025 & 0.0059 & 0.0000 & 0.0000 & 0.0096 & -0.0284 \\
0.0000 & 0.0000 & 0.1723 & 0.0654 & 0.0000 & 0.0000 & -0.0059 & -0.0025 & 0.0000 & 0.0000 & 0.0284 & 0.0096
\end{bmatrix}$$

(5.32h)

The subscripts of the mobility matrix designate the type of mobility information that the matrix contains. The subscript to the left of the slash indicates the joint at which the response is measured; the subscript to the right of the slash indicates the joint at which the forcing function is applied. The numeric subscript indicates the frequency of

37

excitation in per rev. For example, equation (5.32b) represents the mobility of the hub joint due to a 4P forcing function applied at the swashplate joint.

Significant physical insight regarding the ARES-II response may be obtained by studying the mobility matrices presented in equations (5.32). The reader is referred to equation (5.32a), which presents the hub joint response due to 4P hub joint excitations. The first two columns of this matrix identify the response of the hub joint when subjected to a 4P axially directed load. As shown in rows 1 and 2, the axial response is dominant. Rows 5, 6, 9, and 10, however, indicate that normal (vertical) and pitch responses are excited as well. Similarly columns 3 and 4 identify the response of the hub joint when subjected to a 4P side-directed load. The response is primarily to the side; however, coupling exists both in roll (rows 7 and 8) and in yaw (rows 11 and 12).

Out-of-phase results are evident in the 8-per-rev mobility matrices (eqs. (5.32e) through (5.32h)). In equation (5.32e), for instance, the 8P side-directed load at the hub results in a side response that is 70° out of phase with the force; this is due to the proximity of the forcing function frequency (8P or 88 Hz) to the elastic yaw-side-roll mode at 90 Hz (refer to table 4.1 and fig. 4.4).

Two further comments regarding the mobility matrices of equations (5.32) are warranted. First, these matrices have not been generated with a unit sine forcing function as used in section 5.1.1. Since the ARES-II is a relatively stiff structure, minimal response would have been generated by a unit load. Therefore, larger excitation loads were used and the results presented in equations (5.32) normalized to obtain the displacement-per-unit-load values. Second, the results are not entirely indicative of a strictly linear system. Note the submatrices labeled A in equation (5.32a) and the submatrices labeled B in equations (5.32b) and (5.32c). Ideally, the two submatrices labeled A would be identical as would the submatrices labeled B. However, these minor differences exist because of small errors inherent in the DADS and harmonic analysis solutions. The differences are considered minor and no action has been taken to adjust them or to prevent their occurrence.

Finally, a mobility matrix is generated for the entire ARES-II system with the matrices in equations (5.32). A two-step process is used for clarity. First, a mobility matrix is generated for both the 4P and the 8P equations as follows:

$$
\left.\begin{array}{l}
[\mathbf{A}_4] = \begin{bmatrix} [\mathbf{A}_{H/H_4}] & [\mathbf{A}_{H/S_4}] \\ [\mathbf{A}_{S/H_4}] & [\mathbf{A}_{S/S_4}] \end{bmatrix} \\[20pt]
[\mathbf{A}_8] = \begin{bmatrix} [\mathbf{A}_{H/H_8}] & [\mathbf{A}_{H/S_8}] \\ [\mathbf{A}_{S/H_8}] & [\mathbf{A}_{S/S_8}] \end{bmatrix}
\end{array}\right\}
\qquad (5.33)
$$

Second, the final assembly of the system mobility matrix occurs as

$$
[\mathbf{A}] = \begin{bmatrix} [\mathbf{A}_4] & [0] \\ [0] & [\mathbf{A}_8] \end{bmatrix}
\qquad (5.34)
$$

38

The completed mobility equation, then, is

$$
\begin{bmatrix}
\{\mathbf{X}_{H_4}\} \\
\{\mathbf{X}_{S_4}\} \\
\{\mathbf{X}_{H_8}\} \\
\{\mathbf{X}_{S_8}\}
\end{bmatrix}_A
= [\mathbf{A}]
\begin{bmatrix}
\{\mathbf{F}_{H_4}\} \\
\{\mathbf{F}_{S_4}\} \\
\{\mathbf{F}_{H_8}\} \\
\{\mathbf{F}_{S_8}\}
\end{bmatrix}
\tag{5.35}
$$

where

$$
\{\mathbf{X}_{H_n}\} = \left\{ x_{H_{nc}} \quad x_{H_{ns}} \quad y_{H_{nc}} \quad y_{H_{ns}} \quad z_{H_{nc}} \quad z_{H_{ns}} \quad \theta_{x_{H_{nc}}} \quad \theta_{x_{H_{ns}}} \quad \theta_{y_{H_{nc}}} \quad \theta_{y_{H_{ns}}} \quad \theta_{z_{H_{nc}}} \quad \theta_{z_{H_{ns}}} \right\}^T
$$

$$
\{\mathbf{X}_{S_n}\} = \left\{ x_{S_{nc}} \quad x_{S_{ns}} \quad y_{S_{nc}} \quad y_{S_{ns}} \quad z_{S_{nc}} \quad z_{S_{ns}} \quad \theta_{x_{S_{nc}}} \quad \theta_{x_{S_{ns}}} \quad \theta_{y_{S_{nc}}} \quad \theta_{y_{S_{ns}}} \quad \theta_{z_{S_{nc}}} \quad \theta_{z_{S_{ns}}} \right\}^T
$$

$$
\{\mathbf{F}_{H_n}\} = \left\{ F_{x_{H_{nc}}} \quad F_{x_{H_{ns}}} \quad F_{y_{H_{nc}}} \quad F_{y_{H_{ns}}} \quad F_{z_{H_{nc}}} \quad F_{z_{H_{ns}}} \quad M_{x_{H_{nc}}} \quad M_{x_{H_{ns}}} \quad M_{y_{H_{nc}}} \quad M_{y_{H_{ns}}} \quad M_{z_{H_{nc}}} \quad M_{z_{H_{ns}}} \right\}^T
$$

$$
\{\mathbf{F}_{S_n}\} = \left\{ F_{x_{S_{nc}}} \quad F_{x_{S_{ns}}} \quad F_{y_{S_{nc}}} \quad F_{y_{S_{ns}}} \quad F_{z_{S_{nc}}} \quad F_{z_{S_{ns}}} \quad M_{x_{S_{nc}}} \quad M_{x_{S_{ns}}} \quad M_{y_{S_{nc}}} \quad M_{y_{S_{ns}}} \quad M_{z_{S_{nc}}} \quad M_{z_{S_{ns}}} \right\}^T
$$

5.3.1.3. ARES-II motion matrix.

The motion matrix is developed by actuating the ARES-II model in each of the three translational and three rotational motions individually, then processing the response at the hub and swashplate interface joints. Thus, only six DADS runs are required, one for each motion. The actuated motion analysis developed in section 4.1.2 is used to generate the actuator schedules for the motions. For translational motions a nominal amplitude of 0.01 in. is used, and for rotational motions a nominal amplitude of 0.05° is used. All motions are actuated at 4 per rev by using sine excitations. The resulting response at each of the interface joints is analyzed by using the harmonic analysis, then scaled by the appropriate input amplitude to provide a displacement-per-unit-displacement relationship. These relationships are used to generate a motion matrix for the hub $[\mathbf{B}_{H_4}]$ and the swashplate $[\mathbf{B}_{S_4}]$ interface joints. These two component matrices are shown in the following equations:

For hub interface joint response due to 4P pylon actuation,

$$
[\mathbf{B}_{H_4}] =
\begin{bmatrix}
0.6944 & -0.0819 & 0.0007 & 0.0000 & 0.5361 & -0.0988 & 0.0017 & -0.0018 & 26.7396 & -0.9595 & -0.0004 & 0.0014 \\
0.0819 & 0.6944 & 0.0000 & 0.0007 & 0.0988 & 0.5361 & 0.0018 & 0.0017 & 0.9595 & 26.7396 & -0.0014 & -0.0004 \\
0.0118 & -0.0011 & 0.6180 & -0.0608 & 0.0118 & -0.0011 & -17.8883 & -0.1389 & 0.1335 & -0.0128 & 0.3049 & 2.1252 \\
0.0011 & 0.0118 & 0.0608 & 0.6180 & 0.0011 & 0.0118 & 0.1389 & -17.8883 & 0.0128 & 0.1335 & -2.1252 & 0.3049 \\
0.0038 & -0.0054 & -0.0001 & 0.0000 & 1.0305 & -0.1051 & 0.0007 & -0.0001 & 0.7274 & -0.6736 & -0.0006 & 0.0010 \\
0.0054 & 0.0038 & 0.0000 & -0.0001 & 0.1051 & 1.0305 & 0.0001 & 0.0007 & 0.6736 & 0.7274 & -0.0010 & -0.0006 \\
-0.0001 & 0.0000 & -0.0084 & 0.0020 & -0.0001 & 0.0000 & 1.0898 & 0.0032 & -0.0014 & 0.0001 & -0.0106 & 0.0475 \\
0.0000 & -0.0001 & -0.0020 & -0.0084 & 0.0000 & -0.0001 & -0.0032 & 1.0898 & -0.0001 & -0.0014 & -0.0475 & -0.0106 \\
0.0116 & -0.0030 & 0.0000 & 0.0000 & 0.0268 & -0.0045 & 0.0001 & -0.0001 & 1.5320 & -0.0439 & 0.0000 & 0.0001 \\
0.0030 & 0.0116 & 0.0000 & 0.0000 & 0.0045 & 0.0268 & 0.0001 & 0.0001 & 0.0439 & 1.5320 & -0.0001 & 0.0000 \\
0.0000 & 0.0000 & -0.0113 & 0.0007 & 0.0000 & 0.0000 & -0.0395 & 0.0022 & -0.0001 & 0.0000 & 1.3329 & -0.0088 \\
0.0000 & 0.0000 & -0.0007 & -0.0113 & 0.0000 & 0.0000 & -0.0022 & -0.0395 & 0.0000 & -0.0001 & 0.0088 & 1.3329
\end{bmatrix}
$$

$$
\tag{5.36a}
$$

For swashplate interface joint response due to 4P pylon actuation,

$$[\mathbf{B}_{S_4}] = \begin{bmatrix}
0.6000 & -0.0573 & 0.0006 & 0.0000 & 0.3162 & -0.0617 & 0.0013 & -0.0013 & 14.1799 & -0.5953 & -0.0003 & 0.0009 \\
0.0573 & 0.6000 & 0.0000 & 0.0006 & 0.0617 & 0.3162 & 0.0013 & 0.0013 & 0.5953 & 14.1799 & -0.0009 & -0.0003 \\
0.0107 & -0.0010 & 0.5498 & -0.0446 & 0.0107 & -0.0010 & -8.9523 & -0.1156 & 0.1219 & -0.0116 & 0.2184 & 2.5199 \\
0.0010 & 0.0107 & 0.0446 & 0.5498 & 0.0010 & 0.0107 & 0.1156 & -8.9523 & 0.0116 & 0.1219 & -2.5199 & 0.2184 \\
0.0038 & -0.0054 & 0.0000 & 0.0000 & 1.0302 & -0.1050 & 0.0007 & -0.0006 & 0.7257 & -0.6732 & -0.0002 & 0.0010 \\
0.0054 & 0.0038 & 0.0000 & 0.0000 & 0.1050 & 1.0302 & 0.0006 & 0.0007 & 0.6732 & 0.7257 & -0.0010 & -0.0002 \\
-0.0001 & 0.0000 & -0.0081 & 0.0019 & -0.0001 & 0.0000 & 1.0808 & 0.0035 & -0.0014 & 0.0001 & -0.0105 & 0.0487 \\
0.0000 & -0.0001 & -0.0019 & -0.0081 & 0.0000 & -0.0001 & -0.0035 & 1.0808 & -0.0001 & -0.0014 & -0.0487 & -0.0105 \\
0.0112 & -0.0029 & 0.0000 & 0.0000 & 0.0266 & -0.0045 & 0.0001 & -0.0001 & 1.5185 & -0.0430 & 0.0000 & 0.0001 \\
0.0029 & 0.0112 & 0.0000 & 0.0000 & 0.0045 & 0.0266 & 0.0001 & 0.0001 & 0.0430 & 1.5185 & -0.0001 & 0.0000 \\
0.0000 & 0.0000 & -0.0112 & 0.0007 & 0.0000 & 0.0000 & -0.0395 & 0.0022 & -0.0001 & 0.0000 & 1.3326 & -0.0088 \\
0.0000 & 0.0000 & -0.0007 & -0.0112 & 0.0000 & 0.0000 & -0.0022 & -0.0395 & 0.0000 & -0.0001 & 0.0088 & 1.3326
\end{bmatrix}$$

$$(5.36b)$$

The motion matrix defining the 4-per-rev response is

$$[\mathbf{B}_4] = \begin{bmatrix} [\mathbf{B}_{H_4}] & [0] \\ [0] & [\mathbf{B}_{S_4}] \end{bmatrix} \tag{5.37}$$

Therefore, since 8-per-rev motions are not actuated, developing additional matrices for the 8P response is unnecessary. The completed ARES-II system motion matrix is

$$[\mathbf{B}] = \begin{bmatrix} [\mathbf{B}_4] & [0] \\ [0] & [\mathbf{I}] \end{bmatrix} \tag{5.38}$$

where the identity matrix is necessary to expand the matrix size to 48×48 like the mobility matrix $[\mathbf{A}]$.

To drive the ARES-II by using the motion matrix $[\mathbf{B}]$ a control vector $\{\mathbf{U}\}$ is necessary. This control vector is a 12-element vector defining the cosine and sine components of the desired motions of the simulated c.g. referred to in section 4.1.2. However, because of the manner in which the motion matrix has been developed (i.e., $[\mathbf{B}_{H_4}]$ and $[\mathbf{B}_{S_4}]$ on the diagonal), it is necessary to use the vector twice. Therefore, the completed motion equation is

$$\begin{bmatrix} \{\mathbf{X}_{H_4}\} \\ \{\mathbf{X}_{S_4}\} \\ \{\mathbf{X}_{H_8}\} \\ \{\mathbf{X}_{S_8}\} \end{bmatrix}_B = [\mathbf{B}] \begin{bmatrix} \{\mathbf{U}\} \\ \{\mathbf{U}\} \\ \{0\} \\ \{0\} \end{bmatrix} \tag{5.39}$$

where the vectors $\mathbf{X}$ were defined in equation (5.35), and

$$\{\mathbf{U}\} = \left\{ U_{x_c} \ \ U_{x_s} \ \ U_{y_c} \ \ U_{y_s} \ \ U_{z_c} \ \ U_{z_s} \ \ U_{\theta_{x_c}} \ \ U_{\theta_{x_s}} \ \ U_{\theta_{y_c}} \ \ U_{\theta_{y_s}} \ \ U_{\theta_{z_c}} \ \ U_{\theta_{z_s}} \right\}^T$$

5.3.2. Basic Research Rotor Impedance Model

The CAMRAD-II model discussed in section 4.2 is used to develop the impedance model of the BRR. The development of the impedance matrix is, however, more complicated than that required for the sample system of

40

section 5.1.3. Several factors must be considered. First, the rotor system is an inherently nonlinear system. Therefore, to apply an impedance-matching approach to a rotor system, care must be used to ensure that the response is within a linear range. This requires the establishment of a steady-state, fixed-hub (or motionless hub) condition about which small perturbations may be made. Therefore, the loads at the rotor system hub and swashplate interface joints represent the loads due to the operation at the fixed-hub condition plus an incremental load due to the motion of the rotor system. Second, because the rotor control system (i.e., pitch links and swashplate) is massless in the CAMRAD-II model of the BRR, the swashplate interface joint loads are dependent only upon the aerodynamic and dynamic forces in the rotor system. Therefore, the impedance equation must generate forces and moments at both the hub and swashplate interface joints based on the fixed-hub condition loads and motion at the hub joint. No additional loads caused by motion of the swashplate are introduced. Finally, it must be recognized that 4P hub motions generate changes in both 4P and 8P loads because of the changing aerodynamic environment. The same may be said of 8P hub motions. This cross coupling must be considered in the development of the impedance matrix.

5.3.2.1. Fixed-hub load conditions. The choice of meaningful fixed-hub, or motionless hub, load conditions is an important aspect of the impedance-matching approach because, in general, the developed impedance matrices are valid only for a small motion about the fixed-hub condition due to system nonlinearity. For this study, a set of flight conditions that are representative of $1g$ steady flight for a helicopter with gross weight of 8000 lb has been chosen. The performance parameters required to match these conditions are provided as a function of advance ratio μ in table 5.1. CAMRAD-II runs are made for each advance ratio; this allows trim procedures internal to CAMRAD-II to converge to control positions that satisfy the performance parameters. For each of these runs, the rotor is trimmed so that first-harmonic flapping is removed with respect to the rotor shaft, a procedure typical in model rotor system analysis. At each of the flight conditions, the resulting control positions are recorded and a fixed-hub load vector consisting of the 4- and 8-per-rev hub and swashplate loads is defined. This vector is denoted by $\{F_0\}$ and is generated as shown in the following equation:

$$\{F_0\} = \begin{Bmatrix} \{F_{H_4}\} \\ \{F_{S_4}\} \\ \{F_{H_8}\} \\ \{F_{S_8}\} \end{Bmatrix} \tag{5.40}$$

5.3.2.2. Hub motion load conditions. Because rotor systems are inherently nonlinear, no assurance exists that an impedance matrix can be developed by using only a cosine or a sine excitation as for fully linear systems. This study determined that it is necessary, in general, to consider both cosine and sine excitations in the development of an impedance model of a rotor system. A similar approach has been observed in the literature (e.g., ref. 6). This requirement is most likely because of the nonlinear effects introduced to the rotor system by the vortex wake; this is supported by the rotor impedance matrices developed for the flight speed range in which the rotor system

Table 5.1. Performance Parameters for Fixed-Hub
Load Conditions

μ	C_L	C_D
0.05	0.0058	−0.000011
0.10	0.0058	−0.000043
0.15	0.0058	−0.000098
0.20	0.0058	−0.000174
0.25	0.0058	−0.000256
0.30	0.0058	−0.000392
0.35	0.0058	−0.000533

behavior is considered to be the most linear $0.15 \le \mu \le 0.30$. For these flight conditions, the rotor impedance matrices were found to be more typical in form to those developed for fully linear systems. Additionally, CAMRAD-II runs made with a uniform inflow distribution undisturbed by a vortex wake were observed to produce impedance matrices typical in form to those for linear systems. Comprehending the nature of this effect would require study beyond the scope of this research. For this study, it was necessary to excite a rotor system with both cosine and sine hub motions for all flight conditions to develop an appropriate rotor impedance model.

A series of 24 CAMRAD-II runs is made for each advance ratio to define the load characteristics of the BRR under hub motion. These runs include individual cosine and sine excitations for the three translations and the three rotations at both 4P and 8P. For translational hub excitations, an amplitude of 0.01 in. is used, and for rotational hub excitations, an amplitude of 0.05° is used. Because pure hub motions are required to develop these loads, inputting both translational and rotational motions is necessary in order to obtain pure rotational hub motion with the CAMRAD-II model of the BRR. The actuated pylon joint (fig. 4.5) is placed below the hub so that input rotational motion induces both rotation and translation at the hub. For each of the runs, the control positions generated for the fixed-hub conditions were used. In no case did the actuated motion cause the first-harmonic flapping with respect to the shaft to go out of trim by more than 0.1°.

5.3.2.3. Generating impedance matrix.

Because the impedance matrix should permit the calculation of interface loads due to hub motion only, accounting for the fixed-hub loads is necessary when the impedance matrix is developed. Mathematically, this is written as

$$\{F_I\} = \{F_0\} + [C]\{X_I\}$$

(5.41)

Therefore, to develop the impedance matrix $[C]$, the equation

$$[C_{ab}] = \frac{\{F_{I_b}\} - \{F_{0_b}\}}{\{X_{I_a}\}} \qquad (a = 1, 2, ..., 6; \; b = 1, 2, ..., 6)$$

(5.42)

is used where the subscripts a and b denote matrix element location.

For clarity, a two-step process is employed to develop the rotor system impedance matrix. First, matrices are developed based on harmonic response due to harmonic excitation. These matrices are shown in the following equations:

$$\left. \begin{array}{ll} [C_{4/4}] = \begin{bmatrix} [C_{H_{4/4}}] & [0] \\ [C_{S_{4/4}}] & [0] \end{bmatrix} & C_{4/8} = \begin{bmatrix} C_{H_{4/8}} & [0] \\ C_{S_{4/8}} & [0] \end{bmatrix} \\[4em] [C_{8/4}] = \begin{bmatrix} [C_{H_{8/4}}] & [0] \\ [C_{S_{8/4}}] & [0] \end{bmatrix} & C_{8/8} = \begin{bmatrix} C_{H_{8/8}} & [0] \\ C_{S_{8/8}} & [0] \end{bmatrix} \end{array} \right\}$$

(5.43)

The subscripts denote the interface joint for the response (H for hub and S for swashplate), the response harmonic to the left of the slash, and the excitation harmonic to the right of the slash. The matrices [0] are used because the impedance load at the interface joints depends on hub joint motion but not swashplate joint motion. Second, the final assembly of the system impedance matrix occurs as follows:

$$[C] = \begin{bmatrix} [C_{4/4}] & [C_{4/8}] \\ [C_{8/4}] & [C_{8/8}] \end{bmatrix}$$

(5.44)

42

A set of the component matrices required to develop the impedance matrix for $\mu = 0.10$, a highly nonlinear flight condition, is shown in the following equations:

For 4P hub interface joint loads due to 4P hub actuation,

$$
[\mathbf{C}_{H_{4/4}}] = 10^4 \times
\begin{bmatrix}
0.8256 & 0.0125 & -0.0013 & -0.0246 & 0.0114 & -0.0073 & -0.0087 & 0.0204 & -0.0785 & -0.0176 & -0.0993 & 0.0703 \\
-0.0102 & 0.8286 & 0.0202 & 0.0037 & 0.0178 & 0.0024 & 0.0375 & -0.0282 & -0.0376 & -0.0751 & -0.1081 & 0.0144 \\
-0.0046 & 0.0253 & 0.8226 & 0.0106 & 0.0097 & 0.0017 & 0.0702 & 0.0055 & -0.0448 & -0.0176 & -0.0757 & 0.0274 \\
-0.0238 & -0.0028 & -0.0129 & 0.8262 & 0.0127 & 0.0100 & 0.0212 & 0.0545 & -0.0139 & -0.0288 & -0.0967 & -0.0243 \\
-0.0011 & 0.0022 & -0.0014 & -0.0016 & 0.7547 & 0.0335 & 0.0280 & 0.0207 & -0.0193 & -0.0262 & -0.0803 & -0.0848 \\
-0.0015 & 0.0008 & -0.0019 & 0.0002 & -0.0203 & 0.7363 & -0.0008 & -0.0048 & -0.0605 & -0.0221 & 0.0345 & 0.0518 \\
-0.0377 & -0.0310 & -0.0398 & -0.0118 & 0.0652 & -0.0781 & 4.7546 & 1.1236 & 0.0286 & -0.9574 & -0.5711 & 0.6210 \\
0.0259 & -0.0198 & -0.0031 & -0.0337 & 0.1344 & -0.0843 & -0.5825 & 4.6405 & 0.6463 & -0.4314 & -0.8440 & 0.5540 \\
-0.0501 & 0.0509 & -0.1226 & -0.1342 & 0.2925 & 0.1655 & -0.1202 & 1.2477 & 3.5257 & 0.0922 & -2.8765 & 0.2625 \\
-0.0037 & 0.0081 & 0.0302 & -0.0526 & 0.2203 & 0.0835 & -0.5749 & -0.0619 & -0.8938 & 4.2094 & -1.5096 & -0.0426 \\
-0.0288 & -0.0112 & -0.0342 & 0.0002 & 0.4766 & -0.1810 & -0.0143 & 0.3993 & 0.2083 & -0.0580 & -0.1922 & 6.7245 \\
0.0035 & -0.0055 & -0.0127 & -0.0312 & 0.4258 & 0.4290 & -0.1431 & -0.2952 & -0.4960 & -0.0067 & -8.1871 & 0.5865
\end{bmatrix}
$$

(5.45a)

For 4P hub interface joint loads due to 8P hub actuation,

$$
[\mathbf{C}_{H_{4/8}}] = 10^4 \times
\begin{bmatrix}
0.0001 & -0.0021 & -0.0005 & 0.0009 & 0.0003 & -0.0001 & 0.0017 & -0.0073 & -0.0065 & 0.0266 & 0.0021 & -0.0052 \\
-0.0012 & 0.0009 & -0.0001 & 0.0016 & -0.0003 & 0.0000 & 0.0036 & -0.0176 & -0.0041 & 0.0203 & -0.0048 & 0.0128 \\
-0.0004 & -0.0031 & -0.0018 & -0.0031 & 0.0025 & 0.0001 & -0.0120 & -0.0072 & -0.0213 & -0.0067 & -0.0060 & -0.0248 \\
0.0000 & -0.0016 & 0.0010 & 0.0026 & -0.0004 & 0.0065 & 0.0147 & -0.0138 & -0.0048 & 0.0216 & 0.0067 & 0.0022 \\
0.0123 & 0.0137 & 0.0178 & 0.0163 & 0.0083 & 0.0228 & -0.0216 & 0.0508 & 0.1349 & 0.1138 & 0.1316 & 0.1348 \\
0.0081 & 0.0144 & 0.0001 & 0.0062 & 0.0004 & 0.0076 & -0.0580 & 0.0743 & 0.0399 & -0.0009 & -0.0408 & 0.0519 \\
-0.0002 & 0.0328 & 0.0094 & -0.5996 & 0.0089 & 0.0690 & 0.0967 & -0.1441 & 0.3468 & 0.4883 & 0.1241 & 0.3411 \\
-0.0008 & 0.0017 & 0.0148 & 0.1827 & -0.0237 & -0.0190 & 0.0333 & 0.1566 & 0.1226 & -0.1036 & -0.0639 & 0.0890 \\
-0.0061 & -0.0342 & -0.0050 & -1.3330 & -0.0319 & -0.0337 & -0.0673 & 0.0509 & -0.1552 & -0.0565 & -0.2739 & -0.2546 \\
-0.0018 & -0.0342 & -0.0011 & -0.2651 & 0.0178 & -0.0391 & 0.0763 & 0.1101 & -0.4218 & -0.3658 & 0.0437 & -0.4112 \\
-0.0433 & -0.1293 & -0.0736 & 3.7321 & -0.0290 & -0.1371 & 0.1951 & -0.3260 & -0.8648 & -0.6110 & -0.5392 & -0.9326 \\
-0.0225 & -0.0490 & 0.0145 & 0.4054 & 0.0243 & -0.0209 & 0.3279 & -0.4412 & 0.0135 & 0.5080 & 0.4125 & 0.0675
\end{bmatrix}
$$

(5.45b)

For 8P hub interface joint loads due to 4P hub actuation,

$$
[\mathbf{C}_{H_{8/4}}] = 10^4 \times
\begin{bmatrix}
0.0026 & 0.0041 & 0.0026 & 0.0002 & 0.0065 & 0.0035 & 0.0180 & 0.0582 & 0.0600 & 0.0303 & 0.0019 & 0.0297 \\
0.0031 & 0.0035 & 0.0041 & 0.0040 & 0.0061 & 0.0036 & 0.0464 & 0.0447 & 0.0952 & 0.0823 & 0.0438 & 0.0204 \\
-0.0059 & -0.0068 & -0.0072 & -0.0047 & -0.0067 & -0.0042 & -0.0494 & -0.0587 & -0.1429 & -0.1259 & -0.0532 & -0.0539 \\
-0.0001 & -0.0005 & -0.0010 & -0.0047 & -0.0041 & 0.0035 & -0.0285 & 0.0238 & -0.0346 & -0.0195 & -0.0543 & -0.0140 \\
0.0089 & 0.0056 & 0.0067 & -0.0081 & 0.0021 & 0.0129 & 0.1674 & 0.1394 & 0.0401 & 0.0552 & -0.1283 & 0.0938 \\
0.0421 & 0.0353 & 0.0361 & 0.0263 & 0.0658 & 0.0224 & 0.5152 & 0.6610 & 0.7478 & 0.8181 & 0.2448 & 0.2691 \\
-0.0190 & -0.0275 & -0.0222 & -0.0099 & -0.0319 & -0.0152 & -0.1804 & -0.1851 & -0.3536 & -0.3439 & 0.1058 & 0.0397 \\
0.0182 & 0.0201 & 0.0046 & 0.0041 & 0.0254 & 0.0081 & -0.0127 & 0.3161 & 0.3670 & 0.1848 & -0.0291 & 0.4987 \\
-0.0055 & 0.0020 & 0.0090 & 0.0205 & 0.0029 & 0.0179 & 0.1391 & -0.0041 & 0.5911 & 0.1475 & 0.3062 & -0.0986 \\
-0.0316 & -0.0295 & -0.0300 & -0.0100 & -0.0455 & -0.0468 & -0.3246 & -0.2295 & -0.7601 & -0.4087 & 0.1365 & -0.2660 \\
-0.1271 & -0.0838 & -0.0992 & -0.0847 & -0.1850 & -0.0398 & -1.4289 & -1.4209 & -2.1158 & -2.2583 & -1.1741 & -0.8416 \\
0.1380 & 0.1093 & 0.1083 & 0.0473 & 0.1829 & 0.1200 & 1.6127 & 2.0162 & 2.3352 & 2.6169 & 0.5789 & 1.1202
\end{bmatrix}
$$

(5.45c)

43

For 8P hub interface joint loads due to 8P hub actuation,

$$[\mathbf{C}_{H_{8/8}}] = 10^5 \times \begin{bmatrix}
0.3497 & -0.0107 & 0.0051 & 0.0005 & 0.0004 & 0.0008 & 0.0020 & 0.0027 & 0.0291 & -0.0054 & 0.0066 & 0.0029 \\
0.0113 & 0.3502 & -0.0070 & 0.0154 & 0.0150 & 0.0010 & -0.0046 & 0.0052 & 0.0164 & 0.0300 & 0.0065 & 0.0057 \\
-0.0053 & -0.0084 & 0.3488 & -0.0264 & -0.0251 & -0.0031 & -0.0231 & 0.0041 & -0.0109 & -0.0009 & -0.0112 & -0.0099 \\
0.0072 & -0.0052 & 0.0108 & 0.0073 & 0.0066 & -0.0010 & -0.0068 & -0.0287 & -0.0057 & 0.0005 & -0.0022 & -0.0041 \\
-0.0007 & -0.0005 & -0.0004 & 0.0559 & 0.0540 & -0.0410 & 0.0082 & -0.0129 & 0.0012 & 0.0056 & -0.0436 & -0.1086 \\
0.0034 & 0.0061 & 0.0049 & 0.0050 & 0.0036 & 0.3381 & -0.0233 & 0.0084 & 0.0747 & 0.0503 & 0.1639 & 0.0015 \\
0.0025 & -0.0052 & -0.0055 & 0.0079 & -0.0040 & 0.0004 & 2.1830 & -0.0639 & -0.0627 & -0.0535 & -0.0332 & -0.0610 \\
0.0039 & 0.0065 & -0.0008 & 0.2161 & -0.0013 & 0.0001 & 0.0557 & 2.1796 & 0.0532 & -0.0209 & 0.0467 & -0.0032 \\
0.0058 & -0.0019 & 0.0032 & -0.3078 & -0.0007 & -0.0002 & 0.0233 & 0.0659 & 2.1922 & -0.0437 & 0.0088 & 0.0295 \\
0.0011 & 0.0008 & -0.0026 & 0.0968 & 0.0006 & -0.0048 & -0.0323 & 0.0179 & 0.0009 & 2.1769 & -0.0492 & -0.0363 \\
-0.0136 & -0.0186 & -0.0139 & 0.6445 & -0.0649 & -0.1811 & 0.1166 & -0.0568 & -0.2078 & -0.1365 & 6.1916 & -3.2330 \\
0.0057 & 0.0144 & 0.0120 & 0.2088 & 0.1645 & -0.0453 & -0.0409 & 0.0240 & 0.2184 & 0.1697 & 3.2380 & 6.4803
\end{bmatrix}$$

(5.45d)

For 4P swashplate interface joint loads due to 4P hub actuation,

$$[\mathbf{C}_{S_{4/4}}] = 10^3 \times \begin{bmatrix}
-0.0138 & 0.0021 & -0.0051 & -0.0018 & -0.0075 & -0.0019 & -0.0543 & 0.1119 & 0.1151 & -0.1799 & 0.0212 & -0.0745 \\
-0.0060 & -0.0093 & -0.0010 & -0.0047 & -0.0032 & 0.0046 & -0.2261 & -0.0119 & 0.0514 & 0.1905 & 0.0058 & 0.0565 \\
0.0010 & -0.0033 & -0.0036 & 0.0006 & -0.0035 & 0.0017 & -0.3062 & 0.0576 & -0.0228 & 0.1821 & 0.0442 & 0.0526 \\
0.0089 & 0.0079 & 0.0020 & -0.0019 & 0.0073 & 0.0045 & -0.0474 & -0.1903 & -0.0988 & 0.0913 & -0.0157 & 0.1211 \\
0.0194 & -0.0190 & 0.0300 & -0.0326 & -0.0696 & -0.0342 & -0.0882 & 0.1642 & -0.2141 & -0.0552 & -3.6747 & -1.4332 \\
0.0254 & 0.0325 & 0.0304 & 0.0532 & 0.0583 & -0.0568 & -0.0284 & 0.0396 & 0.0575 & 0.5948 & 1.7857 & -3.0352 \\
0.2049 & -0.0415 & 0.0668 & 0.0273 & 0.0981 & 0.0300 & -0.0712 & -1.4626 & -1.7935 & 3.1471 & -0.3432 & 1.0809 \\
0.1129 & 0.1581 & 0.0204 & 0.0663 & 0.0707 & -0.0579 & 3.1639 & -0.3705 & -1.0518 & -2.5459 & 0.0485 & -0.6286 \\
0.0236 & 0.0437 & 0.0662 & -0.0022 & 0.0759 & -0.0184 & 4.6688 & -1.1728 & 0.0187 & -2.1509 & -0.4502 & -0.5214 \\
-0.1143 & -0.0912 & -0.0286 & 0.0388 & -0.1001 & -0.0745 & 1.3385 & 2.8577 & 1.3036 & -1.8980 & 0.1669 & -1.7056 \\
0.0048 & -0.0051 & 0.0084 & -0.0093 & -0.0197 & -0.0098 & -0.0085 & 0.0476 & -0.0538 & -0.0340 & -1.0384 & -0.4082 \\
0.0064 & 0.0083 & 0.0084 & 0.0149 & 0.0159 & -0.0161 & -0.0150 & 0.0221 & 0.0248 & 0.1705 & 0.5031 & -0.8615
\end{bmatrix}$$

(5.45e)

For 4P swashplate interface joint loads due to 8P hub actuation,

$$[\mathbf{C}_{S_{4/8}}] = 10^3 \times \begin{bmatrix}
-0.0082 & -0.0079 & -0.0032 & -0.0042 & -0.0033 & -0.0069 & 0.0169 & -0.0245 & -0.1007 & -0.0731 & -0.1062 & -0.0763 \\
-0.0016 & -0.0036 & 0.0015 & 0.0005 & 0.0017 & -0.0043 & 0.0225 & -0.0337 & -0.0182 & -0.0499 & 0.0066 & -0.0812 \\
-0.0014 & -0.0049 & 0.0014 & 0.0029 & 0.0027 & -0.0027 & 0.0174 & -0.0378 & -0.0272 & -0.0183 & -0.0081 & -0.1002 \\
0.0057 & 0.0070 & 0.0010 & 0.0061 & 0.0041 & 0.0075 & 0.0053 & -0.0121 & 0.0850 & 0.0699 & 0.1088 & 0.0464 \\
-0.0477 & -0.0106 & -0.0460 & -0.0313 & -0.0075 & -0.0234 & 0.0949 & -0.5579 & -0.2422 & 0.1665 & -0.1210 & -0.1945 \\
-0.0140 & 0.0367 & 0.0490 & -0.0029 & 0.0168 & 0.0613 & -0.0048 & 0.1159 & 0.2004 & 0.1439 & 0.2055 & 0.1151 \\
0.1124 & 0.1027 & 0.0498 & 0.0672 & 0.0554 & 0.0927 & -0.1926 & 0.2197 & 1.3875 & 1.0121 & 1.5158 & 0.8231 \\
0.0400 & 0.0732 & -0.0167 & 0.0103 & -0.0129 & 0.0873 & -0.3101 & 0.4783 & 0.5247 & 0.9226 & 0.2210 & 1.3114 \\
0.0452 & 0.0939 & -0.0085 & -0.0289 & -0.0288 & 0.0603 & -0.3016 & 0.6659 & 0.6928 & 0.4599 & 0.4292 & 1.6796 \\
-0.0771 & -0.0944 & -0.0199 & -0.0908 & -0.0648 & -0.0997 & -0.1600 & 0.2726 & -1.1909 & -0.8928 & -1.6105 & -0.4436 \\
-0.0137 & -0.0030 & -0.0132 & -0.0091 & -0.0024 & -0.0067 & 0.0264 & -0.1559 & -0.0706 & 0.0450 & -0.0379 & -0.0520 \\
-0.0044 & 0.0098 & 0.0138 & -0.0011 & 0.0045 & 0.0167 & -0.0006 & 0.0319 & 0.0505 & 0.0343 & 0.0518 & 0.0265
\end{bmatrix}$$

(5.45f)

For 8P swashplate interface joint loads due to 4P hub actuation,

$$[C_{S_{8/4}}] = 10^3 \times \begin{bmatrix}
-0.0055 & -0.0076 & -0.0038 & -0.0004 & -0.0095 & -0.0018 & -0.0046 & -0.0594 & -0.0860 & -0.0755 & 0.0408 & -0.1493 \\
0.0024 & -0.0045 & -0.0042 & -0.0038 & -0.0035 & -0.0062 & -0.0057 & 0.0173 & -0.0468 & -0.0387 & 0.0865 & 0.0350 \\
-0.0007 & 0.0063 & 0.0055 & 0.0031 & 0.0038 & 0.0060 & 0.0092 & -0.0061 & 0.0457 & 0.0559 & -0.0891 & -0.0549 \\
-0.0041 & -0.0045 & -0.0013 & 0.0019 & -0.0058 & -0.0013 & 0.0197 & -0.0425 & -0.0630 & -0.0448 & 0.0827 & -0.1365 \\
-0.0267 & -0.0297 & -0.0412 & -0.0098 & -0.0306 & -0.0216 & -0.3239 & -0.4213 & -0.3923 & -0.4334 & 0.2449 & -0.4621 \\
-0.0183 & -0.0274 & -0.0274 & -0.0437 & -0.0380 & -0.0147 & -0.2268 & -0.3427 & -0.4945 & -0.5183 & 0.1661 & 0.0989 \\
0.0733 & 0.1213 & 0.0655 & 0.0108 & 0.1410 & 0.0409 & 0.0316 & 0.7768 & 1.2959 & 1.2321 & -0.8264 & 1.9072 \\
-0.0458 & 0.0513 & 0.0559 & 0.0568 & 0.0305 & 0.0851 & 0.1220 & -0.4033 & 0.3934 & 0.3921 & -0.9636 & -0.8724 \\
0.0302 & -0.0635 & -0.0604 & -0.0423 & -0.0209 & -0.0773 & -0.0652 & 0.2957 & -0.3321 & -0.4998 & 1.0959 & 1.3223 \\
0.0560 & 0.0829 & 0.0382 & -0.0086 & 0.1003 & 0.0397 & -0.1789 & 0.6268 & 1.1259 & 0.8686 & -1.4917 & 1.8268 \\
-0.0077 & -0.0102 & -0.0130 & -0.0034 & -0.0100 & -0.0075 & -0.0936 & -0.1219 & -0.1252 & -0.1384 & 0.0910 & -0.1275 \\
-0.0041 & -0.0070 & -0.0077 & -0.0129 & -0.0097 & -0.0043 & -0.0673 & -0.0866 & -0.1286 & -0.1386 & 0.0346 & 0.0595
\end{bmatrix}$$

(5.45g)

For 8P swashplate interface joint loads due to 8P hub actuation,

$$[C_{S_{8/8}}] = 10^4 \times \begin{bmatrix}
0.0083 & -0.0013 & 0.0000 & -0.0007 & -0.0002 & -0.0004 & 0.0084 & 0.0167 & -0.0263 & -0.0029 & -0.0065 & 0.0989 \\
-0.0029 & -0.0005 & 0.0002 & 0.0002 & -0.0003 & -0.0002 & -0.0168 & 0.0060 & -0.0016 & -0.0230 & -0.0039 & -0.0477 \\
-0.0019 & 0.0009 & 0.0000 & 0.0000 & 0.0009 & -0.0004 & 0.0191 & 0.0022 & 0.0102 & 0.0212 & 0.0021 & -0.0418 \\
0.0000 & -0.0008 & 0.0000 & -0.0006 & 0.0006 & 0.0003 & -0.0003 & 0.0193 & -0.0211 & 0.0067 & -0.0029 & -0.0049 \\
-0.0247 & -0.0032 & -0.0020 & 0.0010 & -0.0217 & 0.0156 & 0.0067 & 0.0088 & -0.0366 & -0.0109 & -0.0578 & -0.1989 \\
0.1782 & -0.0031 & -0.0051 & -0.0024 & -0.0209 & -0.0270 & 0.0019 & -0.0067 & -0.0622 & -0.0408 & -0.0896 & 2.0997 \\
-0.1261 & 0.0210 & -0.0008 & 0.0108 & 0.0028 & 0.0049 & -0.0682 & -0.2340 & 0.3730 & 0.1005 & 0.0891 & -1.5497 \\
0.0516 & 0.0044 & -0.0030 & -0.0049 & 0.0052 & -0.0002 & 0.2407 & -0.0351 & -0.0443 & 0.3184 & 0.0405 & 0.7920 \\
0.0106 & -0.0082 & 0.0006 & 0.0015 & -0.0087 & 0.0038 & -0.2735 & -0.0817 & -0.0699 & -0.2952 & -0.0036 & 0.3968 \\
-0.0047 & 0.0142 & 0.0005 & 0.0077 & -0.0035 & 0.0005 & 0.0536 & -0.2678 & 0.3212 & -0.0260 & 0.0714 & 0.0510 \\
-0.0066 & -0.0012 & -0.0006 & 0.0002 & -0.0063 & 0.0045 & -0.0013 & 0.0030 & -0.0140 & -0.0077 & -0.0173 & -0.0507 \\
0.0501 & -0.0007 & -0.0014 & -0.0006 & -0.0060 & -0.0077 & -0.0004 & -0.0052 & -0.0131 & -0.0141 & -0.0247 & 0.5904
\end{bmatrix}$$

(5.45h)

As shown, the form of the matrices are not indicative of a linear system. The reader is referred to equation (5.45a), which presents the impedance matrix component for the 4P hub interface joint response due to 4P actuation. The submatrix labeled A shows that, unlike the mobility and motion matrices, the diagonal elements of the submatrices are unequal for the impedance matrix. Similarly, the off-diagonal submatrix terms are not equal and opposite as for the mobility and motion matrices.

5.3.2.4. System linearity. Because the impedance matrices generated for the BRR are not typical of those for fully linear systems, immediate concern is raised as to the applicability of the impedance-matching approach to the rotor system. Therefore, a study has been performed which validates the impedance matrices for translational 4P hub motions with amplitudes of 0.015 in. and rotational 4P hub motions with amplitudes of 0.10°. Figure 5.3 shows representative results for 4P axial hub motions ranging from –0.015 to 0.015 in. As shown, the axial hub load response for the range of motion shown remains linear with respect to the imposed hub motions. This type of response indicates that the impedance-matching method is applicable for the range of motions expected from this study.

5.3.3. System Coupling

The final step necessary to couple the BRR system to the ARES-II is the generation and application of the system coupling equations. These equations are generated in a manner similar to that used for the sample model (section 5.1.4). The motion of the interface joints is most easily defined by observing the system from the point of
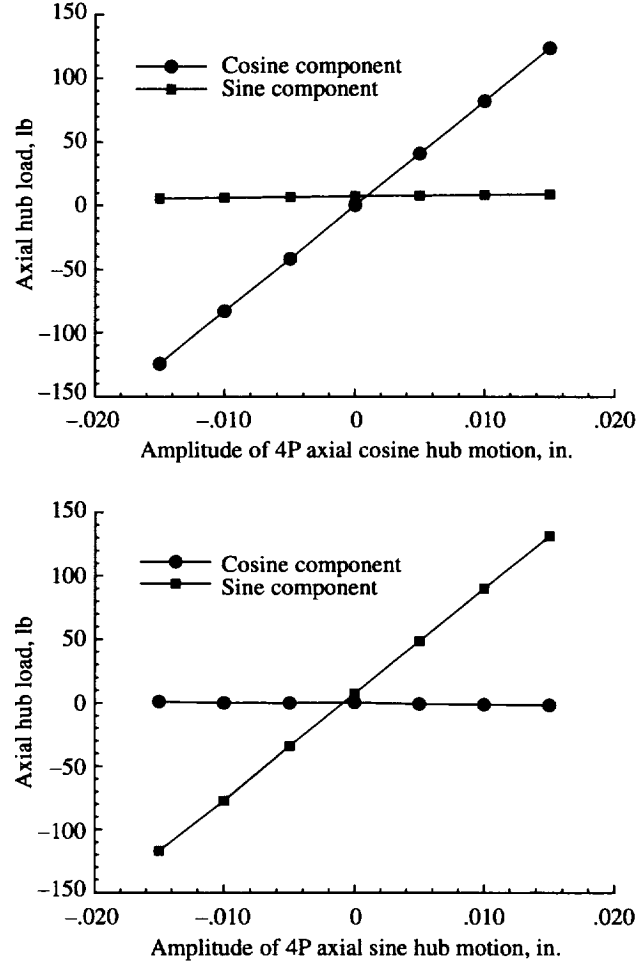
Figure 5.3. BRR model linearity for axial cosine and sine hub motion excitations.

view of ARES-II. Utilizing the mobility equation (eq. (5.35)), the motion equation (eq. (5.39)), and the linear theory of superposition, the motion of the interface joints on the ARES-II may be expressed as

$$\{X_I\} = [A]\{F_I\} + [B]\{U\}$$ (5.46)

Load compatibility is enforced at the interface joints by substituting the rotor impedance equation (eq. (5.41)) into equation (5.46). Displacement compatibility is then enforced by solving for the interface joint displacements $\{X_I\}$ as follows:

$$\{X_I\} = \Big[[I] - [A][C]\Big]^{-1}\Big\{[A]\{F_0\} + [B]\{U\}\Big\}$$ (5.47)

The interface joint forces $\{F_I\}$ are determined by substituting equation (5.47) into equation (5.41) which gives

$$\{F_I\} = \{F_0\} + [C]\Big[[I] - [A][C]\Big]^{-1}\Big\{[A]\{F_0\} + [B]\{U\}\Big\}$$ (5.48)

46

5.3.4. System Loads

The development of system loads throughout the ARES-II testbed is of interest. Of particular importance for this study are the loads generated at each of the system balances. Therefore, a general set of equations has been developed to define the loads in the ARES-II. The approach taken has been to generate two sets of matrices. The first set [D] defines the loads transfer from the interface joints to locations throughout the ARES-II, and the second set [E] defines the effect of actuation on ARES-II component loads.

The load transfer matrices are developed in a manner identical to that used to develop the system mobility matrices in section 5.3.1.2. The only difference is that a load response due to load excitation is developed instead of a motion response due to load excitation. The DADS runs used to develop the mobility matrix are used to define the load response; hence, no additional runs are required to develop the matrix [D]. The matrices defining the effects of actuation on system loads are developed in a manner identical to the motion matrix development described in section 5.3.1.3. Again, the DADS runs that have already been made supply all information necessary to develop the matrix [E]. The loads vector {L} may then be established by using

$$\{L\} = [D]\{F_I\} + [E]\{U\} \qquad (5.49)$$

6. Presentation of Results

Results from independent, uncoupled analysis of the ARES-II and the BRR models are presented in sections 6.1 and 6.2; coupled analysis results are presented in section 6.3. Because of the volume of results presented, tables and figures for section 6 are placed at the end of the section rather than integrated in the text.

6.1. ARES-II Motion Actuation

The actuator motion analysis of section 4.1.2 was used to develop time-varying actuator length schedules for all ARES-II actuation in DADS. For all results presented, a simulated center of gravity was chosen which was placed on the rotor shaft centerline and 10.0 in. above the fixed-system balance center. Figure 6.1 presents a representative actuator length schedule for 0.01 in. 4P axial sine motion of an inflexible ARES-II model by using the equations developed in section 4.1.2. However, application of motions to the DADS elastic model of the ARES-II produces a different response. Table 6.1 presents the response at the hub interface joint using actuator schedules that command 0.01 in. 4P sine translation and 0.05° 4P sine rotation. The columns of table 6.1 represent the 4P sine motion commanded. The rows represent the cosine and sine components of the hub interface joint response of the elastic model due to the commanded motion. As shown by the table, the desired motion is either attenuated or amplified, phase shift is evident, and some significant coupling of pylon motion exists.

When the elastic model of the ARES-II is considered, the Stewart platform must account for the dynamic response of the system to produce the desired motion. The motion matrix for the hub $[B_{H_4}]$ from equation (5.36a) may be used to calculate a control vector that provides a specified hub interface joint motion as follows:

$$\{U\} = [B_{H_4}]^{-1}\{X_{H_4}\} \qquad (6.1)$$

Figure 6.2 presents the actuator schedule required to obtain a pure 0.01 in. 4P axial (x direction) translational motion of the rotor hub interface joint when flexibility is included in the model. A comparison of figure 6.2 with figure 6.1 indicates the difference in actuator motion required to obtain pure hub motions for the flexible model.

47

6.2. BRR Fixed-Hub Loads

A fixed-hub load vector $\{F_0\}$ was obtained with the CAMRAD-II model of the BRR for each forward flight condition listed in table 5.1. The results for the 4P components of the load are presented in figure 6.3 along with the total magnitude of the load transmitted to the fixed system by the hub and swashplate interface joint loads. For this figure, the total magnitude has been calculated with

$$F_{\text{total}} = \sqrt{(F_{H_c} + F_{S_c})^2 + (F_{H_s} + F_{S_s})^2}$$

$$M_{\text{total}} = \sqrt{(M_{H_c} + M_{S_c})^2 + (M_{H_s} + M_{S_s})^2}$$

This formulation neglects the effect of lateral swashplate loads on the total hub moment; however, these loads are small for all cases.

The trends observed for total magnitude as a function of flight speed are typical of those encountered with all rotor systems. Typically, low-speed flight ($\mu \approx 0.05$) vibrations are generally minimal but increase rapidly through $\mu \approx 0.10$ because of a phenomenon called transition in which many blade-vortex interactions occur. Vibratory loads through the cruising range ($\mu \approx 0.20$ to 0.25) are generally low, but loads increase again at the higher flight speeds ($\mu \geq 0.30$). Of particular note is the magnitude of the fixed-system swashplate loads at the high speeds ($\mu \geq 0.30$) for normal force and pitching and rolling moments. If these loads were neglected as has been common practice throughout much of the literature, an inaccurate assessment (up to 30 percent error) of the total fixed-system loads would result. Additionally, for the ARES-II configuration in which the loads sensed by both the rotating- and fixed-system balances are important; neglecting the swashplate loads would result in a serious deficiency in the balance loads prediction.

6.3. BRR/ARES-II Coupled Results

Because the system coupling method developed in section 5.3.3 requires only simple matrix operations, coupled rotor-testbed solutions for a wide range of ARES-II motions may be obtained in a very short time. Because of this, a large volume of results have been obtained from this study. Selected results have been chosen for presentation in this section. Tables 6.2 and 6.3 present representative interface joint motions and loads and allow the comparison of the uncoupled rotor loads with the coupled rotor loads. Tables 6.4 and 6.5 present the loads at the fixed-system and rotating-system balances.

The notation used throughout the tables is straightforward. Displacements are identified as translational (or linear) motions along an axis (L_X, L_Y, L_Z), or as rotational (or angular) motions about an axis (A_X, A_Y, A_Z). Interface joint locations are identified with either H for the hub or S for the swashplate. Amplitudes are identified by their frequency (4P or 8P) and the component (cosine or sine). For example, H8S refers to an 8P sine component amplitude at the hub interface joint. Forces and moments are presented in units of pounds and inch-pounds. Displacements are presented in units of inches and degrees.

The rotor-testbed coupled results in tables 6.2 and 6.3 are obtained with equations (5.47) and (5.48). Table 6.2 presents the motion and loads for the three forward flight speeds: $\mu = 0.10$ (transition), $\mu = 0.20$ (cruise), and $\mu = 0.30$ (high speed). No pylon actuation was used. Table 6.3 presents the motion and loads for representative pylon actuation schedules at a low-speed advance ratio $\mu = 0.10$. Results are included for 0.01 in. 4P sine actuation of the three translational motions (tables 6.3(b) through (d)), and for 0.05° 4P sine actuation of the pitch motion (table 6.3(e)). Also presented are results for 0.01 in. 4P cosine actuation in the axial direction (table 6.3(a)) to demonstrate representative differences in results due to cosine versus sine actuation.

The balance loads results for the coupled system are obtained with equation (5.49). Table 6.4 presents the balance loads for $\mu = 0.10$ without pylon actuation. Therefore, these results may be compared with those presented in

48

table 6.2(a). Table 6.5 presents the balance loads for the five pylon actuation schedules used to generate the results in table 6.3.

The fidelity of the balance measurements for normal force and pitch and roll moments are presented in figure 6.4 for the coupled system without actuated motion. In this figure, the balance moments shown are corrected for the moments produced by the interface joint lateral forces and presented throughout the forward flight speed range. The correction equations are

$$
\left.\begin{array}{l}
M_{x_{RB_{corr}}} = M_{x_{RB}} + 4.213 F_{H_y} \\[2mm]
M_{y_{RB_{corr}}} = M_{y_{RB}} - 4.213 F_{H_x} \\[2mm]
M_{x_{FB_{corr}}} = M_{x_{FB}} + 23.538 F_{H_y} + 15.318 F_{S_y} \\[2mm]
M_{y_{FB_{corr}}} = M_{y_{FB}} - 23.538 F_{H_x} - 15.318 F_{S_x}
\end{array}\right\}
\tag{6.2}
$$

Table 6.6 presents the results obtained by using the control vector inputs necessary to obtain 0.01 in. 4P axial sine motion at the hub interface joint for the coupled rotor-testbed. The control inputs were established by using an iterative solution technique to minimize the phase shift and coupling evident in the results presented in table 6.3(b). No closed-form method of calculating the proper control inputs as for the stand-alone ARES-II (section 6.1) is possible. As shown, significant changes in control inputs are necessary to achieve proper hub motion, particularly for the sine components of the axial and pitch actuation.

Several observations regarding the results obtained for the coupled system are offered as follows:

1. Although the loads due to coupling (i.e., the impedance forces and moments) $[C]\{X_I\}$ are generally small for the unactuated cases (table 6.2), they are significant enough that considering their effects is useful, particularly for the axial and side loads where the loads due to coupling can be as large as or larger than the uncoupled loads $\{F_0\}$. A case could be made for neglecting the loads due to coupling for the normal force and the moments because their contributions are small for the unactuated results.

2. When the pylon is actuated, including the loads due to coupling becomes critical in the analysis. Some of the load may be attributed to the dynamic load associated with actuating the rotor system. However, a significant portion of the load is due to the change in the aerodynamic response of the rotor.

3. The motion response is greatly affected by the rotor system for the actuated cases. Comparison of the results of the testbed alone (table 6.1) with the results for the coupled rotor-testbed (table 6.3) indicates that significantly different hub motions may be expected when the rotor is coupled to the ARES-II. All motions have been observed to grow for the coupled system. For the axial motion, the growth is fortuitous because a response close to that requested by the control vector results. This response is, however, dependent upon the rotor system and flight parameters selected.

4. The motion response is typically amplified compared with the input control vector $\{U\}$ for the actuated cases. The exception to this is for side motion in which the motion is attenuated. Some motions can be significantly larger than expected based on the input control vector. For example, the displacements associated with pitch actuation (table 6.3(e)) are nearly three times larger than the input. Additionally, the axial response (L_X) for these conditions exceeds twice the range established for the linear response range of the rotor

49

system. To ensure validity of the results, more CAMRAD-II runs would have to be made to determine the boundaries of the linear range. Furthermore, as indicated in table 6.5(e), the pitching moment at the fixed-system balance is excessive for the actuated pitch motion. These loads are in excess of the balance limits and would damage the balance.

5. Because of the observations in paragraph 4 and the phase shift and coupled rotor pylon motions evident throughout the results, it is apparent that a closed-loop control system must be implemented to account for the dynamic response of the system and provide the desired motion at the rotor hub. A comparison of table 6.6, in which the inputs are chosen to provide the desired hub interface joint motion, and table 6.3(b), in which the desired motions are input for the control vector, illustrates the importance of a closed-loop control system for proper performance of the ARES-II.

6. The measurement potential of the rotating balance loads is much better than that of the fixed-system balance. Significant loads due to the dynamic response of the ARES-II are apparent throughout the results of the fixed-system balance loads. The rotating balance shows minimal effect due to dynamic response. Therefore, if a reliable means of measuring the swashplate interface loads during wind tunnel testing is identified (e.g., strain-gauge pitch links), better system loads may be obtained by using the rotating balance rather than the fixed-system balance

Table 6.1. Hub Interface Joint Response Due to Actuated 4P Sine Motion

[No rotor model]

Type of hub joint response	Commanded 4P sine motion for—					
	0.01 in. axial	0.01 in. side	0.01 in. normal	0.05° roll	0.05° pitch	0.05° yaw
Axial cos	−0.0008	0.0000	−0.0010	0.0000	−0.0008	0.0000
Axial sin	0.0069	0.0000	0.0054	0.0000	0.0233	0.0000
Side cos	0.0000	−0.0006	0.0000	−0.0001	0.0000	0.0003
Side sin	0.0001	0.0062	0.0001	−0.0156	0.0001	0.0019
Normal cos	−0.0001	0.0000	−0.0011	0.0000	−0.0006	0.0000
Normal sin	0.0000	0.0000	0.0103	0.0000	0.0006	0.0000
Roll cos	0.0000	0.0011	0.0000	0.0002	0.0000	−0.0005
Roll sin	−0.0001	−0.0048	−0.0001	0.0545	−0.0001	0.0024
Pitch cos	−0.0017	0.0000	−0.0026	0.0000	−0.0022	0.0000
Pitch sin	0.0066	0.0000	0.0154	0.0000	0.0766	0.0000
Yaw cos	0.0000	0.0004	0.0000	0.0001	0.0000	−0.0004
Yaw sin	0.0000	−0.0064	0.0000	−0.0020	0.0000	0.0666

Table 6.2. Coupled Rotor-Testbed Results for No Actuated Motion

(a) $\mu = 0.10$

Component	L_X	L_Y	L_Z	A_X	A_Y	A_Z
Input control vector {U}						
4C	0.000000	0.000000	0.000000	0.000000	0.000000	0.000000
4S	0.000000	0.000000	0.000000	0.000000	0.000000	0.000000
Hub and swashplate interface displacements {X$_I$}						
H4C	−0.000172	−0.000594	0.000003	0.004305	−0.000708	−0.003719
H4S	0.000866	−0.000251	0.000092	0.001885	0.005145	0.001361
S4C	−0.000082	−0.000140	−0.000004	0.001663	−0.000437	−0.000990
S4S	0.000296	−0.000080	0.000089	0.000391	0.002483	0.000365
H8C	0.000000	0.000055	0.000029	−0.000380	−0.000032	0.000074
H8S	0.000002	−0.000187	−0.000064	0.000186	−0.000077	−0.001580
S8C	0.000001	0.000021	0.000030	−0.000060	0.000035	0.000556
S8S	0.000009	−0.000154	−0.000065	0.000294	−0.000023	−0.001419

Component	F_X	F_Y	F_Z	M_X	M_Y	M_Z
Hub and swashplate interface forces and moments {F$_I$}						
H4C	−1.65	−15.74	19.28	62.01	−2.34	−132.93
H4S	14.20	0.76	8.36	71.31	67.46	52.75
S4C	0.42	−0.11	−0.15	−6.38	0.52	−0.02
S4S	−0.07	−0.04	7.16	1.34	0.26	2.02
H8C	−0.26	1.98	−2.58	−7.05	−2.27	−24.14
H8S	0.75	0.07	5.01	−5.13	−5.59	−6.57
S8C	−0.04	−0.01	0.17	0.56	0.24	0.05
S8S	0.04	0.00	−0.95	−0.61	−0.03	−0.27
Hub and swashplate forces and moments for fixed-hub condition {F$_0$}						
H4C	−0.22	−11.11	19.25	58.31	−3.71	−122.66
H4S	7.22	2.89	7.52	70.28	64.34	57.23
S4C	0.43	−0.10	−0.33	−6.53	0.43	−0.07
S4S	−0.07	−0.04	7.32	1.31	0.33	2.06
H8C	−0.34	−0.31	−2.58	−4.98	−7.73	−20.14
H8S	0.90	0.09	6.06	−2.23	−2.84	10.06
S8C	0.00	−0.04	0.23	−0.12	0.44	0.07
S8S	0.03	0.02	−0.31	−0.46	−0.25	−0.09
Impedance forces and moments [C] {X$_I$}						
H4C	−1.42	−4.64	0.03	3.70	1.37	−10.27
H4S	6.98	−2.13	0.84	1.03	3.12	−4.49
S4C	−0.01	0.00	0.18	0.15	0.09	0.05
S4S	0.00	0.01	−0.15	0.03	−0.07	−0.04
H8C	0.08	2.29	0.00	−2.07	5.46	−4.00
H8S	−0.15	−0.02	−1.06	−2.90	−2.75	−16.63
S8C	−0.04	0.02	−0.06	0.68	−0.19	−0.02
S8S	0.01	−0.01	−0.64	−0.15	0.22	−0.18

51

Table 6.2. Continued

(b) $\mu = 0.20$

Component	L_X	L_Y	L_Z	A_X	A_Y	A_Z
Input control vector {U}						
4C	0.000000	0.000000	0.000000	0.000000	0.000000	0.000000
4S	0.000000	0.000000	0.000000	0.000000	0.000000	0.000000
Hub and swashplate interface displacements {X_I}						
H4C	−0.000096	−0.000353	0.000011	0.002647	−0.000420	−0.000670
H4S	0.000632	−0.000059	0.000035	0.000465	0.003761	0.002128
S4C	−0.000049	−0.000075	0.000009	0.001005	−0.000179	−0.000218
S4S	0.000214	−0.000019	0.000035	0.000055	0.001814	0.000529
H8C	−0.000017	0.000039	0.000111	−0.000072	−0.000082	0.000468
H8S	−0.000010	0.000135	0.000074	−0.000867	−0.000263	0.000386
S8C	−0.000013	0.000031	0.000114	−0.000061	0.000037	0.000494
S8S	0.000006	0.000053	0.000076	−0.000174	0.000076	0.001194

Component	F_X	F_Y	F_Z	M_X	M_Y	M_Z
Hub and swashplate interface forces and moments {F_I}						
H4C	0.05	−9.02	6.78	41.07	−9.08	−20.08
H4S	10.70	1.73	−0.95	24.78	48.09	79.31
S4C	0.23	−0.16	3.76	−3.75	1.18	1.08
S4S	−0.26	0.05	2.63	3.76	−0.23	0.74
H8C	−1.27	1.25	−8.23	3.12	−1.21	−3.52
H8S	−1.13	4.59	−6.42	−13.28	−11.21	−39.74
S8C	−0.01	−0.06	1.33	0.05	0.54	0.39
S8S	−0.01	−0.04	0.63	−0.07	0.40	0.19
Hub and swashplate forces and moments for fixed-hub condition {F_0}						
H4C	0.89	−6.29	6.66	39.81	−8.27	−17.03
H4S	5.60	2.24	−1.34	24.43	45.76	79.99
S4C	0.24	−0.16	3.78	−3.81	1.21	1.09
S4S	−0.26	0.05	2.75	3.80	−0.22	0.78
H8C	−0.80	0.06	−11.49	3.27	−0.81	−4.95
H8S	−0.79	−0.19	−9.36	−9.98	−10.16	−47.82
S8C	−0.01	−0.06	1.33	−0.01	0.46	0.39
S8S	−0.01	−0.03	0.69	−0.02	0.35	0.20
Impedance forces and moments [C] {X_I}						
H4C	−0.84	−2.74	0.12	1.26	−0.81	−3.05
H4S	5.10	−0.51	0.38	0.35	2.33	−0.69
S4C	0.00	0.00	−0.01	0.06	−0.02	0.00
S4S	0.00	0.00	−0.12	−0.04	−0.01	−0.04
H8C	−0.47	1.20	3.26	−0.15	−0.41	1.43
H8S	−0.34	4.78	2.94	−3.30	−1.05	8.08
S8C	−0.01	0.00	0.00	0.07	0.08	0.00
S8S	0.00	0.00	−0.05	−0.05	0.06	−0.01

Table 6.2. Concluded

(c) $\mu = 0.30$

Component	L_X	L_Y	L_Z	A_X	A_Y	A_Z
Input control vector {U}						
4C	0.000000	0.000000	0.000000	0.000000	0.000000	0.000000
4S	0.000000	0.000000	0.000000	0.000000	0.000000	0.000000
Hub and swashplate interface displacements {X_I}						
H4C	−0.000248	−0.000408	−0.000002	0.003031	−0.001280	−0.000712
H4S	0.000589	0.000212	0.000055	−0.001620	0.003460	0.002437
S4C	−0.000108	−0.000094	−0.000004	0.001078	−0.000562	−0.000214
S4S	0.000200	0.000033	0.000052	−0.000729	0.001724	0.000657
H8C	−0.000035	0.000007	0.000100	0.000078	−0.000354	0.000455
H8S	−0.000010	0.000201	0.000096	−0.000956	−0.000325	0.000903
S8C	−0.000011	0.000017	0.000102	−0.000008	0.000023	0.000153
S8S	0.000010	0.000102	0.000098	−0.000291	0.000092	0.001979

Component	F_X	F_Y	F_Z	M_X	M_Y	M_Z
Hub and swashplate interface forces and moments {F_I}						
H4C	−1.85	−9.50	3.91	52.23	−24.10	−22.05
H4S	11.00	9.27	8.30	−6.10	37.29	88.27
S4C	0.97	0.30	7.95	−14.08	−8.16	2.16
S4S	−0.93	0.02	0.39	13.41	1.57	0.13
H8C	−0.49	−0.16	−4.59	1.76	−17.05	11.94
H8S	−1.99	7.23	−8.11	−0.69	−10.63	−53.83
S8C	−0.43	0.03	−1.33	6.42	1.29	−0.29
S8S	0.01	−0.30	0.87	−0.79	3.92	0.36
Hub and swashplate forces and moments for fixed-hub condition {F_0}						
H4C	0.49	−6.19	4.04	55.23	−24.67	−15.62
H4S	6.33	1.76	7.73	−3.88	40.23	104.27
S4C	0.98	0.31	8.02	−14.16	−8.28	2.18
S4S	−0.93	0.01	0.53	13.29	1.58	0.17
H8C	0.67	−0.18	−7.08	1.14	−16.33	15.64
H8S	−1.67	0.26	−11.60	3.25	−9.54	−66.27
S8C	−0.45	0.03	−1.48	6.79	1.35	−0.33
S8S	0.00	−0.31	0.86	−0.78	4.10	0.36
Impedance forces and moments [C] {X_I}						
H4C	−2.34	−3.31	−0.14	−3.01	0.57	−6.43
H4S	4.68	7.50	0.57	−2.22	−2.95	−16.00
S4C	−0.01	−0.01	−0.07	0.08	0.12	−0.02
S4S	−0.01	0.00	−0.14	0.11	−0.01	−0.04
H8C	−1.16	0.02	2.49	0.61	−0.72	−3.70
H8S	−0.33	6.97	3.49	−3.94	−1.09	12.44
S8C	0.02	0.00	0.14	−0.37	−0.07	0.04
S8S	0.00	0.01	0.01	−0.01	−0.19	0.00

Table 6.3. Coupled Rotor-Testbed Results for Actuated Motion

(a) 0.01 in. 4P axial cosine actuation; $\mu = 0.10$

Component	L_X	L_Y	L_Z	A_X	A_Y	A_Z
Input control vector {U}						
4C	0.010000	0.000000	0.000000	0.000000	0.000000	0.000000
4S	0.000000	0.000000	0.000000	0.000000	0.000000	0.000000
Hub and swashplate interface displacements {X_I}						
H4C	0.010146	−0.000448	0.000095	0.004010	0.025044	−0.004780
H4S	0.002971	−0.000358	0.000265	0.002768	0.012598	0.001454
S4C	0.006981	−0.000032	0.000086	0.001466	0.017423	−0.001232
S4S	0.001412	−0.000090	0.000261	0.000777	0.007917	0.000356
H8C	0.000017	0.000137	0.000024	−0.000819	0.000401	0.000242
H8S	0.000008	−0.000531	−0.000148	0.000745	−0.000271	−0.004271
S8C	−0.000016	0.000060	0.000025	−0.000155	0.000043	0.001358
S8S	0.000029	−0.000420	−0.000152	0.000822	−0.000043	−0.003970

Component	F_X	F_Y	F_Z	M_X	M_Y	M_Z
Hub and swashplate interface forces and moments {F_I}						
H4C	83.11	−14.72	22.92	62.23	8.06	−173.05
H4S	33.20	−3.26	9.81	78.27	71.01	58.84
S4C	0.32	−0.09	−0.02	−4.80	0.50	0.01
S4S	−0.10	0.03	7.55	1.94	−0.72	2.12
H8C	1.04	4.24	−2.35	−13.54	12.23	−55.77
H8S	1.30	−0.27	11.83	−6.11	−17.48	−11.61
S8C	−0.21	0.04	−0.35	3.05	0.00	−0.11
S8S	0.05	−0.08	−2.43	−1.10	1.35	−0.66
Hub and swashplate forces and moments for fixed-hub condition {F_0}						
H4C	−0.22	−11.11	19.25	58.31	−3.71	−122.66
H4S	7.22	2.89	7.52	70.28	64.34	57.23
S4C	0.43	−0.10	−0.33	−6.53	0.43	−0.07
S4S	−0.07	−0.04	7.32	1.31	0.33	2.06
H8C	−0.34	−0.31	−2.58	−4.98	−7.73	−20.14
H8S	0.90	0.09	6.06	−2.23	−2.84	10.06
S8C	0.00	−0.04	0.23	−0.12	0.44	0.07
S8S	0.03	0.02	−0.31	−0.46	−0.25	−0.09
Impedance forces and moments [C] {X_I}						
H4C	83.34	−3.61	3.67	3.92	11.77	−50.39
H4S	25.98	−6.16	2.28	7.99	6.67	1.61
S4C	−0.12	0.02	0.31	1.74	0.07	0.08
S4S	−0.03	0.08	0.24	0.63	−1.05	0.06
H8C	1.38	4.55	0.24	−8.56	19.96	−35.63
H8S	0.40	−0.36	5.76	−3.88	−14.64	−21.67
S8C	−0.21	0.08	−0.58	3.16	−0.44	−0.19
S8S	0.02	−0.10	−2.12	−0.64	1.60	−0.58

Table 6.3. Continued

(b) 0.01 in. 4P axial sine actuation; $\mu = 0.10$

Component	L_X	L_Y	L_Z	A_X	A_Y	A_Z
Input control vector {U}						
4C	0.000000	0.000000	0.000000	0.000000	0.000000	0.000000
4S	0.010000	0.000000	0.000000	0.000000	0.000000	0.000000
Hub and swashplate interface displacements {X_I}						
H4C	−0.002280	−0.000559	−0.000160	0.003915	−0.008200	−0.004179
H4S	0.011221	−0.000041	0.000184	0.001161	0.031117	0.001325
S4C	−0.001201	−0.000151	−0.000167	0.001450	−0.005849	−0.001072
S4S	0.007370	0.000047	0.000180	0.000029	0.020460	0.000376
H8C	0.000007	0.000095	0.000030	−0.000605	0.000174	0.000145
H8S	0.000007	−0.000370	−0.000109	0.000477	−0.000149	−0.003004
S8C	−0.000008	0.000040	0.000031	−0.000104	0.000040	0.000936
S8S	0.000019	−0.000295	−0.000112	0.000576	−0.000034	−0.002776

Component	F_X	F_Y	F_Z	M_X	M_Y	M_Z
Hub and swashplate interface forces and moments {F_I}						
H4C	−20.11	−13.06	20.16	64.38	−10.89	−151.60
H4S	99.70	3.34	9.58	65.10	79.69	50.92
S4C	0.38	−0.05	−0.35	−5.60	−0.11	−0.08
S4S	−0.07	0.08	7.69	1.67	−1.48	2.16
H8C	0.42	2.93	−2.60	−11.48	4.37	−39.57
H8S	1.13	−0.10	8.80	−5.97	−10.72	−8.98
S8C	−0.15	0.08	−0.18	2.39	−0.78	−0.07
S8S	−0.01	−0.04	−1.86	−0.03	0.92	−0.52
Hub and swashplate forces and moments for fixed-hub condition {F_0}						
H4C	−0.22	−11.11	19.25	58.31	−3.71	−122.66
H4S	7.22	2.89	7.52	70.28	64.34	57.23
S4C	0.43	−0.10	−0.33	−6.53	0.43	−0.07
S4S	−0.07	−0.04	7.32	1.31	0.33	2.06
H8C	−0.34	−0.31	−2.58	−4.98	−7.73	−20.14
H8S	0.90	0.09	6.06	−2.23	−2.84	10.06
S8C	0.00	−0.04	0.23	−0.12	0.44	0.07
S8S	0.03	0.02	−0.31	−0.46	−0.25	−0.09
Impedance forces and moments [C] {X_I}						
H4C	−19.89	−1.95	0.91	6.08	−7.18	−28.94
H4S	92.48	0.44	2.06	−5.18	15.36	−6.31
S4C	−0.05	0.05	−0.02	0.94	−0.55	−0.01
S4S	0.00	0.12	0.38	0.36	−1.80	0.10
H8C	0.76	3.24	−0.02	−6.50	12.09	−19.43
H8S	0.24	−0.19	2.74	−3.74	−7.88	−19.04
S8C	−0.15	0.12	−0.42	2.51	−1.22	−0.15
S8S	−0.05	−0.06	−1.55	0.43	1.16	−0.43

55

Table 6.3. Continued

(c) 0.01 in. 4P side sine actuation; $\mu = 0.10$

Component	L_X	L_Y	L_Z	A_X	A_Y	A_Z
Input control vector {U}						
4C	0.000000	0.000000	0.000000	0.000000	0.000000	0.000000
4S	0.000000	0.010000	0.000000	0.000000	0.000000	0.000000
Hub and swashplate interface displacements {X_I}						
H4C	−0.000297	−0.001664	−0.000001	0.007887	−0.001438	−0.003178
H4S	0.000810	0.007533	0.000090	−0.014586	0.004835	−0.004463
S4C	−0.000121	−0.000739	−0.000008	0.004077	−0.000847	−0.000581
S4S	0.000277	0.005673	0.000087	−0.010071	0.002302	−0.005397
H8C	−0.000002	0.000067	0.000040	−0.000419	−0.000059	0.000160
H8S	0.000002	−0.000127	−0.000060	0.000113	−0.000037	−0.001114
S8C	0.000001	0.000028	0.000041	−0.000081	0.000040	0.000624
S8S	0.000005	−0.000105	−0.000062	0.000202	−0.000024	−0.001018

Component	F_X	F_Y	F_Z	M_X	M_Y	M_Z
Hub and swashplate interface forces and moments {F_I}						
H4C	−4.57	−25.56	19.35	67.41	−5.37	−126.51
H4S	13.27	65.13	8.84	63.14	65.69	49.54
S4C	0.39	−0.14	−0.38	−5.94	1.13	−0.08
S4S	−0.13	−0.02	7.85	2.22	0.03	2.21
H8C	−0.53	2.12	−3.42	−7.25	−2.56	−23.13
H8S	0.96	−0.29	4.81	−5.37	−4.44	−3.41
S8C	0.00	0.01	0.29	0.00	−0.19	0.08
S8S	0.00	0.05	−1.01	0.04	−0.55	−0.29
Hub and swashplate forces and moments for fixed-hub condition {F_0}						
H4C	−0.22	−11.11	19.25	58.31	−3.71	−122.66
H4S	7.22	2.89	7.52	70.28	64.34	57.23
S4C	0.43	−0.10	−0.33	−6.53	0.43	−0.07
S4S	−0.07	−0.04	7.32	1.31	0.33	2.06
H8C	−0.34	−0.31	−2.58	−4.98	−7.73	−20.14
H8S	0.90	0.09	6.06	−2.23	−2.84	10.06
S8C	0.00	−0.04	0.23	−0.12	0.44	0.07
S8S	0.03	0.02	−0.31	−0.46	−0.25	−0.09
Impedance forces and moments [C] {X_I}						
H4C	−4.35	−14.45	0.10	9.10	−1.66	−3.84
H4S	6.05	62.24	1.32	−7.15	1.35	−7.70
S4C	−0.05	−0.04	−0.05	0.59	0.69	−0.01
S4S	−0.06	0.03	0.54	0.91	−0.30	0.15
H8C	−0.19	2.43	−0.84	−2.27	5.17	−2.99
H8S	0.07	−0.39	−1.25	−3.14	−1.60	−13.48
S8C	0.00	0.04	0.05	0.11	−0.63	0.01
S8S	−0.03	0.03	−0.70	0.49	−0.30	−0.21

Table 6.3. Continued

(d) 0.01 in. 4P normal sine actuation; $\mu = 0.10$

Component	L_X	L_Y	L_Z	A_X	A_Y	A_Z
Input control vector {U}						
4C	0.000000	0.000000	0.000000	0.000000	0.000000	0.000000
4S	0.000000	0.000000	0.010000	0.000000	0.000000	0.000000
Hub and swashplate interface displacements {X_I}						
H4C	-0.002530	-0.000574	-0.001324	0.004019	-0.009618	-0.004126
H4S	0.008906	-0.000037	0.010624	0.001136	0.035705	0.001467
S4C	-0.001268	-0.000153	-0.001325	0.001511	-0.007031	-0.001065
S4S	0.004307	0.000049	0.010590	0.000021	0.026734	0.000408
H8C	0.000014	0.000089	0.000020	-0.000590	0.000335	0.000058
H8S	0.000004	-0.000486	-0.000116	0.000605	-0.000247	-0.003919
S8C	-0.000013	0.000036	0.000021	-0.000089	0.000034	0.000929
S8S	0.000023	-0.000389	-0.000119	0.000757	-0.000033	-0.003599

Component	F_X	F_Y	F_Z	M_X	M_Y	M_Z
Hub and swashplate interface forces and moments {F_I}						
H4C	-22.07	-13.76	8.89	63.41	-15.92	-149.19
H4S	80.54	3.38	86.05	64.39	83.18	56.28
S4C	0.35	-0.01	-0.59	-5.08	-0.69	-0.15
S4S	0.02	0.11	6.99	0.40	-2.07	1.96
H8C	0.85	2.82	-1.89	-12.15	10.31	-43.74
H8S	1.12	0.22	9.63	-7.86	-15.89	-13.26
S8C	-0.16	0.14	-0.29	2.65	-1.52	-0.12
S8S	-0.06	-0.04	-2.25	0.61	1.04	-0.63
Hub and swashplate forces and moments for fixed-hub condition {F_0}						
H4C	-0.22	-11.11	19.25	58.31	-3.71	-122.66
H4S	7.22	2.89	7.52	70.28	64.34	57.23
S4C	0.43	-0.10	-0.33	-6.53	0.43	-0.07
S4S	-0.07	-0.04	7.32	1.31	0.33	2.06
H8C	-0.34	-0.31	-2.58	-4.98	-7.73	-20.14
H8S	0.90	0.09	6.06	-2.23	-2.84	10.06
S8C	0.00	-0.04	0.23	-0.12	0.44	0.07
S8S	0.03	0.02	-0.31	-0.46	-0.25	-0.09
Impedance forces and moments [C] {X_I}						
H4C	-21.84	-2.66	-10.36	5.10	-12.21	-26.53
H4S	73.32	0.48	78.52	-5.89	18.85	-0.95
S4C	-0.08	0.09	-0.26	1.46	-1.12	-0.08
S4S	0.09	0.15	-0.33	-0.91	-2.39	-0.10
H8C	1.19	3.13	0.70	-7.17	18.03	-23.60
H8S	0.23	0.13	3.56	-5.63	-13.04	-23.32
S8C	-0.16	0.17	-0.53	2.77	-1.95	-0.19
S8S	-0.09	-0.05	-1.94	1.07	1.28	-0.54

Table 6.3. Concluded

(e) 0.05° 4P pitch sine actuation; $\mu = 0.10$

Component	L_X	L_Y	L_Z	A_X	A_Y	A_Z
Input control vector {U}						
4C	0.000000	0.000000	0.000000	0.000000	0.000000	0.000000
4S	0.000000	0.000000	0.000000	0.000000	0.050000	0.000000
Hub and swashplate interface displacements {X_I}						
H4C	−0.004462	−0.000414	−0.000951	0.002686	−0.017315	−0.006197
H4S	**0.036147**	0.000062	0.000951	0.000475	**0.149276**	0.001169
S4C	−0.002167	−0.000150	−0.000958	0.000812	−0.012095	−0.001479
S4S	0.016474	0.000076	0.000941	−0.000235	0.118428	0.000350
H8C	0.000043	0.000272	0.000035	−0.001572	0.001102	0.000468
H8S	0.000025	−0.001179	−0.000306	0.001741	−0.000468	−0.009324
S8C	−0.000045	0.000124	0.000036	−0.000303	0.000065	0.002660
S8S	0.000061	−0.000924	−0.000315	0.001822	−0.000082	−0.008778

Component	F_X	F_Y	F_Z	M_X	M_Y	M_Z
Hub and swashplate interface forces and moments {F_I}						
H4C	−40.69	−5.94	21.87	65.56	−32.03	−231.03
H4S	306.05	4.78	17.19	51.84	150.92	46.72
S4C	0.08	0.26	−0.76	−0.43	−3.79	0.23
S4S	0.11	0.45	9.52	−0.02	−7.55	2.66
H8C	3.16	7.48	−2.83	−28.32	35.42	−109.40
H8S	2.73	−0.86	25.11	−10.89	−33.12	−20.56
S8C	−0.57	0.40	−1.53	9.12	−3.93	−0.54
S8S	−0.16	−0.22	−5.69	1.30	4.34	−1.56
Hub and swashplate forces and moments for fixed-hub condition {F_0}						
H4C	−0.22	−11.11	19.25	58.31	−3.71	−122.66
H4S	7.22	2.89	7.52	70.28	64.34	57.23
S4C	0.43	−0.10	−0.33	−6.53	0.43	−0.07
S4S	−0.07	−0.04	7.32	1.31	0.33	2.06
H8C	−0.34	−0.31	−2.58	−4.98	−7.73	−20.14
H8S	0.90	0.09	6.06	−2.23	−2.84	10.06
S8C	0.00	−0.04	0.23	−0.12	0.44	0.07
S8S	0.03	0.02	−0.31	−0.46	−0.25	−0.09
Impedance forces and moments [C] {X_I}						
H4C	−40.47	5.17	2.62	7.26	−28.32	−108.37
H4S	298.83	1.88	9.66	−18.45	86.59	−10.52
S4C	−0.35	0.36	−0.43	6.10	−4.22	−0.16
S4S	0.18	0.50	2.21	−1.33	−7.87	0.60
H8C	3.51	7.79	−0.25	−23.34	43.14	−89.26
H8S	1.84	−0.95	19.04	−8.66	−30.27	−30.63
S8C	−0.57	0.44	−1.77	9.24	−4.37	−0.61
S8S	−0.19	−0.23	−5.38	1.76	4.59	−1.48

Table 6.4. Coupled Rotor-Testbed Results for Balance Loads With No Actuation and $\mu = 0.10$

Component	L_X	L_Y	L_Z	A_X	A_Y	A_Z
Input control vector {U}						
4C	0.000000	0.000000	0.000000	0.000000	0.000000	0.000000
4S	0.000000	0.000000	0.000000	0.000000	0.000000	0.000000
Fixed-system balance forces and moments						
	F_X	F_Y	F_Z	M_X	M_Y	M_Z
4C	−2.51	−10.75	17.18	431.29	−76.44	−207.41
4S	13.60	−1.94	29.26	78.72	604.52	81.62
8C	−1.19	−4.45	3.10	−26.03	22.29	99.79
8S	3.01	4.46	−7.26	9.16	−39.08	−259.68
Rotating-system balance forces and moments						
4C	−1.76	−16.13	19.28	129.29	−9.53	−132.95
4S	14.74	0.68	8.43	68.44	128.59	52.77
8C	−0.26	1.82	−2.50	−15.72	−3.39	−24.14
8S	0.76	−0.37	4.83	−4.34	−2.41	−6.63

Table 6.5. Coupled Rotor-Testbed Results for Balance Loads With Actuated Motion

(a) 0.01 in. 4P axial cosine actuation; $\mu = 0.10$

Component	L_X	L_Y	L_Z	A_X	A_Y	A_Z
Input control vector {U}						
4C	0.010000	0.000000	0.000000	0.000000	0.000000	0.000000
4S	0.000000	0.000000	0.000000	0.000000	0.000000	0.000000
Fixed-system balance forces and moments						
	F_X	F_Y	F_Z	M_X	M_Y	M_Z
4C	281.67	−9.12	96.53	403.60	4573.81	−259.71
4S	50.26	−5.05	60.29	182.04	1616.29	81.09
8C	−2.73	−10.12	2.25	−53.92	46.87	240.02
8S	7.49	13.13	−16.67	38.19	−95.22	−727.70
Rotating-system balance forces and moments						
4C	89.98	−15.33	22.98	125.14	373.36	−173.08
4S	35.14	−3.36	9.99	92.55	215.35	58.87
8C	1.05	3.95	2.25	−32.23	16.67	−55.76
8S	1.35	−1.49	−16.67	−1.91	−11.94	−11.77

(b) 0.01 in. 4P axial sine actuation; $\mu = 0.10$

Component	L_X	L_Y	L_Z	A_X	A_Y	A_Z
Input control vector {U}						
4C	0.000000	0.000000	0.000000	0.000000	0.000000	0.000000
4S	0.010000	0.000000	0.000000	0.000000	0.000000	0.000000
Fixed-system balance forces and moments						
	F_X	F_Y	F_Z	M_X	M_Y	M_Z
4C	−38.90	−8.60	−10.85	370.35	−1080.83	−225.16
4S	298.53	0.41	107.09	6.98	5282.36	83.55
8C	−2.06	−7.14	3.06	−38.51	36.22	165.62
8S	5.30	9.19	−12.38	24.94	−67.96	−508.44
Rotating-system balance forces and moments						
4C	−21.64	−13.47	20.05	120.26	−99.05	−151.62
4S	107.24	3.08	9.70	51.20	516.49	50.94
8C	0.42	2.72	−2.52	−24.41	6.16	−39.57
8S	1.17	−0.96	8.49	−3.41	−5.88	−9.10

Table 6.5. Continued

(c) 0.01 in. 4P side sine actuation; μ = 0.10

Component	L_X	L_Y	L_Z	A_X	A_Y	A_Z
Input control vector {U}						
4C	0.000000	0.000000	0.000000	0.000000	0.000000	0.000000
4S	0.000000	0.010000	0.000000	0.000000	0.000000	0.000000
Fixed-system balance forces and moments						
	F_X	F_Y	F_Z	M_X	M_Y	M_Z
4C	−5.07	−34.87	15.21	803.95	−176.86	−118.20
4S	12.46	271.96	29.62	−2967.45	564.00	−1237.03
8C	−1.55	−4.71	4.43	−30.34	26.98	114.29
8S	2.65	3.44	−6.91	8.63	−34.14	−187.94
Rotating-system balance forces and moments						
4C	−4.77	−28.03	19.35	177.35	−25.09	−126.51
4S	13.76	69.94	8.90	−122.60	122.77	49.46
8C	−0.53	2.01	−3.31	−16.58	−4.80	−23.12
8S	0.97	−0.53	4.64	−3.39	−0.36	−3.46

(d) 0.01 in. 4P normal sine actuation; μ = 0.10

Component	L_X	L_Y	L_Z	A_X	A_Y	A_Z
Input control vector {U}						
4C	0.000000	0.000000	0.000000	0.000000	0.000000	0.000000
4S	0.000000	0.000000	0.100000	0.000000	0.000000	0.000000
Fixed-system balance forces and moments						
	F_X	F_Y	F_Z	M_X	M_Y	M_Z
4C	−36.06	−9.15	−76.10	386.21	−1454.16	−223.49
4S	104.74	0.38	643.67	4.13	6517.03	90.51
8C	−2.17	−7.33	1.88	−35.06	37.39	160.87
8S	5.96	11.59	−13.09	29.54	−75.54	−657.14
Rotating-system balance forces and moments						
4C	−23.74	−14.12	7.95	122.30	−112.69	−149.21
4S	86.21	3.90	93.52	50.41	435.56	56.30
8C	0.86	2.56	−1.83	−24.58	13.95	−43.74
8S	1.17	−1.00	9.30	−5.99	−11.10	−13.41

61

Table 6.5. Concluded

(e) 0.05° 4P pitch sine actuation; $\mu = 0.10$

Component	L_X	L_Y	L_Z	A_X	A_Y	A_Z
Input control vector {U}						
4C	0.000000	0.000000	0.000000	0.000000	0.000000	0.000000
4S	0.000000	0.000000	0.000000	0.000000	0.050000	0.000000
Fixed-system balance forces and moments						
	F_X	F_Y	F_Z	M_X	M_Y	M_Z
4C	−69.47	−2.04	−68.55	199.58	−2308.30	−313.26
4S	294.59	2.46	538.40	−53.98	**16243.61**	78.74
8C	−5.86	−19.37	2.74	−95.82	96.75	464.69
8S	15.30	29.99	−34.56	92.89	−193.90	−1608.42
Rotating-system balance forces and moments						
4C	−43.73	−5.91	21.20	91.26	−210.40	−231.08
4S	328.86	4.79	17.85	31.73	1492.91	46.72
8C	3.18	6.99	−2.73	−61.48	48.93	−109.39
8S	2.86	−3.61	24.25	−0.45	−21.39	−20.92

Table 6.6. Coupled Rotor-Testbed Results for Actuated Motion Corrected for
Proper Motion at Hub Interface Joint

[0.01 in. 4P axial sine actuation; $\mu = 0.10$]

Component	L_X	L_Y	L_Z	A_X	A_Y	A_Z
Input control vector {U}						
4C	0.001434	-0.001213	-0.000122	-0.003473	0.002847	0.002258
4S	0.025596	-0.000581	0.000042	-0.001358	-0.025542	-0.001503
Hub and swashplate interface displacements {X_I}						
H4C	-0.000014	0.000008	0.000001	0.000008	-0.000001	0.000005
H4S	0.009910	0.000006	-0.000001	0.000006	0.000097	0.000004
S4C	-0.000008	-0.000123	-0.000007	-0.002067	0.000455	0.002937
S4S	0.010421	-0.000076	-0.000004	-0.001159	-0.009225	-0.001084
H8C	0.000002	0.000077	0.000030	-0.000499	0.000071	0.000128
H8S	0.000004	-0.000262	-0.000084	0.000322	-0.000120	-0.002159
S8C	-0.000005	0.000031	0.000031	-0.000085	0.000036	0.000742
S8S	0.000013	-0.000211	-0.000087	0.000409	-0.000027	-0.001977

| Component	F_X	F_Y	F_Z	M_X	M_Y	M_Z
Hub and swashplate interface forces and moments {F_I}						
H4C	-1.35	-9.03	20.93	63.41	-3.83	-142.85
H4S	89.32	3.30	7.73	67.01	57.86	57.54
S4C	0.46	-0.13	-0.51	-6.99	0.81	-0.12
S4S	-0.16	0.03	7.64	2.82	-0.53	2.14
H8C	0.16	2.39	-2.61	-9.68	0.76	-30.76
H8S	0.94	-0.03	6.70	-4.71	-8.58	-7.22
S8C	-0.11	0.04	-0.01	1.64	-0.33	-0.02
S8S	0.01	-0.03	-1.35	-0.26	0.52	-0.38
Hub and swashplate forces and moments for fixed-hub condition {F_0}						
H4C	-0.22	-11.11	19.25	58.31	-3.71	-122.66
H4S	7.22	2.89	7.52	70.28	64.34	57.23
S4C	0.43	-0.10	-0.33	-6.53	0.43	-0.07
S4S	-0.07	-0.04	7.32	1.31	0.33	2.06
H8C	-0.34	-0.31	-2.58	-4.98	-7.73	-20.14
H8S	0.90	0.09	6.06	-2.23	-2.84	10.06
S8C	0.00	-0.04	0.23	-0.12	0.44	0.07
S8S	0.03	0.02	-0.31	-0.46	-0.25	-0.09
Impedance forces and moments [C]{X_I}						
H4C	-1.13	2.08	1.68	5.10	-0.12	-20.19
H4S	82.10	0.40	0.20	-3.27	-6.48	0.31
S4C	0.02	-0.03	-0.18	-0.45	0.38	-0.05
S4S	-0.09	0.07	0.32	1.51	-0.86	0.08
H8C	0.50	2.70	-0.03	-4.71	8.49	-10.62
H8S	0.05	-0.12	0.64	-2.48	-5.74	-17.28
S8C	-0.11	0.08	-0.25	1.75	-0.77	-0.09
S8S	-0.03	-0.04	-1.04	0.20	0.77	-0.29
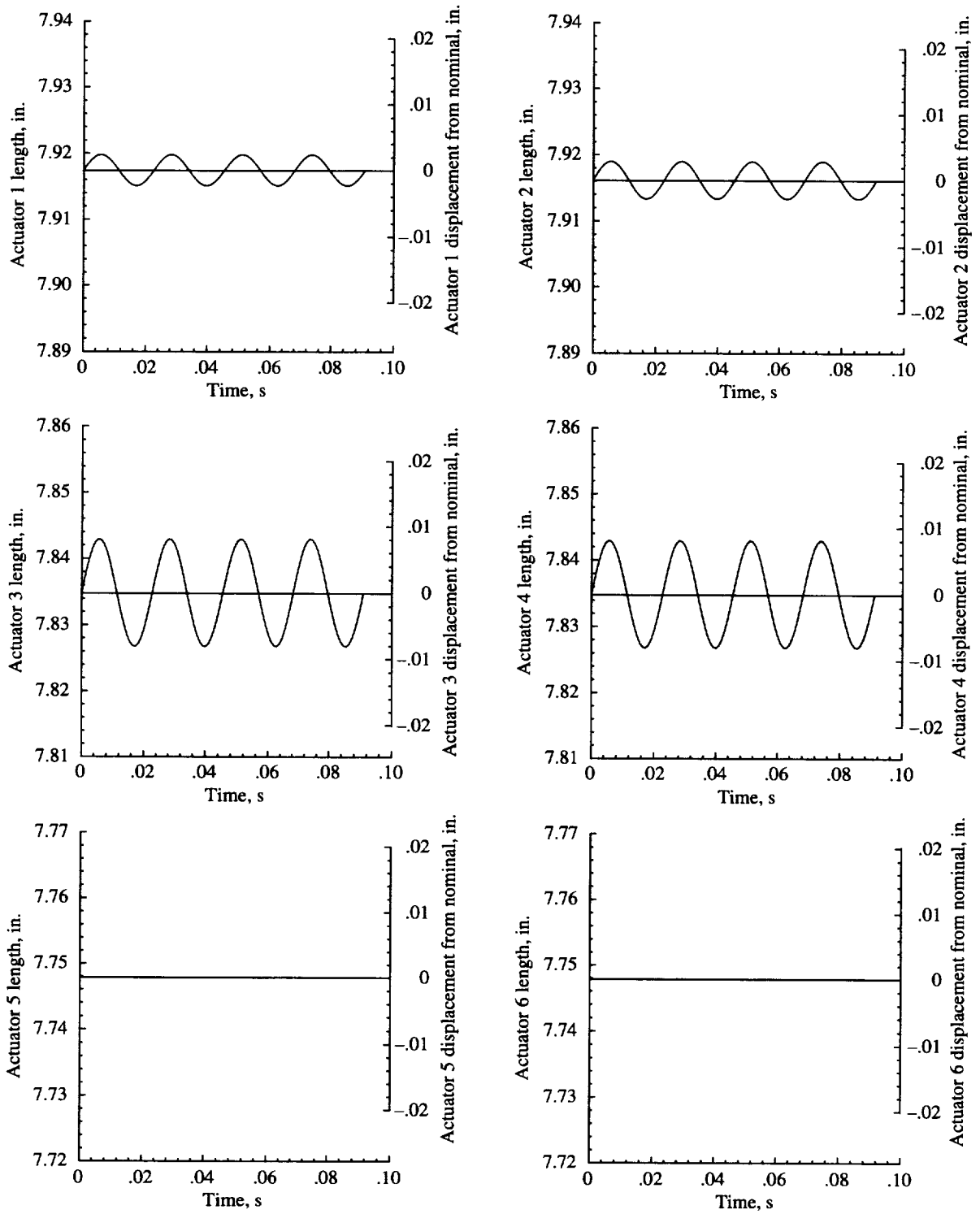
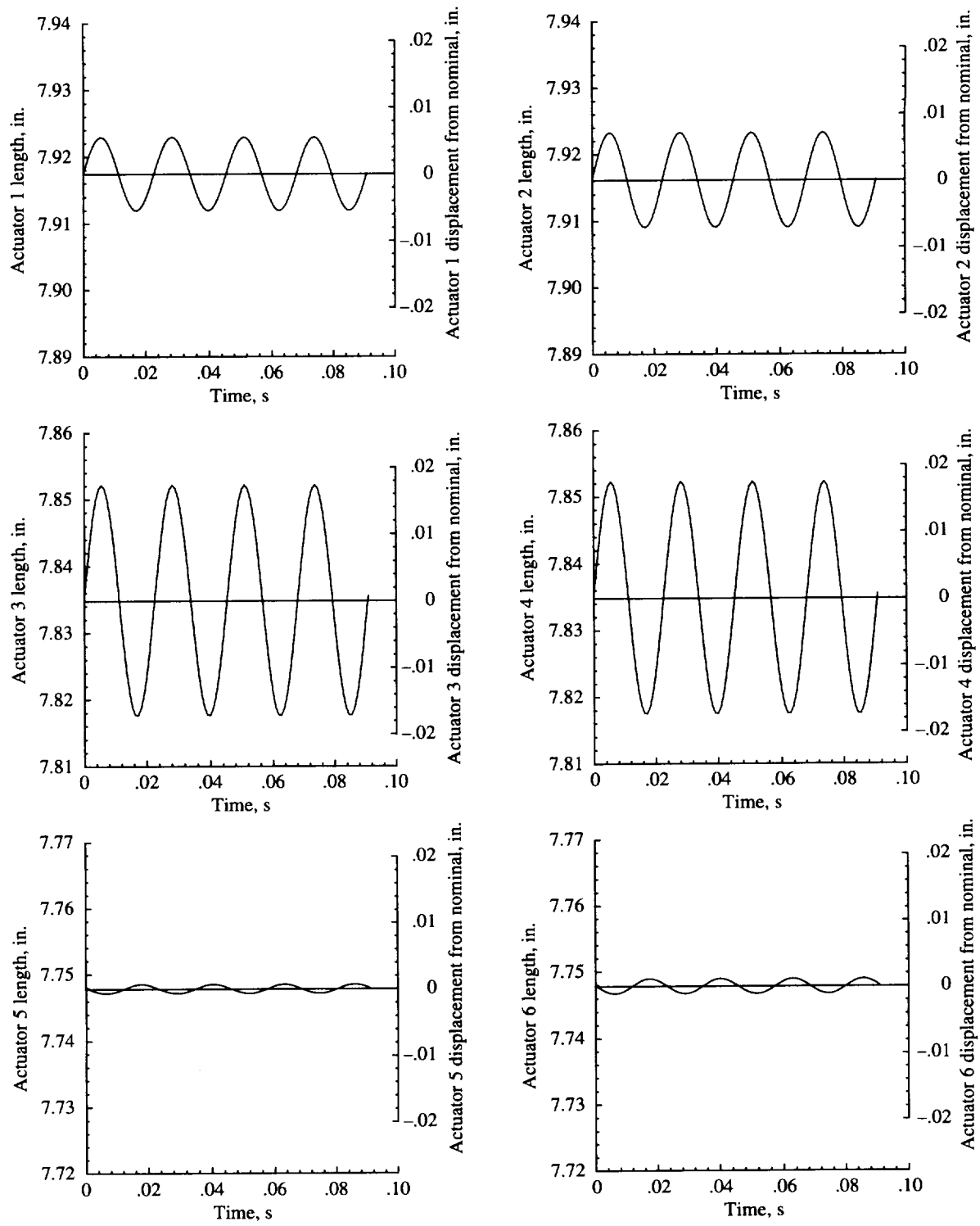Figure 6.1. Actuator lengths for 0.01 in. 4P sine actuation of inflexible ARES-II.

Figure 6.2. Actuator lengths for 0.01 in. 4P sine actuation of elastic ARES-II.
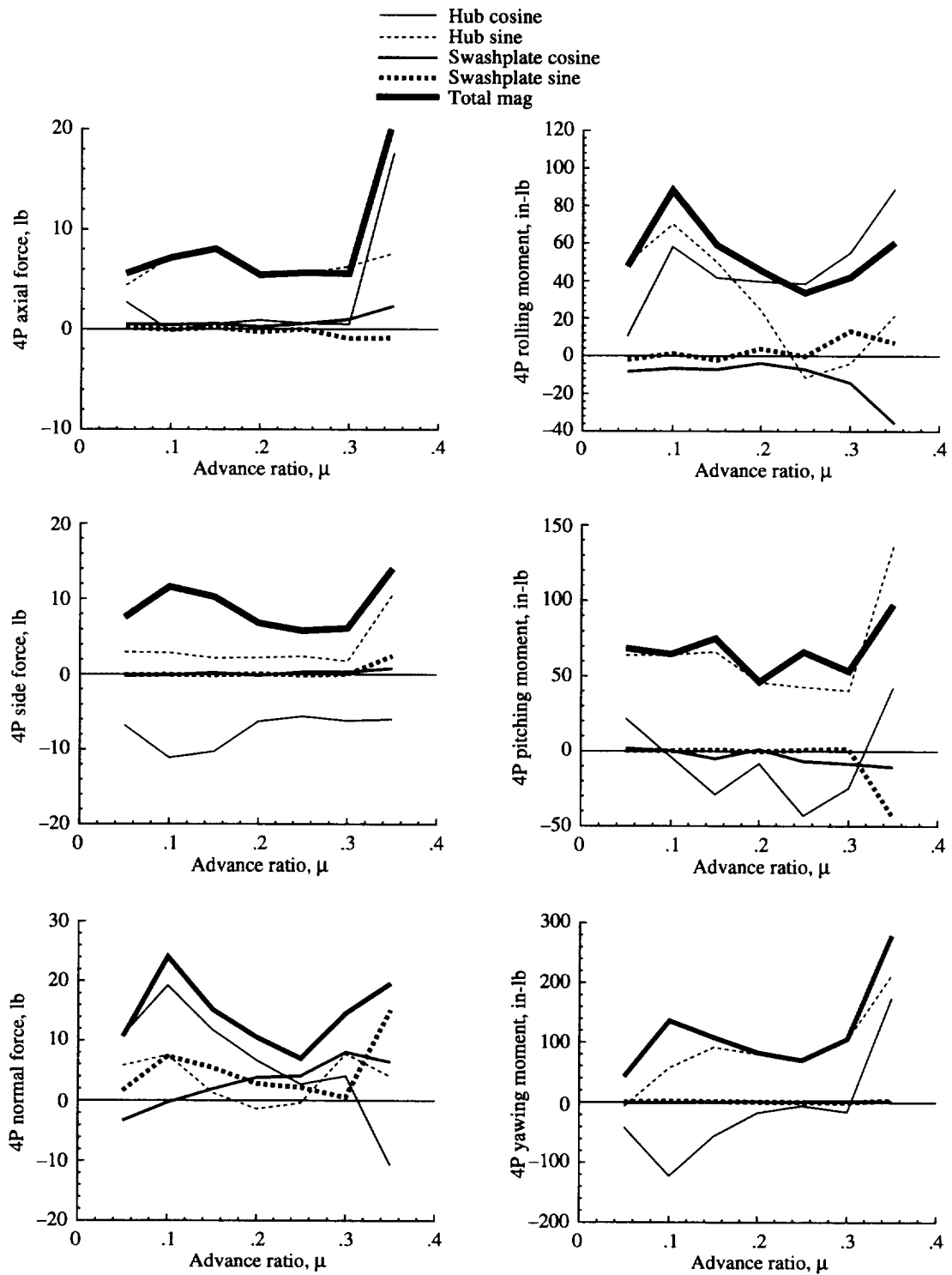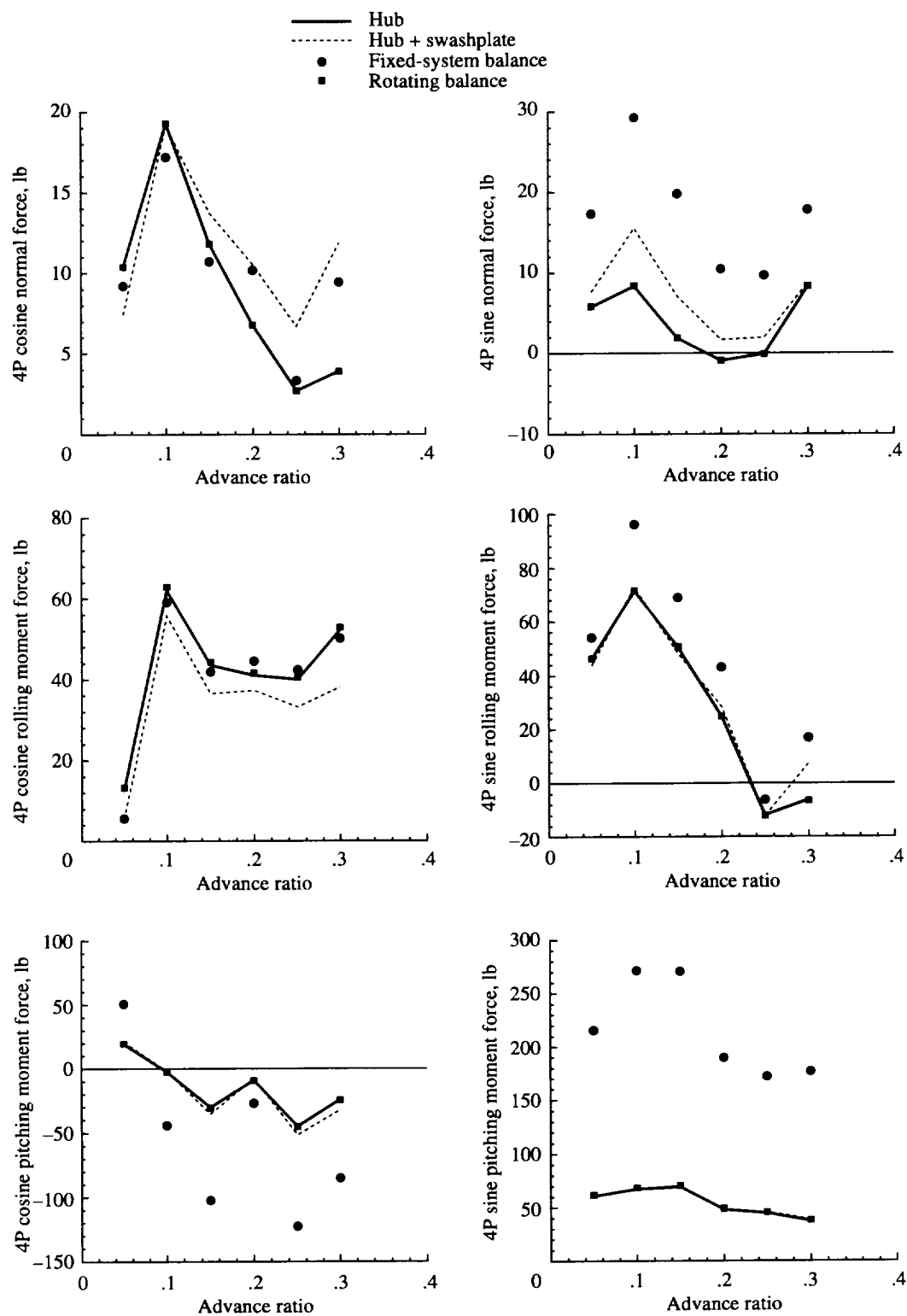
Figure 6.3. Fixed-system loads for uncoupled BRR model.

Figure 6.4. Balance loads compared with hub interface joint loads.

7. Conclusions

A method for coupling an aeroelastically scaled model rotor system to the ARES-II (second generation version of the Aeroelastic Rotor Experimental System) rotor research testbed has been developed. The method requires the development of individual analytical models of the ARES-II and the rotor system to be coupled. For this study the Basic Research Rotor (BRR), a generic research rotor, is used. The development of individual models of the testbed and the rotor system is used to an advantage by selecting analyses that are best suited to model each system. For the ARES-II model, the Dynamic Analysis and Design System (DADS) multibody dynamics analysis is used. For the rotor system, the second generation version of the Comprehensive Analytical Model of Rotorcraft Aerodynamics and Dynamics (CAMRAD-II) is used. Other analyses are suitable for use in place of DADS and CAMRAD-II.

Impedance matching is used to couple the BRR to the ARES-II. Impedance matching requires that the structures to be coupled be represented with a linear model. This representation is of no consequence for the ARES-II, a linear system. However, since rotor systems are inherently nonlinear systems, care must be exercised to ensure the proper application of the impedance-matching approach. For the BRR, fixed-hub forward flight trim conditions for 1g steady flight are used with a correction applied to account for the loads due to rotor hub motion.

The process used to perform coupled rotor-testbed analysis is as follows:

1. Develop a mobility matrix [A] for the ARES-II by using the DADS model. This matrix is generated by applying 4P and 8P dynamic loads at the interface joints and characterizing the 4P and 8P motion at the interface joints.

2. Develop a motion matrix [B] for the ARES-II by using the DADS model. This matrix is generated by prescribing motions of the Stewart platform and characterizing the motion at the interface joints.

3. Develop the fixed-hub load conditions (no motion) at the interface joints for the BRR by using the CAMRAD-II model. Then the impedance matrix [C] is generated by prescribing hub motions and characterizing the loads at the interface joints.

4. The resulting mobility, motion, and impedance matrices are coupled through simple matrix equations.

This study has shown that the impedance-matching approach is a viable method for the analysis of model rotor systems coupled to the ARES-II aeroelastic rotor research testbed. The impedance-matching method has been used to an advantage by generating independent models of the ARES-II and the BRR system. Thus, to couple alternate rotor systems to the ARES-II requires only the generation of the impedance model for the new rotor system. Additionally, the experimental verification of the ARES-II model will be eased because it may be exercised in a stand-alone mode for comparison with shake and actuation tests. This study has extended the impedance-matching techniques evident in the literature by including the effects of actuated hub motion and by using two interface joints between the rotor system and the testbed.

Based on the experience developed in rotor-body coupling techniques during this study and the examination of the results, the following conclusions were found:

1. Although impedance matching is a linear theory approach, the effect of rotor system nonlinearity must be considered throughout the analysis. The rotor impedance matrices for this study have been developed by using both cosine and sine harmonic hub motions with checks to ensure that the rotor system response remained in the linear range.

2. The effect of both hub and control system (swashplate) loads is necessary to properly model the coupled rotor-testbed system. Control system loads have been shown to be of particular importance for the calculation of normal force and pitching and rolling moments. Neglecting the swashplate load path has been shown to result in fixed-system load errors of up to 30 percent.

3. Significant ARES-II body motion coupling and phase lag are evident in the actuated motion results for both the stand-alone ARES-II and for the coupled rotor-testbed system. Stewart platform control vectors required to obtain pure hub motion uncontaminated by body coupling or phase lag may be developed for the stand-alone ARES-II

with simple matrix manipulations. However, no closed-form method of calculating the required control vector is possible for the coupled rotor-testbed system. Therefore, the analytical results indicate that a closed-loop control system is necessary to generate desired hub motions.

4. Based on the analytical results, the ARES-II rotating balance is expected to be a more reliable loads measurement device than the fixed-system balance. The results suggest that the rotating balance is essentially free of loads contamination due to system dynamic response. The fixed-system balance results indicate significant errors for all load cases examined.

8. References

1. Reichert, G.: Helicopter Vibration Control—A Survey. *Vertica*, vol. 5, no. 1, 1981, pp. 1–20.

2. Gerstenberger, Walter; and Wood, Edward R.: Analysis of Helicopter Aeroelastic Characteristics in High-Speed Flight. *AIAA J.*, vol. 1, no.10, Oct. 1963, pp. 2366–2381.

3. Staley, J. A.; and Sciarra, J. J.: Coupled Rotor/Airframe Vibration Prediction Methods. *Rotorcraft Dynamics*, NASA SP-352, 1974, pp. 81–90.

4. Hohenemser, Kurt H.; and Yin, Sheng-Kuang: The Role of Impedance in Vibration Analysis of Rotorcraft. *Vertica*, vol. 3, no. 3/4, 1979, pp. 189–204.

5. Hsu, T.-K.; and Peters, D. A.: Coupled Rotor/Airframe Vibration Analysis by a Combined Harmonic-Balance, Impedance-Matching Method. *J. American Heli. Soc.*, vol. 27, no. 1, Jan. 1982, pp. 25–35.

6. Gabel, R.; and Sankewitsch, V.: Rotor-Fuselage Coupling by Impedance. *Proceedings of the 42nd Annual Forum of the American Helicopter Society*, 1986, pp. 1–11.

7. Johnson, Wayne: *CAMRAD II—Nonlinear Substructure Aeromechanics Analysis. Volume I–III: Theory.* Johnson Aeronaut., 1994.

8. Johnson, Wayne: *CAMRAD II—Nonlinear Substructure Aeromechanics Analysis. Volume IV–VI: Input.* Johnson Aeronaut., 1994.

9. *DADS: Dynamic Analysis and Design System—Reference Manual, Revision 7.5, Volume 1.* Computer Aided Design Software, Inc., 1993.

10. Haug, Edward J.: *Computer Aided Kinematics and Dynamics of Mechanical Systems.* Allyn and Bacon, 1989.

11. Gessow, Alfred; and Myers, Garry C., Jr.: *Aerodynamics of the Helicopter.* MacMillan Co., 1952.

12. Bielawa, Richard L: *Rotary Wing Structural Dynamics and Aeroelasticity.* AIAA, 1992.

13. Johnson, Wayne: *Helicopter Theory.* Princeton Univ. Press, 1980.

14. Bramwell, A. R. S.: *Helicopter Dynamics.* John Wiley & Sons, Inc., 1976.

15. Landgrebe, A. J.: The Wake Geometry of a Hovering Helicopter Rotor and Its Influence on Rotor Performance. *J. American Heli. Soc.*, vol. 17, no. 4, Oct. 1972, pp. 3–15.

16. Kocurek, J. D.; and Tangler, J. L.: A Prescribed Wake Lifting Surface Hover Performance Analysis. *J. American Heli. Soc.*, vol. 22, no. 1, Jan. 1977, pp. 24–35.

17. Scully, Michael P.: *Computation of Helicopter Rotor Wake Geometry and Its Influence on Rotor Harmonic Airloads.* ASRL Tech. Rep. 178-1, MIT, 1975.

18. Johnson, Wayne: A General Free Wake Geometry Calculation for Wings and Rotors. *Proceedings of the 51st Annual American Helicopter Society Forum*, May 1995, pp. 137–153.

19. Yeager, William T., Jr.; Mirick, Paul H.; Hamouda, M-Nabil H.; Wilbur, Matthew L.; Singleton, Jeffery D.; and Wilkie, W. Keats: Rotorcraft Aeroelastic Testing in the Langley Transonic Dynamics Tunnel. *J. American Heli. Soc.*, vol. 38, no. 3, July 1993, pp. 73–82.

Appendix A

Rotating to Nonrotating Coordinate Transformations

In the study of helicopter rotor system dynamics, the transformation of displacements and loads from the rotating frame to the nonrotating frame is of prime importance. This appendix describes the mathematical formulation of such transformations. Special attention is given to four-bladed articulated rotor systems to emphasize the equations necessary for analysis of the Basic Research Rotor (BRR).

Figure A1 illustrates a nonrotating (or fixed-system) coordinate frame represented by the X,Y,Z axes and a rotating-system coordinate frame represented by the x,y,z axes. Although the nonrotating coordinate frame is often also called the fixed system, it should not be confused with the ground-fixed inertial system. The nonrotating coordinate frame is a body-fixed system placed within the helicopter or testbed fuselage. The orientation in use throughout this work is $+X$-axis aft, $+Y$-axis right side, and $+Z$-axis up along the rotor shaft axis with origin placed at the center of rotation. The rotating coordinate frame (x,y,z) is a hub-fixed coordinate system that revolves about the Z-axis with constant angular velocity Ω whose origin is placed at a constant radius e from the Z-axis. For the purposes of this development, the origin of the rotating frame is constrained to lie in the X-Y plane at all times and the distance e is defined as the rotor flap-lag hinge offset. For the BRR, the flap and lag hinges are coincident; this allows for a single value of e. For rotor hubs with noncoincident flap and lag hinges, two values of e are necessary in the transformation formulation. The x- and y-axes are constrained to the X-Y plane and oriented such that the $+x$-axis lies toward the trailing edge and the y-axis lies along the radius of the reference blade. The $+z$-axis is oriented up and is parallel to the Z-axis. The azimuthal position of the rotating frame relative to the nonrotating frame is given by ψ. The azimuth is indexed such that $\psi = 0°$ when the reference blade is over the X-axis. This position corresponds to the one when the $+y$-axis is aligned with the $+X$-axis. The azimuth angle increases with counterclockwise rotation of the rotating frame.

By inspection of figure A1, the displacement, force, and moment relationships between the reference blade root and the nonrotating frame are evident and are

$$\begin{Bmatrix} X \\ Y \\ Z \end{Bmatrix} = \begin{bmatrix} \sin\psi & \cos\psi & 0 \\ -\cos\psi & \sin\psi & 0 \\ 0 & 0 & 1 \end{bmatrix} \begin{Bmatrix} x \\ y \\ z \end{Bmatrix} \tag{A1}$$

$$\begin{Bmatrix} F_X \\ F_Y \\ F_Z \end{Bmatrix} = \begin{bmatrix} \sin\psi & \cos\psi & 0 \\ -\cos\psi & \sin\psi & 0 \\ 0 & 0 & 1 \end{bmatrix} \begin{Bmatrix} F_x \\ F_y \\ F_z \end{Bmatrix} \tag{A2}$$

$$\begin{Bmatrix} M_X \\ M_Y \\ M_Z \end{Bmatrix} = \begin{bmatrix} 0 & 0 & e\sin\psi \\ 0 & 0 & -e\cos\psi \\ -e & 0 & 0 \end{bmatrix} \begin{Bmatrix} F_x \\ F_y \\ F_z \end{Bmatrix} \tag{A3}$$

As a simple example, one may define the vertical shear force in the nonrotating frame (F_Z) due to vertical blade root shear (F_z) by using equation (A2). The result is

$$F_Z = F_z$$

71
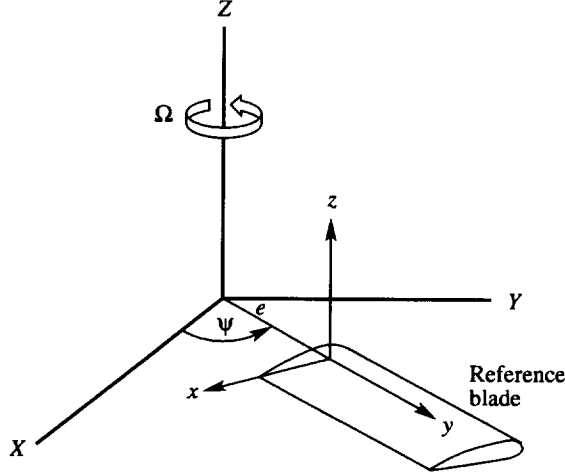
Figure A1. Rotating and nonrotating frame coordinate systems.

However, note that this result only includes the effect of a single blade. For multibladed rotor systems, determining the forces and moments in the nonrotating frame by including the effect of all blades is necessary. Therefore, the equation for the total nonrotating vertical shear is

$$F_{Z_{tot}} = \sum_{b=1}^{N} F_{z_b} \tag{A4}$$

where b is the blade index and N is the number of blades. Assume now a Fourier series to describe the periodic force for each blade:

$$F_{z_b} = \sum_{n=0}^{\infty} (F_{z_{nc}} \cos n\psi_b + F_{z_{ns}} \sin n\psi_b) \tag{A5}$$

where the index n is harmonic number, the subscripts c and s indicate the cosine and sine components of the force, and b is the azimuthal position of the bth blade as described by

$$\psi_b = \psi + \frac{2b\pi}{N} \tag{A6}$$

where ψ is the azimuthal position of the reference blade. Substituting equation (A6) into equation (A5) and the result into (A4) yields the equation for the total nonrotating frame vertical shear as

$$F_{Z_{tot}} = \sum_{b=1}^{N} \sum_{n=0}^{\infty} (F_{z_{nc}} \cos n\psi_b + F_{z_{ns}} \sin n\psi_b) \tag{A7}$$

Further development, however, will show that equation (A7) may be further reduced. To aid in this development several trigonometric identities are used as follows:

$$\sin(\alpha + \beta) = \sin \alpha \cos \beta + \cos \alpha \sin \beta \tag{A8}$$

72

$$\cos(\alpha - \beta) = \cos\alpha\cos\beta + \sin\alpha\sin\beta \tag{A9}$$

$$\cos(\alpha + \beta) = \cos\alpha\cos\beta - \sin\alpha\sin\beta \tag{A10}$$

$$\sin(\alpha - \beta) = \sin\alpha\cos\beta - \cos\alpha\sin\beta \tag{A11}$$

Reduction of equation (A7) is achieved by developing equations for one harmonic at a time, beginning with the 0th harmonic (mean) and working through to the 5th harmonic. Because the BRR is a four-bladed rotor system, $N = 4$ is assumed throughout the remainder of the development.

For $n = 0$, $N = 4$:

$$
\begin{aligned}
F_{Z_{tot}}\Big|_{n=0} &= \sum_{b=1}^{4}\left[F_{z_{0c}}\cos(0\cdot\psi_b) + F_{z_{0c}}\sin(0\cdot\psi_b)\right] \\
&= \sum_{b=1}^{4}\left[F_{z_{0c}}\right] \\
&= 4F_{z_{0c}} \tag{A12}
\end{aligned}
$$

Equation (A12) shows the expected result: the nonrotating frame vertical shear is four times the vertical blade root shear.

For $n = 1$:

$$
\begin{aligned}
F_{Z_{tot}}\Big|_{n=1} &= \sum_{b=1}^{4}\left[F_{Z_{1c}}\cos(\psi_b) + F_{z_{1s}}\sin(\psi_b)\right] \\
&= \sum_{b=1}^{4}\left[F_{Z_{1c}}\cos\left(\psi + \frac{b\pi}{2}\right) + F_{z_{1s}}\sin\left(\psi + \frac{b\pi}{2}\right)\right] \tag{A13}
\end{aligned}
$$

Equations (A10) and (A11) allow for reduction of the cosine and sine terms depending upon blade number.

For blade 1:

$$\cos\left(\psi + \frac{\pi}{2}\right) = -\sin\psi$$

$$\sin\left(\psi + \frac{\pi}{2}\right) = \cos\psi$$

For blade 2:

$$\cos(\psi + \pi) = -\cos\psi$$

$$\sin(\psi + \pi) = -\sin\psi$$

For blade 3:

$$\cos\left(\psi + \frac{3\pi}{2}\right) = \sin\psi$$

$$\sin\left(\psi + \frac{3\pi}{2}\right) = -\cos\psi$$

For blade 4:

$$\cos(\psi + 2\pi) = \cos \psi$$
$$\sin(\psi + 2\pi) = \sin \psi$$

Substituting these expressions into equation (A13) yields

$$
\begin{aligned}
F_{Z_{\text{tot}}}\big|_{n=1} &= F_{z_{1c}}(-\sin \psi - \cos \psi + \sin \psi + \cos \psi) \\
&\quad + F_{z_{1s}}(\cos \psi - \sin \psi - \cos \psi + \sin \psi) \\
&= 0
\end{aligned}
$$

(A14)

Each harmonic may be evaluated similarly.

For $n = 2$:

$$
\begin{aligned}
F_{Z_{\text{tot}}}\big|_{n=2} &= \sum_{b=1}^{4}\left[F_{z_{2c}} \cos 2\left(\psi + \frac{b\pi}{2}\right) + F_{z_{2s}} \sin 2\left(\psi + \frac{b\pi}{2}\right)\right] \\
&= F_{z_{2c}}(-\cos 2\psi + \cos 2\psi - \cos 2\psi + \cos 2\psi) \\
&\quad + F_{z_{2s}}(-\sin 2\psi + \sin 2\psi - \sin 2\psi + \sin 2\psi) \\
&= 0
\end{aligned}
$$

For $n = 3$:

$$
\begin{aligned}
F_{Z_{\text{tot}}}\big|_{n=3} &= \sum_{b=1}^{4}\left[F_{z_{3c}} \cos 3\left(\psi + \frac{b\pi}{2}\right) + F_{z_{3s}} \sin 3\left(\psi + \frac{b\pi}{2}\right)\right] \\
&= F_{z_{3c}}(\sin 3\psi - \cos 3\psi - \sin 3\psi + \cos 3\psi) \\
&\quad + F_{z_{3s}}(-\cos 3\psi - \sin 3\psi + \cos 3\psi + \sin 3\psi) \\
&= 0
\end{aligned}
$$

For $n = 4$:

$$
\begin{aligned}
F_{Z_{\text{tot}}}\big|_{n=4} &= \sum_{b=1}^{4}\left[F_{z_{4c}} \cos 4\left(\psi + \frac{b\pi}{2}\right) + F_{z_{4s}} \sin 4\left(\psi + \frac{b\pi}{2}\right)\right] \\
&= F_{z_{4c}}(\cos 4\psi + \cos 4\psi + \cos 4\psi + \cos 4\psi) \\
&\quad + F_{z_{4s}}(\sin 4\psi + \sin 4\psi + \sin 4\psi + \sin 4\psi) \\
&= 4\left(F_{z_{4c}} \cos 4\psi + F_{z_{4s}} \sin 4\psi \right)
\end{aligned}
$$

Therefore,

$$
\left.\begin{aligned}
F_{Z_{\text{tot}_{4c}}} &= 4 F_{z_{4c}} \\
F_{Z_{\text{tot}_{4s}}} &= 4 F_{z_{4s}}
\end{aligned}\right\}
$$

(A15)

For $n = 5$:

$$F_{Z_{tot}}\Big|_{n=5} = \sum_{b=1}^{4}\left[F_{z_{5_c}}\cos 5\left(\psi + \frac{b\pi}{2}\right) + F_{z_{5_s}}\sin 5\left(\psi + \frac{b\pi}{2}\right)\right]$$

$$= F_{z_5}(-\sin 5\psi - \cos 5\psi + \sin 5\psi + \cos 5\psi)$$

$$+ F_{z_{5_s}}(\cos 5\psi - \sin 5\psi - \cos 5\psi + \sin 5\psi)$$

$$= 0$$

Continued analysis would confirm that rotating frame, vertical blade root shear is converted to vertical nonrotating frame shear only if the harmonic number is an integer multiple of the number of rotor system blades. For a four-bladed rotor system, this may be represented mathematically by

$$\left.\begin{aligned}F_{Z_{tot_{nc}}} &= 4F_{z_{nc}}\\ F_{Z_{tot_{ns}}} &= 4F_{z_{ns}}\end{aligned}\right\} \qquad (n = 0, 4, 8, \ldots) \qquad (A16)$$

An analysis similar to the preceding development of the vertical shear loads may be extended to the transfer of chordwise blade root shears to yawing moments in the nonrotating frame; that is,

$$\left.\begin{aligned}M_{Z_{tot_{nc}}} &= -4eF_{x_{nc}}\\ M_{Z_{tot_{ns}}} &= -4eF_{x_{ns}}\end{aligned}\right\} \qquad (n = 0, 4, 8, \ldots) \qquad (A17)$$

However, the manner in which axial (fore-and-aft) and side loads are generated in the nonrotating frame is not as straightforward. Therefore, the axial load equations are developed to ensure the clarity of the proper procedures.

Equation (A2) shows that the axial nonrotating frame load F_X is generated by a combination of chordwise blade root shears F_x, and blade root axial loads F_y. The total axial load may be represented by

$$F_{X_{tot}} = \sum_{b=1}^{N}(F_x \sin \psi_b + F_y \cos \psi_b) \qquad (A18)$$

where

$$F_x = \sum_{n=0}^{\infty}\left(F_{x_{nc}}\cos n\psi_b + F_{x_{ns}}\sin n\psi_b\right)$$

$$F_y = \sum_{n=0}^{\infty}\left(F_{y_{nc}}\cos n\psi_b + F_{y_{ns}}\sin n\psi_b\right)$$

75

and ψ_b was defined in equation (A6). Expanding equation (A18) yields

$$F_{X_{\text{tot}}} = \sum_{b=1}^{N} \sum_{n=0}^{\infty} \left[\left(F_{x_{nc}} \cos n\psi_b + F_{x_{ns}} \sin n\psi_b \right) \sin \psi_b \right. $$
$$\left. + \left(F_{y_{nc}} \cos n\psi_b + F_{y_{ns}} \sin n\psi_b \right) \cos \psi_b \right] \tag{A19}$$

Again assuming a four-bladed rotor system and using the trigonometric identities in equations (A8) through (A11) give the following results:

For $n = 0$, $N = 4$:

$$F_{X_{\text{tot}}}\big|_{n=0} = \sum_{b=1}^{4} F_{y_{0c}}$$
$$= 4F_{y_{0c}} \tag{A20}$$

For $n = 1$:

$$F_{Z_{\text{tot}}}\big|_{n=1} = \sum_{b=1}^{N} \left\{ \left[F_{x_{1c}} \cos\left(\psi + \frac{b\pi}{2}\right) + F_{x_{1s}} \sin\left(\psi + \frac{b\pi}{2}\right) \right] \sin\left(\psi + \frac{b\pi}{2}\right) \right.$$
$$\left. + \left[F_{y_{1c}} \cos\left(\psi + \frac{b\pi}{2}\right) + F_{y_{1s}} \sin\left(\psi + \frac{b\pi}{2}\right) \right] \cos\left(\psi + \frac{b\pi}{2}\right) \right\}$$

$$= F_{x_{1c}} (-\sin\psi\,\cos\psi - \sin\psi\,\cos\psi - \sin\psi\,\cos\psi + \sin\psi\cos\psi)$$
$$+ F_{x_{1s}} (\cos^2\psi + \sin^2\psi + \cos^2\psi + \sin^2\psi)$$
$$+ F_{y_{1c}} (\sin^2\psi + \cos^2\psi + \sin^2\psi + \cos^2\psi)$$
$$+ F_{y_{1s}} (-\sin\psi\,\cos\psi + \sin\psi\,\cos\psi - \sin\psi\,\cos\psi + \sin\psi\,\cos\psi)$$
$$= 2F_{x_{1s}} + 2F_{y_{1s}} \tag{A21}$$

For $n = 2$:

$$F_{X_{tot}}\big|_{n=2} = \sum_{b=1}^{N} \left\{ \left[F_{x_{2c}} \cos 2\left(\psi + \frac{b\pi}{2}\right) + F_{x_{2s}} \sin 2\left(\psi + \frac{b\pi}{2}\right) \right] \sin \left(\psi + \frac{b\pi}{2}\right) \right.$$

$$\left. + \left[F_{y_{2c}} \cos 2\left(\psi + \frac{b\pi}{2}\right) + F_{y_{2s}} \sin 2\left(\psi + \frac{b\pi}{2}\right) \right] \cos \left(\psi + \frac{b\pi}{2}\right) \right\}$$

$$= F_{x_{2c}} (-\cos 2\psi \cos \psi - \cos 2\psi \sin \psi + \cos 2\psi \cos \psi + \cos 2\psi \sin \psi)$$

$$+ F_{x_{2s}} (-\sin 2\psi \cos \psi - \sin 2\psi \sin \psi + \sin 2\psi \cos \psi + \sin 2\psi \sin \psi)$$

$$+ F_{y_{2c}} (\cos 2\psi \sin \psi - \cos 2\psi \cos \psi - \cos 2\psi \sin \psi + \cos 2\psi \cos \psi)$$

$$+ F_{y_{2s}} (-\sin 2\psi \sin \psi - \sin 2\psi \cos \psi - \sin 2\psi \sin \psi + \sin 2\psi \cos \psi)$$

$$= 0$$

For $n = 3$:

$$F_{X_{tot}}\big|_{n=3} = \sum_{b=1}^{N} \left\{ \left[F_{x_{3c}} \cos \left(\psi + \frac{b\pi}{2}\right) + F_{x_{3s}} \sin \left(\psi + \frac{b\pi}{2}\right) \right] \sin \left(\psi + \frac{b\pi}{2}\right) \right.$$

$$\left. + \left[F_{y_{3c}} \cos \left(\psi + \frac{b\pi}{2}\right) + F_{y_{3s}} \sin \left(\psi + \frac{b\pi}{2}\right) \right] \cos \left(\psi + \frac{b\pi}{2}\right) \right\}$$

$$= F_{x_{3c}} (\sin 3\psi \cos \psi + \cos 3\psi \sin \psi + \sin 3\psi \cos \psi + \cos 3\psi \sin \psi)$$

$$+ F_{x_{3s}} (-\cos 3\psi \cos \psi + \sin 3\psi \sin \psi - \cos 3\psi \cos \psi + \sin 3\psi \sin \psi)$$

$$+ F_{y_{3c}} (-\sin 3\psi \sin \psi + \cos 3\psi \cos \psi - \sin 3\psi \sin \psi + \cos 3\psi \cos \psi)$$

$$+ F_{y_{3s}} (\cos 3\psi \sin \psi + \sin 3\psi \cos \psi + \cos 3\psi \sin \psi + \sin 3\psi \cos \psi)$$

$$= 2F_{x_{3c}} \sin 4\psi - 2F_{x_{3s}} \cos 4\psi + 2F_{y_{3c}} \cos 4\psi + 2F_{y_{3s}} \sin 4\psi$$

$$= 2(F_{x_{3c}} + F_{y_{3s}})\sin 4\psi + 2(-F_{x_{3s}} + F_{y_{3c}}) \cos 4\psi \tag{A22}$$

For $n = 4$:

$$F_{X_{tot}}\Big|_{n=4} = \sum_{b=1}^{N}\left\{\left[F_{x_{4c}}\cos\left(\psi + \frac{b\pi}{2}\right) + F_{x_{4s}}\sin\left(\psi + \frac{b\pi}{2}\right)\right]\sin\left(\psi + \frac{b\pi}{2}\right)\right.$$

$$\left. + \left[F_{y_{4c}}\cos\left(\psi + \frac{b\pi}{2}\right) + F_{y_{4s}}\sin\left(\psi + \frac{b\pi}{2}\right)\right]\cos\left(\psi + \frac{b\pi}{2}\right)\right\}$$

$$= F_{x_{4c}}(\cos 4\psi \cos\psi - \cos 4\psi \sin\psi - \cos 4\psi \cos\psi + \cos 4\psi \sin\psi)$$

$$+ F_{x_{4s}}(\sin 4\psi \cos\psi - \sin 4\psi \sin\psi - \sin 4\psi \cos\psi + \sin 4\psi \sin\psi)$$

$$+ F_{y_{4c}}(-\cos 4\psi \sin\psi - \cos 4\psi \cos\psi + \cos 4\psi \sin\psi + \cos 4\psi \cos\psi)$$

$$+ F_{y_{4s}}(-\sin 4\psi \sin\psi + \sin 4\psi \cos\psi + \sin 4\psi \sin\psi + \sin 4\psi \cos\psi)$$

$$= 0$$

For $n = 5$:

$$F_{X_{tot}}\Big|_{n=5} = \sum_{b=1}^{N}\left\{\left[F_{x_{5c}}\cos\left(\psi + \frac{b\pi}{2}\right) + F_{x_{5s}}\sin\left(\psi + \frac{b\pi}{2}\right)\right]\sin\left(\psi + \frac{b\pi}{2}\right)\right.$$

$$\left. + \left[F_{y_{5c}}\cos\left(\psi + \frac{b\pi}{2}\right) + F_{y_{5s}}\sin\left(\psi + \frac{b\pi}{2}\right)\right]\cos\left(\psi + \frac{b\pi}{2}\right)\right\}$$

$$= F_{x_{5c}}(-\sin 5\psi \cos\psi + \cos 5\psi \sin\psi - \sin 5\psi \cos\psi + \cos 5\psi \sin\psi)$$

$$+ F_{x_{5s}}(\cos 5\psi \cos\psi + \sin 5\psi \sin\psi + \cos 5\psi \cos\psi + \sin 5\psi \sin\psi)$$

$$+ F_{y_{5c}}(\sin 5\psi \sin\psi + \cos 5\psi \cos\psi + \sin 5\psi \sin\psi + \cos 5\psi \cos\psi)$$

$$+ F_{y_{5s}}(-\cos 5\psi \sin\psi + \sin 5\psi \cos\psi - \cos 5\psi \sin\psi + \sin 5\psi \cos\psi)$$

$$= 2F_{x_{5c}}\sin(-4\psi) + 2F_{x_{5s}}\cos 4\psi + 2F_{y_{5c}}\cos 4\psi + 2F_{y_{5s}}\sin 4\psi$$

$$= 2\left(-F_{x_{5c}} + F_{y_{5s}}\right)\sin 4\psi + 2\left(F_{x_{5s}} + F_{y_{5c}}\right)\cos 4\psi \tag{A23}$$

Combining equations (A22) and (A23) yields the following cosine and sine components of the 4-per-rev axial load in the nonrotating frame:

$$\left.\begin{aligned} F_{X_{tot_{4c}}} &= 2(-F_{x_{3s}} + F_{y_{3c}} + F_{x_{5s}} + F_{y_{5c}}) \\ F_{X_{tot_{4s}}} &= 2(F_{x_{3c}} + F_{y_{3s}} - F_{x_{5c}} + F_{y_{5c}}) \end{aligned}\right\} \tag{A24}$$

Finally, the following equations (eqs. (A25) through (A36)) provide a set of general results for each component of force and moment in the nonrotating frame due to blade root shear in the rotating frame. Note that these equations

are valid only for four-bladed rotor systems and that the subscript denoting total has been dropped from the nonrotating frame force and moment terms.

$$F_{X_{nc}} = 2\left(-F_{x_{(n-1)s}} + F_{y_{(n-1)c}} + F_{x_{(n+1)s}} + F_{y_{(n+1)c}}\right) \qquad (n = 0, 4, 8, \ldots) \qquad \text{(A25)}$$

$$F_{X_{ns}} = 2\left(F_{x_{(n-1)c}} + F_{y_{(n-1)s}} - F_{x_{(n+1)c}} + F_{y_{(n+1)s}}\right) \qquad (n = 0, 4, 8, \ldots) \qquad \text{(A26)}$$

$$F_{Y_{nc}} = 2\left(-F_{x_{(n-1)c}} - F_{y_{(n-1)s}} - F_{x_{(n+1)c}} + F_{y_{(n+1)s}}\right) \qquad (n = 0, 4, 8, \ldots) \qquad \text{(A27)}$$

$$F_{Y_{ns}} = 2\left(-F_{x_{(n-1)s}} + F_{y_{(n-1)c}} - F_{x_{(n+1)s}} - F_{y_{(n+1)c}}\right) \qquad (n = 0, 4, 8, \ldots) \qquad \text{(A28)}$$

$$F_{Z_{nc}} = 4F_{z_{nc}} \qquad (n = 0, 4, 8, \ldots) \qquad \text{(A29)}$$

$$F_{Z_{ns}} = 4F_{z_{ns}} \qquad (n = 0, 4, 8, \ldots) \qquad \text{(A30)}$$

$$M_{X_{nc}} = 2e\left(-F_{z_{(n-1)s}} + F_{z_{(n+1)s}}\right) \qquad (n = 0, 4, 8, \ldots) \qquad \text{(A31)}$$

$$M_{X_{ns}} = 2e\left(F_{z_{(n-1)c}} - F_{z_{(n+1)c}}\right) \qquad (n = 0, 4, 8, \ldots) \qquad \text{(A32)}$$

$$M_{Y_{nc}} = 2e\left(F_{z_{(n-1)c}} + F_{z_{(n+1)c}}\right) \qquad (n = 0, 4, 8, \ldots) \qquad \text{(A33)}$$

$$M_{Y_{ns}} = 2e\left(F_{z_{(n-1)s}} + F_{z_{(n+1)s}}\right) \qquad (n = 0, 4, 8, \ldots) \qquad \text{(A34)}$$

$$M_{Z_{nc}} = -4eF_{x_{nc}} \qquad (n = 0, 4, 8, \ldots) \qquad \text{(A35)}$$

$$M_{Z_{ns}} = -4eF_{x_{ns}} \qquad (n = 0, 4, 8, \ldots) \qquad \text{(A36)}$$

Appendix B

ARES-II Model Data

This appendix provides component data necessary for modeling the ARES-II with the Dynamic Analysis and Design System (DADS) software. Although all data are not specifically provided, an experienced DADS user can generate a working model similar to that developed for this study. This appendix is organized into tables of rigid-body, joint, elastic element, and miscellaneous element data. All locations are referenced to an inertial coordinate system oriented in the manner used throughout the report: +X, aft; +Y, right; +Z, up. The bottom center of the stand baseplate is placed at the inertial coordinate system origin.

B1. Rigid Bodies

Table B1 lists the rigid-body components necessary to model the ARES-II. Included in the table are the body center of gravity with respect to the inertial coordinate system, the mass of the body, and the inertia of the body with respect to the center of gravity.

Table B1. ARES-II Model Rigid-Body Components

Body description	Mass, lb-s²/in.	Center of Gravity, in.			Mass moment of inertia about body c.g., lb-in-s²					
		X	Y	Z	I_{xx}	I_{yy}	I_{zz}	I_{xy}	I_{xz}	I_{yz}
Stand base	1.425	0	0	16.304	704.22	706.39	265.79	0	0	0
Stand yoke	0.1067	−0.510	0	68.730	3.3872	0.4592	3.1791	0	0	0
Longeron	0.1571	−4.529	0	71.691	6.4772	5.7451	11.5442	0	−1.2215	0
Fixed-system balance bottom	0.0871	1.400	0	70.796	0.6633	0.6979	1.1559	0	0	0
Fixed-system balance top	0.1350	1.400	0	75.090	1.3665	1.3670	2.1458	0	0	0
Main shaft housing	0.1266	1.010	0	83.220	1.0499	1.0799	0.4970	0	0	0
Main shaft and drive sheave	0.0574	1.400	0	79.660	1.4559	1.4559	0.5157	0	0	0
Intermediate shaft housing	0.0179	−6.574	0	79.409	0.0957	0.1138	0.1037	0	−0.0264	0
Intermediate shaft and drive sheaves	0.0279	−5.125	0	80.884	0.3238	0.3238	0.1767	0	0	0
Drive motor	0.1703	−13.653	0	77.539	1.8022	1.8022	0.8264	0	−0.0166	0
Drive motor sheave	0.0018	−13.795	0	83.337	0.0008	0.0008	0.0010	0	0	0
Rotating balance bottom	0.0020	1.400	0	91.304	0.0016	0.0016	0.0028	0	0	0
Rotating balance top	0.0028	1.400	0	92.577	0.0019	0.0019	0.0034	0	0	0
Mast	0.0064	1.400	0	94.615	0.0164	0.0164	0.0038	0	0	0

B2. Joints

Five joint types are used to model the ARES-II: translational, revolute, spherical, universal, and bracket. The translational joint eliminates all degrees of freedom between two bodies except one linear dof. The revolute joint eliminates all dofs between two bodies except one angular dof. The spherical joint eliminates linear dofs but allows all angular dofs, and the universal joint eliminates all linear and one angular dof. The bracket joint eliminates all degrees of freedom between two bodies effectively making them one larger rigid body. Table B2 lists all joints, their location with respect to the inertial coordinate system, and the bodies that the joints connect.

Table B2. ARES-II Model Joints

Joint type	Joint location, in.			Body 1	Body 2
	X	Y	Z		
Revolute	−0.600	0	74.040	Stand yoke	Longeron
Universal	−7.675	−6.580	74.340	Longeron	Actuator 1 body
Universal	−7.675	6.580	74.340	Longeron	Actuator 2 body
Universal	2.402	−7.100	74.345	Longeron	Actuator 3 body
Universal	2.402	7.100	74.345	Longeron	Actuator 4 body
Universal	8.513	−0.625	75.790	Longeron	Actuator 5 body
Universal	8.513	0.625	75.790	Longeron	Actuator 6 body
Spherical	−5.806	0	70.353	Actuator 1 Rod	Fixed-system balance bottom
Spherical	−5.421	0	70.560	Actuator 2 Rod	Fixed-system balance bottom
Spherical	8.748	−5.724	69.961	Actuator 3 Rod	Fixed-system balance bottom
Spherical	8.748	5.724	69.961	Actuator 4 Rod	Fixed-system balance bottom
Spherical	8.513	−5.450	69.728	Actuator 5 Rod	Fixed-system balance bottom
Spherical	8.513	5.450	69.728	Actuator 6 Rod	Fixed-system balance bottom
Bracket	1.400	0	75.590	Fixed-system balance top	Main shaft housing
Bracket	−2.725	0	80.140	Main shaft housing	Intermediate shaft housing
Revolute	1.400	0	77.710	Main shaft housing	Main shaft and drive sheave
Bracket	1.400	0	90.915	Main shaft and drive sheave	Rotating balance bottom
Revolute	−5.125	0	79.941	Intermediate shaft housing	Intermediate shaft and drive sheaves
Bracket	−9.125	0	78.710	Intermediate shaft housing	Drive motor
Revolute	−13.795	0	82.471	Drive motor	Drive motor sheave
Bracket	1.400	0	92.915	Rotating balance top	Mast

B3. Elastic Elements

Three types of elastic elements are used to model the ARES-II: beam, bushing, and spring-damper. The bushing is a six-degree-of-freedom elastic element with damping. The nature of the beam and spring-damper are self-explanatory. Table B3 provides a list of all elastic elements, their connection locations in inertial coordinates, and the bodies that they connect.

Table B3. ARES-II Model Elastic Elements

Elastic element type	Connection location for body 1, in.			Connection location for body 2, in.			Body 1	Body 2
	X	Y	Z	X	Y	Z		
Spring damper[1]	−17.854	−17.854	0	−17.854	−17.854	0	Pad 1	Stand base
Spring damper[1]	−17.854	−17.854	0	−17.854	17.854	0	Pad 2	Stand base
Spring damper[1]	17.854	17.854	0	17.854	17.854	0	Pad 3	Stand base
Spring damper[1]	17.854	−17.854	0	17.854	−17.854	0	Pad 4	Stand base
Beam[2]	0	0	30.0	0	0	66.840	Stand base	Stand yoke
Bushing[3]	1.400	0	72.590	1.400	0	72.590	Fixed-system balance bottom	Fixed-system balance top
Bushing[4]	1.400	0	91.915	1.400	0	91.915	Rotating balance bottom	Rotating balance top

[1]Sprint-damper properties: $K_z = 6000.0$ lb/in.; $C_z = 20.0$ lb-s/in.

[2]Beam properties: $EI_{xx} = 1.163 \times 10^9$ lb-in²; $EI_{yy} = 1.163 \times 10^9$ lb-in²; $GJ = 8.95 \times 10^8$ lb-in²

[3]Bushing properties:

$K_x = 862,000.0$ lb/in.; $K_y = 512,800.0$ lb/in.; $K_z = 93,400.0$ lb/in.

$K_{\theta_x} = 18.75 \times 10^6$ in-lb/rad; $K_{\theta_y} = 17.44 \times 10^6$ in-lb/rad; $K_{\theta_z} = 26.30 \times 10^6$ in-lb/rad

$C_x = 8.6$ lb-s/in.; $C_y = 5.1$ lb-s/in.; $C_z = 0.9$ lb-s/in.

$C_{\theta_x} = 1875.0$ in-lb-s/rad; $C_{\theta_y} = 1744.00$ in-lb-s/rad; $C_{\theta_z} = 2630.0$ in-lb-s/rad

[4]Bushing properties:

$K_x = 709,000.0$ lb/in.; $K_y = 709,000.0$ lb/in.; $K_z = 2.78 \times 10^6$ lb/in.

$K_{\theta_x} = 2.76 \times 10^6$ in-lb/rad; $K_{\theta_y} = 2.76 \times 10^6$ in-lb/rad; $K_{\theta_z} = 2.82 \times 10^6$ in-lb/rad

$C_x = 7.1$ lb-s/in.; $C_y = 7.1$ lb-s/in.; $C_z = 27.8$ lb-s/in.

$C_{\theta_x} = 276.0$ in-lb-s/rad; $C_{\theta_y} = 276.0$ in-lb-s/rad; $C_{\theta_z} = 282.0$ in-lb-s/rad

B.4. Miscellaneous Elements

The miscellaneous elements consist of constraint and point-of-interest elements. The constraint elements are used to control the length of the ARES-II actuators, hold the longeron in a fixed position relative to the stand, constrain the stand degrees of freedom that are not restrained by the mounting pads (i.e., lateral displacement and yaw), and develop the relationships for the drive train speed reduction ratio. The point-of-interest elements allow for the output of displacement information at a point on a rigid body. Table B4 provides the location of the point-of-interest elements used for the hub and swashplate interface joints.

Table B4. ARES-II Model Point-of-Interest Elements

Body	Location, in.			Purpose
	X	Y	Z	
Main-shaft housing	1.400	0	87.908	Swashplate interface joint
Mast	1.400	0	96.128	Hub interface joint

Appendix C

Basic Research Rotor Model Data

The tables in this appendix provide the input necessary to develop the rotorcraft shell and core models of the Basic Research Rotor. Note that all CAMRAD-II coordinate frames are not necessarily the same as those used in this report. Table C1 provides the basic input data to the rotorcraft shell. Table C2 provides run-time modifications to the shell model and the core model inputs.

During the research program it was noted that results obtained when modeling the R-12 test medium were inconsistent with expected trends. This inconsistency was eliminated if the model and environment parameters were scaled for air. The most obvious differences were for the high-speed flight regime ($\mu \geq 0.30$); however, some differences were noted at the lower speeds. The reason for the inconsistency is unknown as CAMRAD-II executes internally in a nondimensional format. An errant dynamic viscosity term is suspected of affecting the high-speed aerodynamic environment when executing models in the R-12 medium.

To obtain the best possible results the scaled model for R-12 was converted to execute as a scaled model in air. Therefore, the tables reflect the inputs necessary to execute an air-scaled model of the BRR. The geometric scaling remained the same. However, the mass and stiffness scaling has been modified according to the relations

$$m_{air} = 0.396 m_{R-12}$$

$$EI_{air} = 1.973 EI_{R-12}$$

The mass scaling applies to mass moment of inertia scaling and the stiffness scaling applies to the torsional stiffness scaling as well. Because the geometric scaling is the same, displacement results are not scaled. However, forces and moments must be scaled according to the relations

$$F_{R-12} = 0.5054 F_{air}$$

$$M_{R-12} = 0.5054 M_{air}$$

Table C1. BRR CAMRAD-II Shell Inputs

```
!
!  Basic Research Rotor base shell input deck
!
&NLDEF  class='CASE'  &END
&NLVAL  TITLE='Basic Research Rotor',
        OPUNIT=1, TMTASK=1,
        OPDENS=1, ALTMSL=0.
&END
&NLDEF  class='TRIM'  &END
&NLVAL  VTIPIN=3, MTIP=0.65, OPTRIM=0, MPSI=24, MPSIAV=4,
        DOFA=6*0, DOFD=8*0,
&END
&NLDEF  class='TRIM ROTOR', name='ROTOR 1'  &END
&NLVAL  DOFG=0, DOFS=0, DOFM=7*1,33*2, DOFB=8*1,4*0, OPMODE=1,
&END
&NLDEF  class='FLUTTER'  &END
&NLVAL  OPFLUT=0, OPMEAN=1, OPBLD=0, OPSTAB=0, OPAERO=0,
        DOFA=6*0, DOFD=8*0, TASK=1,3*0, OPEIGN=1, MEIGN=2,
&END
&NLDEF  class='FLUTTER ROTOR', name='ROTOR 1'  &END
&NLVAL  OPAERO=0, OPMODE=1, DOFM=7*1,33*2, OPTRAN=1,
&END
&NLDEF  class='AIFRFRAME', type='STRUCTURE'  &END
```

```
&NLVAL TITLE='ARES-2 Testbed - Simple Model',
       CONFIG=0, OPFREE=0, OPTRAN=0, OPAERO=0,
       WEIGHT=1.0, MASSR=0.29984, IXXR=0., IYYR=0., IZZR=2.193752,
                                 IXYR=0., IXZR=0., IYZR=0.       ,
       FSCG =-0.0500, BLCG =0., WLCG =6.17,
       FSRTR= 0.1167, BLRTR=0., WLRTR=8.01,
       ASHAFT=0., HSP=0.685,
&END
&NLDEF class='AIRFRAME', type='CONTROL'  &END
&NLVAL K0=1.0, KC=1.0, KS=1.0,
&END
&NLDEF class='ROTOR', type='STRUCTURE', name='ROTOR 1'  &END
&NLVAL TITLE='Basic Research Blades V.8 on Articulated Hub',
       RADIUS=4.685, NBLADE=4, ROTATE=1, SIGMA=0.0821,
       CONFIG=1, OPAERO=1, GIMBAL=0, CONTRL=2,
       HINGE=3, EFLAP=0.0534, ELAG=0.0534, DLAG=15.96,
       PITCH=1, LOCKP=1, EPITCH=0.08,
       OPTPP=2, ETPP=0.0534,
       LOCKPL=0, EPH=0.08894,
       XSP=0.03113, YSP=0.01939, ZSP=-0.14621,
       XPH=0.02490, YPH=0.04002, ZPH= 0.,
       TWIN=1, TWISTL=0.,
       KNODE=4, RNODE=0.2,0.4,0.6,0.8, OPWING=1, OPPOS=1, NRPOS=0,
        GDAMPU=0.01, GDAMPV=0.01, GDAMPW=0.01, GDAMPT=0.01
       KNODE=5, RNODE=0.1221, 0.2, 0.4, 0.6, 0.8, DRELST=0.07,
       NPROP=10,
       RPROP=0., 0.05339, 0.05341, 0.08, 0.1220, 0.1222,
             0.16, 0.18, 0.20, 1.0,
       KP=5*0.02043, 2*0.01350, 0.00451, 2*0.00669,
       EIFLAP=2*9.865E5, 3*189244.0, 2*13179.0,   309.2, 2*197.3,
       EILAG= 2*11.838E5, 3*189244.0, 2*24051.0, 15145.0, 2*5919.0,
       GJ=    2*9.865E5, 3*151394.0, 2*11178.0,   429.7, 2*268.3,
       EA=    10*414330.0,
       MASS=  2*0.1188,   3*0.05576, 2*0.02895,  0.00653, 2*0.00634,
       ITHETA=2*0.003168, 3*0.000170, 2*0.000075, 0.000012, 2*0.000053,
       IPOLAR=2*0.003168, 3*0.000170, 2*0.000075, 0.000012, 2*0.000053
&END
&NLDEF class='ROTOR', type='AERODYNAMICS', name='ROTOR 1'  &END
&NLVAL OPSCEN=1, CHORD=0.3021, NPANEL=19, REDGE=0.19,0.28,0.35,
       0.42,0.48,0.54,0.59,0.64,0.69,0.73,0.77,0.81,0.84,0.87,
       0.90,0.92,0.94,0.96,0.98,1.0
&END
&NLDEF class='ROTOR', type='INFLOW', name='ROTOR 1'  &END
&NLVAL OPSCEN=1  &END
&NLDEF class='TABLES'  &END
&NLVAL  &END
!----------------------------------------------------------------------
&NLDEF action='end of shell'  &END
&NLDEF action='end of core'   &END
```

```
!
!  BRR model w/ hub motion
!
setenv BLADEAIRFOIL1 lr0012.tab
setenv SHELLINPUT thesis1.dat
camrad > thesis1.out <<'endofinput'
 &NLJOB NCASES=1  &END
 !====================================================================
 &NLDEF class='CASE'  &END
 &NLVAL TMTASK=1,
        OPDENS=1, ALTMSL=0.
 &END
 &NLDEF class='TRIM'  &END
 &NLVALRELAXC=0.1, WINDIN=2, WVEL=0.05,
        OPTRIM=1, MTRIM=4,
            MNAME(1)='CL/S'  , VNAME(1)='COLL'  , CLTRIM= 0.07065,
            MNAME(2)='CX/S'  , VNAME(2)='PITCH' , CXTRIM=-0.00013,
            MNAME(3)='BETAS', VNAME(3)='LATCYC', BSTRIM=0.0,
            MNAME(4)='BETAC', VNAME(4)='LNGCYC', BCTRIM=0.0,
            COLL=11.14, PITCH=0.15, LATCYC=-3.37, LNGCYC=0.89,
        ITERU=1, ITERP=1, NWPRNT=1, TOLERT=0.5, LEVEL=3,
 &END
 &NLDEF class='TRIM ROTOR', name='ROTOR 1'  &END
 &NLVAL MHSEN=3, MCSEN=3, MPSEN=3,
        GDAMPM=40*0.01
 &END
 &NLDEF class='FLUTTER'  &END
 &NLVAL OPEIGN=0, MPSIAV=1  &END
 &NLDEF class='FLUTTER ROTOR', name='ROTOR 1'  &END
 &NLVAL &END
 &NLDEF class='AIRFRAME', type='STRUCTURE'  &END
 &NLVAL &END
 &NLDEF class='ROTOR', type='STRUCTURE', name='ROTOR 1'  &END
 &NLVAL OPAERO=1, OPPOS=4, NRPOS=2,
 &END
 &NLDEF class='ROTOR', type='AERODYNAMIC', name='ROTOR 1'  &END
 &NLVAL &END
 &NLDEF class='ROTOR', type='WAKE', name='ROTOR 1'  &END
 &NLVAL OPFW=1, OPNW=1, OPLL=1, OPAX=0,
        KNW=4, KRU=6, KFW=96, KDW=96,
        OPRWG=1, FK2TWG=0.9, TWIST=0.,
        OPCORE=0, CORE(1)=0.2,
        OPFWG=2, MFWG=6, COREWG=0.2, MBWG=4, DQWG=2*0.0003,
        ITERWG=2, RLXWG=0.5, RFWG=0.04,0.5, RNWG=0.04,0.125,
        RUDWG=0.5, OPDWG=1, MPSIWG=24, OPDISP=3,1
 &END
 !====================================================================
 &NLDEF action='end of shell' &END
 !====================================================================
 !
 ! Begin CORE input
 !
 !====================================================================
 !  Set in proper hub mass and inertia properties
 !  Add Hub Displacement and Hub Rotation sensors and output
 !  Add Non-rotating force and moment sensors and outputs which include
 !          hub mass
 &NLDEF class='COMPONENT', type='RIGID BODY', name='ROTOR 1 HUB'  &END
```

```
&NLVAL MASS=0.663, IXX=0.0377, IYY=0.0377, IZZ=0.0647,
                   IXY=0.   , IXZ=0.   , IYZ=0.   ,
       NSEN=8, KSEN=8, SENV(5)=5,6,7,8,
                SNAME(5)='HUB DISPLACEMENT', SLABL(5)='HUB DISP',
                SNAME(6)='HUB ROTATION'    , SLABL(6)='HUB ROT' ,
                SNAME(7)='NONROTATING HUB FORCE (w/ HUB)' ,
                SNAME(8)='NONROTATING HUB MOMENT (w/ HUB)',
                KINDQ(5)=4*1, IDENTQ(5)=4*1, QUANT(5)=1,7,41,42,
                KINDR(5)=2*6, FRAMER(5)=2*'',  SCALE(5)=4*1.0
&END
!
&NLDEF class='OUTPUT', type='', name='HUB DISPLACEMENT'  &END
&NLVAL KINDY=4, YNAMEC='ROTOR 1 HUB', YNAMEV='HUB DISPLACEMENT',
       TMPART='ROTOR 1 HUB LOAD SENSOR',
       TNPART='ROTOR 1 HUB LOAD SENSOR',
       FLPART='ROTOR 1 HUB',
       NTPRNT=1, NHPRNT=1, MTIME=24, MHARM=10, OPHARM=1
&END
!
&NLDEF class='OUTPUT', type='', name='HUB ROTATION'  &END
&NLVAL KINDY=4, YNAMEC='ROTOR 1 HUB', YNAMEV='HUB ROTATION',
       TMPART='ROTOR 1 HUB LOAD SENSOR'
       TNPART='ROTOR 1 HUB LOAD SENSOR',
       FLPART='ROTOR 1 HUB',
       NTPRNT=1, NHPRNT=1, MTIME=24, MHARM=10, OPHARM=1
&END
!
&NLDEF class='OUTPUT', type='', name='NONROTATING HUB FORCE'  &END
&NLVAL KINDY=4, YNAMEC='ROTOR 1 HUB', YNAMEV='NONROTATING HUB FORCE (w/ HUB)',
       TMPART='ROTOR 1 HUB LOAD SENSOR',
       TNPART='ROTOR 1 HUB LOAD SENSOR',
       FLPART='ROTOR 1 HUB',
       NTPRNT=1, NHPRNT=1, MTIME=24, MHARM=10, OPHARM=1
&END
!
&NLDEF class='OUTPUT', type='', name='NONROTATING HUB MOMENT'  &END
&NLVAL KINDY=4, YNAMEC='ROTOR 1 HUB', YNAMEV='NONROTATING HUB MOMENT (w/ HUB)',
       TMPART='ROTOR 1 HUB LOAD SENSOR',
       TNPART='ROTOR 1 HUB LOAD SENSOR',
       FLPART='ROTOR 1 HUB',
       NTPRNT=1, NHPRNT=1, MTIME=24, MHARM=10, OPHARM=1
&END
!
&NLDEF class='OUTPUT', type='', name='NONROTATING SWASHPLATE LOAD'  &END
&NLVAL KINDY=4, YNAMEC='PYLON', YNAMEV='NONROTATING SWASHPLATE LOAD',
       TMPART='ROTOR 1 HUB LOAD SENSOR',
       TNPART='ROTOR 1 HUB LOAD SENSOR',
       FLPART='ROTOR 1 HUB',
       NTPRNT=1, NHPRNT=1, MTIME=24, MHARM=10, OPHARM=1
&END
!========================================================================
!  Delete unused components
&NLDEF class='COMPONENT', type='RIGID BODY', name='AIRFRAME ROTOR 1',
       action='delete'
&END
!========================================================================
!  Build PYLON ROTOR 1 component from AIRFRAME ROTOR 1 input
&NLDEF class='COMPONENT', type='RIGID BODY', name='PYLON ROTOR 1'  &END
&NLVAL LABEL='PY RTR 1', DEBUG=0,
       TMPART='AIRFRAME',
```

```
           TNPART='ROTORCRAFT',
           FLPART='AIRFRAME',
           FRAME='AIRFRAME', OPMTRX=0,
           KINDFC=0, KINDRM=2,
           RNAME='PYLON ROTOR 1 RIGID BODY', RLABL='P R 1 RB',
           JNTDOF=0,
           NLOC=1, CEREP=0, ZCJ=3*0.,
           NJOINT=0,
           NCNXN=1, CCREP=0, ZCJ=3*0., CNXJNT=0, CNXLOC=1,
           NSDINT=2, SDICNX=1,1,
           SDNAME(1)='PYLON/PYLON ROTOR 1', SDLABL(1)='P /PR 1',
           SDNAME(2)='PYLON ROTOR 1/HUB 1', SDLABL(2)='PR1/H 1',
           MASS=0.
 &END
 !==============================================================================
 ! Modify existing rigid body components
 &NLDEF class='COMPONENT', type='RIGID BODY', name='ROTOR 1 HUB'   &END
 &NLVAL SDNAME(1)='PYLON ROTOR 1/HUB 1', SDLABL(1)='P /H 1'   &END
 !
 &NLDEF class='COMPONENT', type='RIGID BODY', name='ROTOR 1 SWASHPLATE'   &END
 &NLVAL SDNAME(1)='PYLON/SWASHPLATE 1', SDLABL='P /SP 1'   &END
 !==============================================================================
 ! Add PYLON component
 &NLDEF class='COMPONENT', type='RIGID BODY', name='PYLON'   &END
 &NLVAL LABEL='PYLON', DEBUG=0,
           TMPART='AIRFRAME',
           TNPART='ROTORCRAFT',
           FLPART='AIRFRAME',
           FRAME='AIRFRAME', OPMTRX=0,
           KINDFC=0, KINDRM=2,
           RNAME='PYLON RIGID BODY', RLABL='PYLON R',
           JNTDOF=6,
           NLOC=3, CEREP=3*0, ZEB= 0., 0.,  0.,
                                   0., 0.,  1.0067,
                                   0., 0.,  0.3217,
           NJOINT=1, CJREP=0, ZJE=3*0., JNTLOC=1, KINDJ=3, KINDJL=3, KINDJA=3,
           AXISL=1,2,3, GAINL=3*1.0        , TYPEL=3*1, JNTEL=1,2,3,
           AXISA=1,2,3, GAINA=3*0.0174533, TYPEA=3*1, JNTEA=4,5,6,
           NSPRNG=6, KTYPE=6*1, CTYPE=6*1,
                   KLIN=3*1.E20,3*1.E8, KEQUIV=3*1.E20,3*1.E8,
                   CLIN=6*0.          , CEQUIV=6*0.,
           OFFSET=6*0., BIAS=6*0., OPTENS=0,
           NCNXN=3, CCREP=3*0, ZCJ=9*0., CNXJNT=1,2*0, CNXLOC=1,2,3,
           NSDINT=3, SDICNX=1,2,3, TORQ=3*0,
           SDNAME(1)='AIRFRAME/PYLON',       SDLABL(1)='AF/P',
           SDNAME(2)='PYLON/PYLON ROTOR 1', SDLABL(2)='P /PR 1',
           SDNAME(3)='PYLON/SWASHPLATE 1',   SDLABL(3)='P /SP 1',
           NSEN=2, OPDEFN=2*1,
               SNAME(1)='HUB MOTION SENSOR',           SLABL(1)='HUB SEN',
               SNAME(2)='NONROTATING SWASHPLATE LOAD', SLABL(2)='NR SP LD',
               LENS=6,6,
               KSEN=12, SENV=6*1,6*2, SENE=1,2,3,4,5,6,1,2,3,4,5,6,
               KINDQ=6*2,6*1, IDENTQ=1,2,3,4,5,6,6*3,
               QUANT=6*21,3*41,3*42, AXIS=1,2,3,1,2,3,1,2,3,1,2,3,
               SCALE=3*1.0,3*0.0174533,6*1.0, OPSCL=12*0,
               SENAME( 1)='HUB MOTION LX', SELABL( 1)='HUB LX',
               SENAME( 2)='HUB MOTION LY', SELABL( 2)='HUB LY',
               SENAME( 3)='HUB MOTION LZ', SELABL( 3)='HUB LZ',
               SENAME( 4)='HUB MOTION AX', SELABL( 4)='HUB AX',
               SENAME( 5)='HUB MOTION AY', SELABL( 5)='HUB AY',
```

```
                SENAME( 6)='HUB MOTION AZ',  SELABL( 6)='HUB AZ',
                SENAME( 7)='NR SP LOAD LX'  , SELABL( 7)='NR SP LX',
                SENAME( 8)='NR SP LOAD LY'  , SELABL( 8)='NR SP LY',
                SENAME( 9)='NR SP LOAD LZ'  , SELABL( 9)='NR SP LZ',
                SENAME(10)='NR SP LOAD AX'  , SELABL(10)='NR SP AX',
                SENAME(11)='NR SP LOAD AY'  , SELABL(11)='NR SP AY',
                SENAME(12)='NR SP LOAD AZ'  , SELABL(12)='NR SP AZ',
        NCON=1, CNAME='HUB MOTION INPUT', CLABL='HUB MOTN', LENC=6,
        OPACT=6*2, CONVKC=6*1, CONEKC=1,2,3,4,5,6,
        MASS=0.
&END
&NLDEF class='RESPONSE', type='RIGID', name='DOF PYLON RIGID'  &END
&NLVAL KINDR=1,
        RNAMEC='PYLON', RNAMEV='PYLON RIGID BODY',
        OPFILT=1, KINDRM=2, REPLIN=1, REPANG=2,
        WTCLIN=.05, WTCANG=.02, WTPLIN=.05, WTPANG=.02,
        KINDN=3, KINDDN=1, CNREP=4,
        CNOM(1,1)= -1.,   0.,   0.,
        CNOM(1,2)=  0.,   1.,   0.,
        CNOM(1,3)=  0.,   0.,  -1.,
        ZNOM=-0.1667, 0., -0.8333,
        QREF=3*0, QINIT=3*0, QOPSYM=3*0, QTMRED=3*1, QTNRED=3*1, QFLRED=3*1,
        PREF=3*0, PINIT=3*0, POPSYM=3*0, PTMRED=3*1, PTNRED=3*1, PFLRED=3*1,
&END
!================================================================================
!  Modify AIRFRAME normal modes component
&NLDEF class='COMPONENT', type='LINEAR NORMAL MODES', name='AIRFRAME'  &END
&NLVAL ZEB(1,1)=-0.1667, 0., -0.8333,
        NSDINT=1, SDICNX=1,
        SDNAME(1)='AIRFRAME/PYLON', SDLABL(1)='AF/P'
&END
!================================================================================
!  Delete old structural dynamic interfaces
&NLDEF class='INTERFACE', type='SD', name='AIRFRAME/AIRFRAME ROTOR 1',
        action='delete'
&END
&NLDEF class='INTERFACE', type='SD', name='AIRFRAME ROTOR 1/HUB 1',
        action='delete'
&END
&NLDEF class='INTERFACE', type='SD', name='AIRFRAME/SWASHPLATE 1',
        action='delete'
&END
!================================================================================
!  Build new structural dynamic interfaces
&NLDEF class='INTERFACE', type='SD', name='AIRFRAME/PYLON'  &END
&NLVAL LABEL='AF/P', DEBUG=0,
        TMPART='AIRFRAME',
        TNPART='ROTORCRAFT',
        FLPART='AIRFRAME',
        ANAMEC='AIRFRAME', ANAMEV='AIRFRAME/PYLON',
        BNAMEC='PYLON'    , BNAMEV='AIRFRAME/PYLON',
        KINDSD=1, AXESC=0, OPELIM=1, NXELIM=0
&END
!
&NLDEF class='INTERFACE', type='SD', name='PYLON/PYLON ROTOR 1'  &END
&NLVAL LABEL='P /PR 1', DEBUG=0,
        TMPART='AIRFRAME',
        TNPART='ROTORCRAFT',
        FLPART='AIRFRAME',
        ANAMEC='PYLON',           ANAMEV='PYLON/PYLON ROTOR 1',
```

```
          BNAMEC='PYLON ROTOR 1', BNAMEV='PYLON/PYLON ROTOR 1',
          KINDSD=1, AXESC=0, OPELIM=1, NXELIM=0
&END
!
&NLDEF class='INTERFACE', type='SD', name='PYLON ROTOR 1/HUB 1'  &END
&NLVAL LABEL='PR 1/H 1', DEBUG=0,
          TMPART='ROTOR 1 HUB',
          TNPART='ROTORCRAFT',
          FLPART='ROTOR 1 HUB',
          ANAMEC='PYLON ROTOR 1', ANAMEV='PYLON ROTOR 1/HUB 1',
          BNAMEC='ROTOR 1 HUB'  , BNAMEV='PYLON ROTOR 1/HUB 1',
          KINDSD=1, AXESC=0, OPELIM=1, NXELIM=0
&END
!
&NLDEF class='INTERFACE', type='SD', name='PYLON/SWASHPLATE 1'  &END
&NLVAL LABEL='P /SP 1', DEBUG=0,
          TMPART='ROTOR 1 HUB',
          TNPART='ROTORCRAFT',
          FLPART='ROTOR 1 HUB',
          ANAMEC='PYLON'                , ANAMEV='PYLON/SWASHPLATE 1',
          BNAMEC='ROTOR 1 SWASHPLATE', BNAMEV='PYLON/SWASHPLATE 1',
          KINDSD=1, AXESC=0, OPELIM=1, NXELIM=0
&END
!===============================================================================
!  Delete old RESPONSEs
&NLDEF class='RESPONSE', type='RIGID', name='DOF AIRFRAME ROTOR 1 RIGID BODY',
          action='delete'
&END
&NLDEF class='RESPONSE', type='VARIABLE', name='INT AIRFRAME/SWASHPLATE 1',
          action='delete'
&END
&NLDEF class='RESPONSE', type='VARIABLE', name='INT AIRFRAME/AIRFRAME ROTOR 1',
          action='delete'
&END
&NLDEF class='RESPONSE', type='VARIABLE', name='INT AIRFRAME ROTOR 1/HUB 1',
          action='delete'
&END
!===============================================================================
!  Create new RESPONSEs
&NLDEF class='RESPONSE', type='RIGID', name='DOF PYLON ROTOR 1 RIGID BODY'
&END
&NLVAL DEBUG=0, KINDR=1,
          RNAMEC='PYLON ROTOR 1',
          RNAMEV='PYLON ROTOR 1 RIGID BODY',
          OPFILT=1, KINDRM=2, REPLIN=1, REPANG=2,
          WTCLIN=.05, WTCANG=.02, WTPLIN=.05, WTPANG=.02,
          KINDN=3, KINDDN=1, CNREP=4,
          CNOM(1,1)= -1.,   0.,   0.,
          CNOM(1,2)=  0.,   1.,   0.,
          CNOM(1,3)=  0.,   0.,  -1.,
          ZNOM=-0.1667, 0., -1.84,
          QREF=3*0, QINIT=3*0, QOPSYM=3*0, QTMRED=3*1, QTNRED=3*1, QFLRED=3*1,
          PREF=3*0, PINIT=3*0, POPSYM=3*0, PTMRED=3*1, PTNRED=3*1, PFLRED=3*1,
&END
!
&NLDEF class='RESPONSE', type='VARIABLE', name='INT PYLON/SWASHPLATE 1'  &END
&NLVAL DEBUG=0, KINDR=2,
          RNAMEC='',
          RNAMEV='PYLON/SWASHPLATE 1',
          OPFILT=0, MVAR=6, KINDN=3,
```

```
         XNOM=6*0., WTCONV=3*1.3,3*0.6, WTPERT=3*1.3,3*0.6, WTMODE=6*0.,
         XREF=6*0., XINIT=6*0., TMRED=6*1, TNRED=6*1, FLRED=6*1, OPSYM=6*0
&END
!
&NLDEF class='RESPONSE', type='VARIABLE', name='INT PYLON/PYLON ROTOR 1'  &END
&NLVAL DEBUG=0, KINDR=2,
         RNAMEC='',
         RNAMEV='PYLON/PYLON ROTOR 1',
         OPFILT=0, MVAR=6, KINDN=3,
         XNOM=6*0., WTCONV=3*1.3,3*0.6, WTPERT=3*1.3,3*0.6, WTMODE=6*0.,
         XREF=6*0., XINIT=6*0., TMRED=6*1, TNRED=6*1, FLRED=6*1, OPSYM=6*0
&END
!
&NLDEF class='RESPONSE', type='VARIABLE', name='INT PYLON ROTOR 1/HUB 1'  &END
&NLVAL DEBUG=0, KINDR=2,
         RNAMEC='',
         RNAMEV='PYLON ROTOR 1/HUB 1',
         OPFILT=0, MVAR=6, KINDN=3,
         XNOM=6*0., WTCONV=3*1.3,3*0.6, WTPERT=3*1.3,3*0.6, WTMODE=6*0.,
         XREF=6*0., XINIT=6*0., TMRED=6*1, TNRED=6*1, FLRED=6*1, OPSYM=6*0
&END
!==============================================================================
!  Hub motion input/output and connections
&NLDEF class='OUTPUT', type='', name='HUB MOTION SENSOR'  &END
&NLVAL KINDY=4, YNAMEC='PYLON', YNAMEV='HUB MOTION SENSOR',
         TMPART='ROTOR 1 HUB LOAD SENSOR',
         TNPART='NO SOLUTION',
         FLPART='NO SOLUTION',
         NTPRNT=1, NHPRNT=1, MTIME=24, MHARM=10, OPHARM=1
&END
!
&NLDEF class='RESPONSE', type='VARIABLE', name='OUT HUB MOTION SENSOR'  &END
&NLVAL KINDR=4, RNAMEV='HUB MOTION SENSOR',
         MVAR=6, KINDN=3, XNOM=6*0., WTMODE=6*0., XREF=6*0., XINIT=6*0.,
         OPSYM=6*0, WTCONV=3*0.05,3*1.0, WTPERT=3*0.05,3*1.0,
         TMRED=6*1, TNRED=6*1, FLRED=6*1
&END
!
&NLDEF class='INPUT', type='', name='HUB MOTION LX HHC INPUT'  &END
&NLVAL LABEL='LX HHC', NCNXN=1,
         FNAMEC='HUB MOTION OSC AMP LX',
         FNAMEV='HUB MOTION LX HHC INPUT',
         LENGTH=17,
         UENAME='MEAN', '1C', '1S', '2C', '2S', '3C', '3S', '4C', '4S',
                        '5C', '5S', '6C', '6S', '7C', '7S', '8C', '8S',
         UELABL='MEAN', '1C', '1S', '2C', '2S', '3C', '3S', '4C', '4S',
                        '5C', '5S', '6C', '6S', '7C', '7S', '8C', '8S',
&END
!
&NLDEF class='RESPONSE', type='VAR', name='INP HUB MOTION LX HHC INPUT'  &END
&NLVAL KINDR=3, RNAMEV='HUB MOTION LX HHC INPUT',
         MVAR=17, KINDN=3, XNOM=17*0., WTMODE=17*0., XREF=17*0.,
!
!                        Axial hub motions are set in here -- MEAN, 1PC, 1PS, 2PC, 2PS, ...
!
         XINIT=0., 6*0., 0., 0., 6*0., 0., 0.,
         OPSYM=17*0, WTCONV=17*0.05, WTPERT=17*0.05,
         TMRED=17*1, TNRED=17*1, FLRED=17*1
&END
!
```

```
&NLDEF class='COMPONENT', type='FOURIER', name='HUB MOTION OSC AMP LX'  &END
&NLVAL LABEL='HUB MOTN', MHARM=8, NBHARM=0, NEHARM=8, TYPEA=2,
       PERIOD='ROTOR 1', AZREF=0., GAIN=1.0, OPDRVF=0, OPDRVX=0,
       FONAME='HUB MOTION LX HHC INPUT', FOLABL='LX HHC',
       XNAME='HUB MOTION OSC AMP LX'   , XLABL='LX HHC'
&END
!
&NLDEF class='INTERFACE', type='IO', name='HUB MOTION OSC AMP LX'  &END
&NLVAL LABEL='AMP LX',
       TMPART='ROTOR 1 CONTROL', TMPASS=1,
       TNPART='NO SOLUTION',
       FLPART='NO SOLUTION',
       XNAMEC='HUB MOTION OSC AMP LX',
       XNAMEV='HUB MOTION OSC AMP LX',
       NCNXN=1,
       FNAMEC='HUB MOTION', FNAMEV='HUB MOTION OSC AMP LX'
&END
!
&NLDEF class='RESPONSE', type='VARIABLE', name='INT HUB MOTION OSC AMP LX' &END
&NLVAL KINDR=2, RNAMEV='HUB MOTION OSC AMP LX',
       MVAR=1, KINDN=3, XNOM=0., WTMODE=0., XREF=0., XINIT=0.,
       OPSYM=0, WTCONV=0.05, WTPERT=0.05,
       TMRED=1, TNRED=1, FLRED=1
&END
!
&NLDEF class='INPUT', type='', name='HUB MOTION LY HHC INPUT'  &END
&NLVAL LABEL='LY HHC', NCNXN=1,
       FNAMEC='HUB MOTION OSC AMP LY',
       FNAMEV='HUB MOTION LY HHC INPUT'
       LENGTH=17,
       UENAME='MEAN', '1C', '1S', '2C', '2S', '3C', '3S', '4C', '4S',
                      '5C', '5S', '6C', '6S', '7C', '7S', '8C', '8S',
       UELABL='MEAN', '1C', '1S', '2C', '2S', '3C', '3S', '4C', '4S',
                      '5C', '5S', '6C', '6S', '7C', '7S', '8C', '8S',
&END
!
&NLDEF class='RESPONSE', type='VAR', name='INP HUB MOTION LY HHC INPUT'  &END
&NLVAL KINDR=3, RNAMEV='HUB MOTION LY HHC INPUT',
       MVAR=17, KINDN=3, XNOM=17*0., WTMODE=17*0., XREF=17*0.,
!
!                        Side hub motions are set in here -- MEAN, 1PC, 1PS, 2PC, 2PS, ...
!
       XINIT=0., 6*0., 0., 0., 6*0., 0., 0.,
       OPSYM=17*0, WTCONV=17*0.05, WTPERT=17*0.05,
       TMRED=17*1, TNRED=17*1, FLRED=17*1
&END
!
&NLDEF class='COMPONENT', type='FOURIER', name='HUB MOTION OSC AMP LY'  &END
&NLVAL LABEL='HUB MOTN', MHARM=8, NBHARM=0, NEHARM=8, TYPEA=2,
       PERIOD='ROTOR 1', AZREF=0., GAIN=1.0, OPDRVF=0, OPDRVX=0,
       FONAME='HUB MOTION LY HHC INPUT', FOLABL='LY HHC',
       XNAME='HUB MOTION OSC AMP LY'   , XLABL='LY HHC'
&END
!
&NLDEF class='INTERFACE', type='IO', name='HUB MOTION OSC AMP LY'  &END
&NLVAL LABEL='AMP LY',
       TMPART='ROTOR 1 CONTROL', TMPASS=1,
       TNPART='NO SOLUTION',
       FLPART='NO SOLUTION',
       XNAMEC='HUB MOTION OSC AMP LY',
```

```
                XNAMEV='HUB MOTION OSC AMP LY',
                NCNXN=1,
                FNAMEC='HUB MOTION', FNAMEV='HUB MOTION OSC AMP LY'
     &END
     !
     &NLDEF class='RESPONSE', type='VARIABLE', name='INT HUB MOTION OSC AMP LY' &END
     &NLVAL KINDR=2, RNAMEV='HUB MOTION OSC AMP LY',
                MVAR=1, KINDN=3, XNOM=0., WTMODE=0., XREF=0., XINIT=0.,
                OPSYM=0, WTCONV=0.05, WTPERT=0.05,
                TMRED=1, TNRED=1, FLRED=1
     &END
     !
     &NLDEF class='INPUT', type='', name='HUB MOTION LZ HHC INPUT'  &END
     &NLVAL LABEL='LZ HHC', NCNXN=1,
                FNAMEC='HUB MOTION OSC AMP LZ',
                FNAMEV='HUB MOTION LZ HHC INPUT',
                LENGTH=17,
                UENAME='MEAN', '1C', '1S', '2C', '2S', '3C', '3S', '4C', '4S',
                           '5C', '5S', '6C', '6S', '7C', '7S', '8C', '8S',
                UELABL='MEAN', '1C', '1S', '2C', '2S', '3C', '3S', '4C', '4S',
                           '5C', '5S', '6C', '6S', '7C', '7S', '8C', '8S',
     &END
     !
     &NLDEF class='RESPONSE', type='VAR', name='INP HUB MOTION LZ HHC INPUT'  &END
     &NLVAL KINDR=3, RNAMEV='HUB MOTION LZ HHC INPUT',
                MVAR=17, KINDN=3, XNOM=17*0., WTMODE=17*0., XREF=17*0.,
     !
     !                         Normal hub motions are set in here -- MEAN, 1PC, 1PS, 2PC, 2PS, ...
     !
                XINIT=0., 6*0., 0., 0., 6*0., 0., 0.,
                OPSYM=17*0, WTCONV=17*0.05, WTPERT=17*0.05,
                TMRED=17*1, TNRED=17*1, FLRED=17*1
     &END
     !
     &NLDEF class='COMPONENT', type='FOURIER', name='HUB MOTION OSC AMP LZ'  &END
     &NLVAL LABEL='HUB MOTN', MHARM=8, NBHARM=0, NEHARM=8, TYPEA=2,
                PERIOD='ROTOR 1', AZREF=0., GAIN=1.0, OPDRVF=0, OPDRVX=0,
                FONAME='HUB MOTION LZ HHC INPUT', FOLABL='LZ HHC'
                XNAME='HUB MOTION OSC AMP LZ'   , XLABL='LZ HHC'
     &END
     !
     &NLDEF class='INTERFACE', type='IO', name='HUB MOTION OSC AMP LZ'  &END
     &NLVAL LABEL='AMP LZ',
                TMPART='ROTOR 1 CONTROL', TMPASS=1,
                TNPART='NO SOLUTION',
                FLPART='NO SOLUTION',
                XNAMEC='HUB MOTION OSC AMP LZ',
                XNAMEV='HUB MOTION OSC AMP LZ',
                NCNXN=1,
                FNAMEC='HUB MOTION', FNAMEV='HUB MOTION OSC AMP LZ'
     &END
     !
     &NLDEF class='RESPONSE', type='VARIABLE', name='INT HUB MOTION OSC AMP LZ' &END
     &NLVAL KINDR=2, RNAMEV='HUB MOTION OSC AMP LZ',
                MVAR=1, KINDN=3, XNOM=0., WTMODE=0., XREF=0., XINIT=0.,
                OPSYM=0, WTCONV=0.05, WTPERT=0.05,
                TMRED=1, TNRED=1, FLRED=1
     &END
     !
```

```
&NLDEF class='INPUT', type='', name='HUB MOTION AX HHC INPUT'   &END
&NLVAL LABEL='AX HHC', NCNXN=1,
       FNAMEC='HUB MOTION OSC AMP AX',
       FNAMEV='HUB MOTION AX HHC INPUT',
       LENGTH=17,
       UENAME='MEAN', '1C', '1S', '2C', '2S', '3C', '3S', '4C', '4S',
                      '5C', '5S', '6C', '6S', '7C', '7S', '8C', '8S',
       UELABL='MEAN', '1C', '1S', '2C', '2S', '3C', '3S', '4C', '4S',
                      '5C', '5S', '6C', '6S', '7C', '7S', '8C', '8S',
&END
!
&NLDEF class='RESPONSE', type='VAR', name='INP HUB MOTION AX HHC INPUT'   &END
&NLVAL KINDR=3, RNAMEV='HUB MOTION AX HHC INPUT',
       MVAR=17, KINDN=3, XNOM=17*0., WTMODE=17*0., XREF=17*0.,
!
!                       Roll hub motions are set in here -- MEAN, 1PC, 1PS, 2PC, 2PS, ...
!                       Must input some Side motion if want pure roll at hub
!
       XINIT=0., 6*0., 0., 0., 6*0., 0., 0.,
       OPSYM=17*0, WTCONV=17*0.05, WTPERT=17*0.05,
       TMRED=17*1, TNRED=17*1, FLRED=17*1
&END
!
&NLDEF class='COMPONENT', type='FOURIER', name='HUB MOTION OSC AMP AX'   &END
&NLVAL LABEL='HUB MOTN', MHARM=8, NBHARM=0, NEHARM=8, TYPEA=2,
       PERIOD='ROTOR 1', AZREF=0., GAIN=1.0, OPDRVF=0, OPDRVX=0,
       FONAME='HUB MOTION AX HHC INPUT', FOLABL='AX HHC',
       XNAME='HUB MOTION OSC AMP AX'    , XLABL='AX HHC'
&END
!
&NLDEF class='INTERFACE', type='IO', name='HUB MOTION OSC AMP AX'   &END
&NLVAL LABEL='AMP AX',
       TMPART='ROTOR 1 CONTROL', TMPASS=1,
       TNPART='NO SOLUTION',
       FLPART='NO SOLUTION',
       XNAMEC='HUB MOTION OSC AMP AX',
       XNAMEV='HUB MOTION OSC AMP AX',
       NCNXN=1,
       FNAMEC='HUB MOTION', FNAMEV='HUB MOTION OSC AMP AX'
&END
!
&NLDEF class='RESPONSE', type='VARIABLE', name='INT HUB MOTION OSC AMP AX' &END
&NLVAL KINDR=2, RNAMEV='HUB MOTION OSC AMP AX',
       MVAR=1, KINDN=3, XNOM=0., WTMODE=0., XREF=0., XINIT=0.,
       OPSYM=0, WTCONV=0.05, WTPERT=0.05,
       TMRED=1, TNRED=1, FLRED=1
&END
!
&NLDEF class='INPUT', type='', name='HUB MOTION AY HHC INPUT'   &END
&NLVAL LABEL='AY HHC', NCNXN=1,
       FNAMEC='HUB MOTION OSC AMP AY',
       FNAMEV='HUB MOTION AY HHC INPUT',
       LENGTH=17,
       UENAME='MEAN', '1C', '1S', '2C', '2S', '3C', '3S', '4C', '4S',
                      '5C', '5S', '6C', '6S', '7C', '7S', '8C', '8S',
       UELABL='MEAN', '1C', '1S', '2C', '2S', '3C', '3S', '4C', '4S',
                      '5C', '5S', '6C', '6S', '7C', '7S', '8C', '8S',
&END
!
```

93

```
&NLDEF class='RESPONSE', type='VAR', name='INP HUB MOTION AY HHC INPUT'   &END
&NLVAL KINDR=3, RNAMEV='HUB MOTION AY HHC INPUT',
       MVAR=17, KINDN=3, XNOM=17*0., WTMODE=17*0., XREF=17*0.,
!
!                               Pitch hub motions are set in here -- MEAN, 1PC, 1PS, 2PC, 2PS, ...
!                               Must input some Axial motion if want pure roll at hub
!
       XINIT=0., 6*0., 0., 0., 6*0., 0., 0.,
       OPSYM=17*0, WTCONV=17*0.05, WTPERT=17*0.05,
       TMRED=17*1, TNRED=17*1, FLRED=17*1
&END
!
&NLDEF class='COMPONENT', type='FOURIER', name='HUB MOTION OSC AMP AY'   &END
&NLVAL LABEL='HUB MOTN', MHARM=8, NBHARM=0, NEHARM=8, TYPEA=2,
       PERIOD='ROTOR 1', AZREF=0., GAIN=1.0, OPDRVF=0, OPDRVX=0,
       F0NAME='HUB MOTION AY HHC INPUT', F0LABL='AY HHC',
       XNAME='HUB MOTION OSC AMP AY'    , XLABL='AY HHC'
&END
!
&NLDEF class='INTERFACE', type='IO', name='HUB MOTION OSC AMP AY'   &END
&NLVAL LABEL='AMP AY',
       TMPART='ROTOR 1 CONTROL', TMPASS=1,
       TNPART='NO SOLUTION',
       FLPART='NO SOLUTION',
       XNAMEC='HUB MOTION OSC AMP AY',
       XNAMEV='HUB MOTION OSC AMP AY',
       NCNXN=1,
       FNAMEC='HUB MOTION', FNAMEV='HUB MOTION OSC AMP AY'
&END
!
&NLDEF class='RESPONSE', type='VARIABLE', name='INT HUB MOTION OSC AMP AY' &END
&NLVAL KINDR=2, RNAMEV='HUB MOTION OSC AMP AY',
       MVAR=1, KINDN=3, XNOM=0., WTMODE=0., XREF=0., XINIT=0.,
       OPSYM=0, WTCONV=0.05, WTPERT=0.05,
       TMRED=1, TNRED=1, FLRED=1
&END
!
&NLDEF class='INPUT', type='', name='HUB MOTION AZ HHC INPUT'   &END
&NLVAL LABEL='AZ HHC', NCNXN=1,
       FNAMEC='HUB MOTION OSC AMP AZ',
       FNAMEV='HUB MOTION AZ HHC INPUT',
       LENGTH=17,
       UENAME='MEAN', '1C', '1S', '2C', '2S', '3C', '3S', '4C', '4S',
                      '5C', '5S', '6C', '6S', '7C', '7S', '8C', '8S',
       UELABL='MEAN', '1C', '1S', '2C', '2S', '3C', '3S', '4C', '4S',
                      '5C', '5S', '6C', '6S', '7C', '7S', '8C', '8S',
&END
!
&NLDEF class='RESPONSE', type='VAR', name='INP HUB MOTION AZ HHC INPUT'   &END
&NLVAL KINDR=3, RNAMEV='HUB MOTION AZ HHC INPUT',
       MVAR=17, KINDN=3, XNOM=17*0., WTMODE=17*0., XREF=17*0.,
!
!                               Yaw hub motions are set in here -- MEAN, 1PC, 1PS, 2PC, 2PS, ...
!
       XINIT=0., 6*0., 0., 0., 6*0., 0., 0.,
       OPSYM=17*0, WTCONV=17*0.05, WTPERT=17*0.05,
       TMRED=17*1, TNRED=17*1, FLRED=17*1
&END
!
```

```
&NLDEF class='COMPONENT', type='FOURIER', name='HUB MOTION OSC AMP AZ'   &END
&NLVAL LABEL='HUB MOTN', MHARM=8, NBHARM=0, NEHARM=8, TYPEA=2,
       PERIOD='ROTOR 1', AZREF=0., GAIN=1.0, OPDRVF=0, OPDRVX=0,
       F0NAME='HUB MOTION AZ HHC INPUT', F0LABL='AZ HHC',
       XNAME='HUB MOTION OSC AMP AZ'    , XLABL='AZ HHC'
&END
!
&NLDEF class='INTERFACE', type='IO', name='HUB MOTION OSC AMP AZ'  &END
&NLVAL LABEL='AMP AZ',
       TMPART='ROTOR 1 CONTROL', TMPASS=1,
       TNPART='NO SOLUTION',
       FLPART='NO SOLUTION',
       XNAMEC='HUB MOTION OSC AMP AZ',
       XNAMEV='HUB MOTION OSC AMP AZ',
       NCNXN=1,
       FNAMEC='HUB MOTION', FNAMEV='HUB MOTION OSC AMP AZ'
&END
!
&NLDEF class='RESPONSE', type='VARIABLE', name='INT HUB MOTION OSC AMP AZ' &END
&NLVAL KINDR=2, RNAMEV='HUB MOTION OSC AMP AZ',
       MVAR=1, KINDN=3, XNOM=0., WTMODE=0., XREF=0., XINIT=0.,
       OPSYM=0, WTCONV=0.05, WTPERT=0.05,
       TMRED=1, TNRED=1, FLRED=1
&END
!
&NLDEF class='COMPONENT', type='DE', name='HUB MOTION'  &END
&NLVAL LABEL='HUB MOTN',OPMTRX=1, FORMEQ=0, INPTEQ=0, INPTDS=1,
       XNAME='HUB MOTION', XLABL='HUB MOTN', LENX=6,
       NCON=6,
       CNAME(1)='HUB MOTION OSC AMP LX', CLABL(1)='LX', LENC(1)=1,
       CNAME(2)='HUB MOTION OSC AMP LY', CLABL(2)='LY', LENC(2)=1,
       CNAME(3)='HUB MOTION OSC AMP LZ', CLABL(3)='LZ', LENC(3)=1,
       CNAME(4)='HUB MOTION OSC AMP AX', CLABL(4)='AX', LENC(4)=1,
       CNAME(5)='HUB MOTION OSC AMP AY', CLABL(5)='AY', LENC(5)=1,
       CNAME(6)='HUB MOTION OSC AMP AZ', CLABL(6)='AZ', LENC(6)=1,
       OPCON=1, LENV=6, CONV=1,2,3,4,5,6, CONE=6*1
&END
!
&NLDEF class='INTERFACE', type='IO', name='HUB MOTION INPUT'  &END
&NLVAL LABEL='HUB MOTN',
       TMPART='ROTOR 1 CONTROL', TMPASS=2,
       TNPART='NO SOLUTION',
       FLPART='NO SOLUTION',
       XNAMEC='HUB MOTION', XNAMEV='HUB MOTION',
       NCNXN=1,
       FNAMEC='PYLON', FNAMEV='HUB MOTION INPUT'
&END
!
&NLDEF class='RESPONSE', type='VARIABLE', name='HUB MOTION INPUT'  &END
&NLVAL KINDR=2, RNAMEV='HUB MOTION INPUT',
       MVAR=6, KINDN=3, XNOM=0., WTMODE=0., XREF=0., XINIT=0.,
       OPSYM=6*0, WTCONV=3*0.05,3*0.02, WTPERT=3*0.05,,3*0.02,
       TMRED=6*1, TNRED=6*1, FLRED=6*1
&END
!
&NLDEF class='OUTPUT', type='', name='OUT HUB MOTION INPUT'   &END
&NLVAL KINDY=4, YNAMEC='HUB MOTION', YNAMEV='HUB MOTION',
       TMPART='ROTOR 1 HUB LOAD SENSOR',
       TNPART='NO SOLUTION',
       FLPART='NO SOLUTION',
```

```
        NTPRNT=1, NHPRNT=1, MTIME=24, MHARM=10, OPHARM=1
&END
!=========================================================================
&NLDEF action='end of core' &END
'endofinput'
```

REPORT DOCUMENTATION PAGE	Form Approved OMB No. 07704-0188

Public reporting burden for this collection of information is estimated to average 1 hour per response, including the time for reviewing instructions, searching existing data sources, gathering and maintaining the data needed, and completing and reviewing the collection of information. Send comments regarding this burden estimate or any other aspect of this collection of information, including suggestions for reducing this burden, to Washington Headquarters Services, Directorate for Information Operations and Reports, 1215 Jefferson Davis Highway, Suite 1204, Arlington, VA 22202-4302, and to the Office of Management and Budget, Paperwork Reduction Project (0704-0188), Washington, DC 20503.

1. AGENCY USE ONLY (Leave blank)	2. REPORT DATE June 1998	3. REPORT TYPE AND DATES COVERED Technical Publication

4. TITLE AND SUBTITLE	5. FUNDING NUMBERS
Development of a Rotor-Body Coupled Analysis for an Active Mount Aeroelastic Rotor Testbed	WU 581-20-21-01 PR A5008

6. AUTHOR(S)
Matthew L. Wilbur

7. PERFORMING ORGANIZATION NAME(S) AND ADDRESS(ES)	8. PERFORMING ORGANIZATION REPORT NUMBER
U.S. Army Research Laboratory Vehicle Technology Center NASA Langley Research Center Hampton, VA 23681-2199	L-17596

9. SPONSORING/MONITORING AGENCY NAME(S) AND ADDRESS(ES)	10. SPONSORING/MONITORING AGENCY REPORT NUMBER
National Aeronautics and Space Administration Washington, DC 20546-0001 and U.S. Army Research Laboratory Adelphi, MD 20783-1145	NASA/TP-1998-208433 ARL-TR-1313

11. SUPPLEMENTARY NOTES

Wilbur: U.S. Army Research Laboratory, Vehicle Technology Center, Langley Research Center, Hampton, VA.
The information presented in this report was submitted as a thesis in partial fulfillment of the requirements for the degree of Master of Science, George Washington University, Washington, DC, May 1996.

12a. DISTRIBUTION/AVAILABILITY STATEMENT	12b. DISTRIBUTION CODE
Unclassified–Unlimited Subject Category 05 Distribution: Standard Availability: NASA CASI (301) 621-0390	

13. ABSTRACT (Maximum 200 words)

At the Langley Research Center an active mount rotorcraft testbed is being developed for use in the Langley Transonic Dynamics Tunnel. This testbed, the second generation version of the Aeroelastic Rotor Experimental System (ARES-II), can impose rotor hub motions and measure the response so that rotor-body coupling phenomena may be investigated. An analytical method for coupling an aeroelastically scaled model rotor system to the ARES-II is developed in the current study. Models of the testbed and the rotor system are developed in independent analyses, and an impedance-matching approach is used to couple the rotor system to the testbed. The development of the analytical models and the coupling method is examined, and individual and coupled results are presented for the testbed and rotor system. Coupled results are presented with and without applied hub motion, and system loads and displacements are examined. The results show that a closed-loop control system is necessary to achieve desired hub motions, that proper modeling requires including the loads at the rotor hub and rotor control system, and that the strain-gauge balance placed in the rotating system of the ARES-II provided the best loads results.

14. SUBJECT TERMS Helicopters; Model rotor testing; Model rotor testbeds; Stewart platforms; Impedance matching	15. NUMBER OF PAGES 109
	16. PRICE CODE A06

17. SECURITY CLASSIFICATION OF REPORT Unclassified	18. SECURITY CLASSIFICATION OF THIS PAGE Unclassified	19. SECURITY CLASSIFICATION OF ABSTRACT Unclassified	20. LIMITATION OF ABSTRACT

NSN 7540-01-280-5500

Standard Form 298 (Rev. 2-89)
Prescribed by ANSI Std. Z39-18
298-102